Experimental and Numerical Modeling of the Gated and Ungated Ogee Spillway

Chuyao Luo

Thesis submitted to the
Faculty of Engineering
in partial fulfillment of the requirements for the degree of

Master of Applied Science in Civil Engineering

Academic Supervisors: Prof. Abdolmajid Mohammadian, Prof. Ioan Nistor, and Prof. Hanifeh Imanian

University of Ottawa

Department of Civil Engineering

January 2023

Abstract

Spillways are hydraulic structures that allow dams to release and convey surplus water or flood from the reservoir to the downstream channel. The spillway is a safety structure that prevents the overtopping of the dam. Many dam failure disasters were due to the inadequate capacity of the spillway, which fully illustrates the prominence of spillway design. According to the control structure, spillways can be divided into gated and ungated type. The gated spillway provides better control of the managed water level and reduces the elevation of the top of the dam. Researchers have mostly used experimental models to investigate these two types of spillways in previous literature. In the past few years, following the rapid development of numerical simulation technology, there have been more studies on the numerical modeling of spillways. However, most of the literature was about ungated spillways and most of it considered the case of low head ratios, while the case with gates, especially the case of vertical plane gates, was less investigated.

In this study, the hydraulic characteristics, such as velocity, pressure, and discharge coefficient, of the ungated and gated ogee spillways are investigated by means of physical and numerical models for the case of low and high head ratios. The study covered head ratios varying from 1.4 to 4.6 and the relative gate-openings varying from 0.5 to 2. The second main objective of this study was to evaluate the performance of the numerical model to simulate gated and ungated spillways. It mainly employed 2DV OpenFOAM to simulate three turbulence models (realizable k-ε, RNG k-ε, k-ω SST), and the results were compared and calibrated with the experimental results from the physical model tests performed by the author to verify the performance of the numerical model. This study aims to demonstrate that the numerical model can be used as a complementary tool to the physical model to measure the hydraulic performance of ogee spillways.

Acknowledgments

First of all, I would like to acknowledge and express my sincerest gratitude to my academic supervisors, Prof. Abdolmajid Mohammadian, Prof. Ioan Nistor, and Prof. Hanifeh Imanian. I vividly remember that Prof. Mohammadian patiently mentored me on OpenFOAM, leading me to the field of numerical models, imparting the knowledge of hydraulics to me, and supporting my entire research. My co-supervisor, Prof. Nistor, provided me with valuable advice, comprehensive support, and all the necessary and excellent resources for the experiment and this project. Furthermore, my co-supervisor, Prof. Imanian, inspired and suggested me all the time, not only in numerical models but also in the experiment setup. It is thanks to their excellent teaching and encouragement to allow me gradually grasped the application of numerical models in hydraulic studies. Over the past few years, they have advised me not only on my academic work but also on my career development. The weekly meetings and the discussion with them were the most cherished and valuable experiences and memories I had during my Master's study.

Secondly, I would like to extend my gratitude to all the lab technicians, particularly to Mark Lapointe and Leo Denner, who helped me assemble the experimental models and to use the measurement instrumentation. The experiment would not have been successfully completed without their professional help. I would also like to thank the summer exchange student, Théophile Prunaux from France, for assisting me in running many of the experimental tasks. Additionally, I would like to express my thanks to the other staff, and to my colleagues: Margo Muller, Wenjun Zhang, and Shilong Liu, who have contributed to my experiment setup. The enthusiastic help from all of them was key to the completion of my project.

I would like to recognize my fellow colleagues and friends. Especially, Xinyun Wang, who provided me with warm help over the past few years, enabled me to adapt quickly and well to my studies and life here. Besides, I would like to express my thanks to my friends, Xiaotong Ye, and Qin Chen, who provided me with useful suggestions and encouragement to finish my research.

Additionally, I would like to express my gratitude to my lifelong mentors, Dr. Xiaojun Liu, and Ms. Yan Wang, for their guidance and inspiration. Their wisdom and insightful advice have exerted a profound influence on me, motivating me to think critically and study more diligently. I would also like to express my thanks to President Changbo Jiang at the Hunan University of

Technology for providing me with invaluable suggestions and support in the field of water resource engineering.

Finally, I would like to express my deepest gratitude to my parents, Zhong Luo and Guihua Luo, for their unwavering support throughout my academic journey. Their trust, encouragement, love, and understanding have been instrumental in my achievements, sustaining me through the challenges and motivating me to reach my goals.

Table of Contents

List of Figures

List of Tables

List of Symbols

Literature review-Experiment model

Hd	Designed head	m
Cd	Discharge coefficient	
χ	relative head	
H_0	actual head	m
Hr	Head ratio	
zl	gate opening	m
Zl	relative gate opening	
Q_g	Discharge over gated spillway	m^3/s
α	chute slope angle	rad
β	deflection angle	rad
θ	takeoff angle	rad
$\frac{R}{h_0}$	relative curvature of the flip bucket	
Fr_0	Froude number	
D_p	damage potential	
σ_s	cavitation index for the initiation of damage	
σ_f	cavitation index for the flow	
V_r	reference velocity	m/s
D_i	damage index	
t_c	cumulative time of operation	s
ρ	volume mass of water	kg/m^3
g	gravity acceleration	m/s^2
S_f	tailwater submergence factor	
L_c	width of the spillway bay	m
d	tailwater submergence	m
Q_s	discharge (Sinniger's formula)	m^3/s
C_{dg}	Sinniger's discharge coefficient	
G	gate opening	m
C_p	Pressure correction factor	
D	orifice opening	m
$\frac{p}{\gamma}$	mean pressure distribution	
A	the area of the orifice corresponding to the orifice opening	m^2

P_s	spillway height	m
C_{dfw}	free-weir discharge coefficient	
S_c	reduction factor or submergence coefficient	
y_c	critical depth over the still crest	m

Literature review-Numerical model

W_{ab}	interpolation kernel	
ρ_a	density of particle *a*	
m_b	mass of particle *b*	
v_a and v_b	velocity of particles *a* and *b*	m/s
$\mathbf{r}_{ab}$	position distance between particle a and b	m
$\mathbf{v}_{ab}$	difference in velocity between particles a and b	
η	smoothing parameter	
ξ	viscous term parameter	
$\boldsymbol{u}$	velocity vector	m/s
t	time	s
ρ	density of the fluid	kg/m^3
p	pressure	N/m^2
$\boldsymbol{r}$	position vector	
μ	fluid viscosity	$N.s/m^2$
F	flux vector	
k	turbulent kinetic energy	
ε	the turbulent kinetic energy dissipation rate	m^2/s
f_i	Gaussian force	
K	total kinetic energy	
ν	kinematic viscosity	m^2/s
ν_t	turbulent kinematic viscosity	m^2/s
ω	specific dissipation rate	m^2/s

Technical paper

u, v, and w	velocity variables in the x, y, and z directions	m/s

A_x, A_y, A_z	fractional areas of open flow area in the *x*, *y*, and *z* directions respectively	m^2
$\bar{u}_i$	average flow velocity	m/s
g_i	gravitational force	m/s^2
f_i	Reynolds stresses required by the turbulence closure	N/m^2
S_{ij}	strain-rate tensor	
v_t	the turbulent viscosity	m^2/s
C_μ	dynamic viscosity coefficient	
h	water depth above the spillway crest	m
Q	discharge at the inlet	m^3/s
B	width of the spillway	m
g	gravitational acceleration	m/s^2
h_{uf}	height of the upstream spillway	m
Hr	Head ratio	
Zl	Relative gate opening	
Z	Water depth upstream	m
Y	experimental model measured vector	m/s
D	numerical model calculated vector	m/s
N	number of measured vectors	
x_0	normalized head	
Q(g)	Gated discharge calculated by Equation 6	m^3/s
Q(exp)	experimental gated discharge	m^3/s
Q(revised)	Revised gated discharge	m^3/s
Lz	Height of the corner eddy	m
Lx	Length of the corner eddy	m
dm	Vertical location where the maximum velocity occurs	m
$d(Pmin)$	Vertical location where the minimum pressure occurs	m
x	Distance from the spillway axis	m

List of Abbreviations

RANS	Reynolds-Averaged Navier-Stokes
LES	Large Eddy Simulation
DES	Detached Eddy Simulation
2DV	2 Dimensions Vertically
LSPIV	Large Scale Particle Image Velocimetry
PIV	Particle Image Velocimetry
TVA	Tennessee Valley Authority
ADCP	Acoustic Doppler Current Profiler
PFEM	Particle Finite Element Method
SPH	Smoothed Particle Hydrodynamics
WC-MPS	Weakly Compressible Moving Particle Semi-implicit
SFGFEM	Smoothed Fixed Grid Finite Element method
FAVOR	Fractional Area / Volume Obstacle Representation
VOF	Volume-of-Fluid
RNG	Renormalized Group
SST k-ω model	Shear-Stress Transport k-ω model
LRR	Launder-Reece-Rodi
BSL model	Baseline model
FEM	Finite Element Method
ANN	Artificial Neural Network
MLP	Multilayer Perceptron
ADV	Acoustic Doppler Velocimeter
CFD	Computational Fluid Dynamics
OpenFOAM	Open Field Operation And Manipulation
FVM	Finite Volume Method
PCG	Preconditioned Conjugate Gradient
DIC	Diagonal Incomplete Cholesky
BC	Boundary Condition

Chapter 1 Introduction

1.1 Background

A spillway is a hydraulic structure that ensures the safety of dams by allowing the release of surplus water or excess flood water from the impounded reservoir to the downstream channel. As a safety structure, the spillway is designed to prevent the dam from uncontrolled overtopping. Many dam failure disasters are triggered by poor spillway performance or inadequate spillway discharge capacity. It can be seen that the design of the spillway and the investigation of the hydraulic characteristics are highly important.

According to Khatsuria (2005), spillways are also equipped with other functions. For example, spillways can drop the water level in case of emergency and keep the average water level in flood situations, as well as compensate for water supply to maintain the normal river functions.

The selection of spillways varies greatly for different dam types, hydrography, and geographic locations. For example, concrete dams and masonry dams are commonly equipped with ogee spillways. Earth dams are usually equipped with side channel spillways, while shaft spillways are a good choice for a dam located in a narrow canyon (Khatsuria, 2005).

The design of the spillway, as a control structure, is crucial. Depending on the control structure, spillways can be categorized as gated spillways, ungated spillways, and orifice of sluice spillways.

Figure 1-1 Gated spillway (The Greenville News, 2016)

The ungated spillway allows water to be released automatically. When the water level exceeds the height of the crest of the spillway, which is determined by the maximum flood level, the ungated spillway releases it automatically. By contrast, the gated spillway is equipped with vertical plane or radial gates placed at the crest of the spillway to control the upstream water level for flood regulation by controlling the opening of the gates – this requires which needs human operation.

It can be seen that the height of a dam with a gated spillway can be lower than that of an ungated spillway because the gated spillway can be regulated by the gates rather than the height of the dam itself. On the other hand, a gated spillway requires human operation and maintenance, and the crest of a gated spillway requires more release capacity. Therefore, designing a gated or ungated spillway involves consideration of many factors, such as local topography, geological conditions, and climatic and meteorological conditions. In addition, economic conditions need to be considered as well.

Based on the importance of spillway research, many studies have been conducted on this topic. In the past, most of the research has been focused on experimental models, which were used to obtain results used to determine the hydraulic properties of spillways and to propose empirical formulas. In recent decades, numerical models have evolved rapidly, and many of them can produce satisfactory results and save significant time while being cost-efficient. However, the study of numerical models still needs to be constantly compared with experimental models to ensure accuracy.

Figure 1-2 Gated spillway (The Greenville News, 2016)

1.2 Objectives of the study

The principal objective of this project is to examine the hydraulic characteristics of the ogee spillway under the high head ratio, including velocity distribution, pressure, and water surface profile.

First, this study included both experimental and numerical models. The results of the experimental models are compared with those of the numerical models in order to calibrate and validate the latter. This research also aims to demonstrating that a numerical model can be used as a complementary tool to the physical model to provide various hydraulic properties on the ogee spillway.

Secondly, this study aims to investigate the velocity distribution and water surface profile experimentally and numerically under gated and ungated spillways, as well as to evaluate their characteristics and difference.

Furthermore, this study aims to investigate the hydraulic characteristics of the ungated spillway for high head ratios and compare them with results from previous studies to demonstrate their accuracy.

Finally, this study evaluates the accuracy of the results of several turbulence models used in combination with the Reynolds-Averaged Navier-Stokes (RANS) equations and discusses which turbulence model is more suitable for the problem investigated.

1.3 Scope

This research mainly concentrates on the numerical and experimental modeling of the spillway with gates and the high head ratio of the spillway without gates. Given the constraints of experimental conditions and time, the present study has the following limitations:

- Only a vertical plane gated spillway was considered in this study, while other types of gate spillways, such as radial gates, were not studied.
- Due to the limitation of the maximum achievable water level of the experimental flume in the Tilting Flume of the Hydraulic Lab at the University of Ottawa, the experiment on the high head ratio of the ungated spillway could only measure the relative head up to a value of 4.5.

- Due to the limitations of the velocity measurement instrument (Vectrino Profiler), the upstream velocity distribution could only be measured 5 cm above the bottom and 10 cm below the water level. Moreover, since the point at 12cm height is a weak spot, the nearby 1~2cm points cannot be measured accurately.
- The velocity distribution experiment was only investigated upstream of the ogee spillway, and it did not consider the velocity and pressure distribution at the spillway crest nor on the downstream chute.
- There are several numerical models available to simulate flow over spillways. This research only employed the RANS turbulence models of OpenFOAM. LES (Large Eddy Simulation) and DES (Detached Eddy Simulation) models were not considered.
- This study only used structured (regular) grids. Unstructured grids, which could be used for more complex discretization schemes, were not considered.
- To save computational costs, the numerical models in this study are 2 dimensions vertically (2DV) models. The application of 3D models is required to be researched for future work.

1.4 Novelty and contributions

There are two main elements of novelty in this study as follows:

First, this study investigates the high head ratio ungated spillways by using both experimental tests and numerical models. High head ratios are an essential and a deserving topic for further research because they are efficient and, therefore, important for the design of spillways. In recent years, due to changes in climate, many completed spillways have experienced heads that were actually much higher than their original design ones. Most experiments in the past have studied the hydraulic characteristics of spillways with low head ratios, while studies on actual heads much higher than the design heads are inadequate. A significant innovation of this study is to investigate the hydraulic characteristics of spillways with high head ratios through experiments and numerical models to complement this knowledge gap.

The second innovation of this study is the investigation of the hydraulic characteristics of the gated spillway using experimental and numerical models. There are few studies on using vertical plane gates on ogee spillways. This study is the first one that performs a comprehensive investigation of vertical plane gated spillways both experimentally and numerically. The physical

and numerical models are combined to investigate hydraulics properties, such as the velocity distribution of the gated spillway, and compare these characteristics of the gated spillway with those of the ungated spillway at the same inlet discharge to examine the improvement of one over the other.

Concluding, this study provides experimental and numerical modeling insight for the case of high-head ratio ogee spillways. Moreover, this study contributes to the research of gated spillways with vertical plane gates by providing experimental data results and numerical model development. With improvements in mind, the numerical models investigated in this study will hopefully be used for other gated and ungated spillways studies.

1.5 Thesis outline

Chapter 1 covers the introduction aspects related to this work. It includes the background of the research problem at hand, the objectives of the study, its scope, the novelty elements, and contributions, as well as the outline of the thesis.

Chapter 2 provides a detailed literature review that includes four parts. First, it examines the hydraulic properties of the ogee spillways, such as the spillways profiles, discharge, pressure, and hydraulic head ratio. Secondly, it presents research from previous experimental models and some conclusions regarding different flow conditions. Thirdly, it reviews some advanced numerical models in spillway studies. Last but not least, a literature review Discussion is presented.

Chapter 3 consists of the technical paper. The outline of the paper contains the introduction, methodology, results, discussion, and conclusions. The methodology covers the design of the experimental model, the governing equations of the numerical model, the turbulence models used, and other features of the numerical model. Experimental and numerical models of the ungated and gated spillways are compared and discussed. First, the results of the experiment and the numerical model are compared to verify the accuracy of the numerical model. Secondly, the hydraulic characteristics of the gated and ungated spillways are compared to examine the improvement of the hydraulic characteristics of the gated spillway for the same inlet discharge. Finally, general conclusions are drawn based on comparing the results.

Chapter 4 outlines the conclusions and provides recommendations for future work.

Chapter 2 Literature Review

In this literature review, previous studies on spillways and related empirical formulations are presented and discussed. First, this review will describe the hydraulic properties of the spillway, such as ogee spillway profile, discharge, and pressure. Secondly, this review will present previous significant experimental models and some of their conclusions. Thirdly, this review will present some advanced numerical models used in spillway performance research, and finally, a discussion will be presented. The main objectives of the literature review are to (1) provide detailed background on the design of the types of spillways investigated; (2) present previous research on experimental testing and numerical models of spillways that have been surveyed to establish a methodology for this study.

2.1. Spillway hydraulic characteristics

2.1.1 Ogee spillway profile

The Ogee spillway profile contains four parts: the vertical reservoir wall, upstream crest curve, crest power-law arc, and chute tangent line.

The design of the ogee spillway crest profile relates to the efficiency of spillway discharge ability as well as economic benefit, which is crucial. Besides, since minor deviations in the radius of curvature are likely to result in considerable local pressure peaks, it stands to reason that the smoothness of the spillway bottom geometry may greatly determine the pressure distribution at the bottom of the spillway (Hager, 1987).

An ideal crest shape that can provide the perfect discharge ability is similar to the profile of the undernappe of a jet flowing over a sharp-crested weir (*Design of Small Dams*, 1987). All the quantities of the spillway crest are determined by the design head Hd (Hager, 1987).

In the upstream quadrant, the arcs of the circle are decided by the following equations, where x represents the flow direction and z represents the upward direction in the Cartesian coordinates system. (Imanian & Mohammadian, 2019):

$$\left(\frac{x}{H_d}+0.2418\right)^2+\left(\frac{z}{H_d}+0.1360\right)^2=(0.04)^2$$

$$-0.2818\le\frac{x}{H_d}\le-0.2760 \qquad (1.)$$

$$\left(\frac{x}{H_d}+0.1050\right)^2+\left(\frac{z}{H_d}+0.2190\right)^2=(0.2)^2$$

$$-0.276\le\frac{x}{H_d}\le-0.175 \quad (2.)$$

$$\left(\frac{x}{H_d}\right)^2+\left(\frac{z}{H_d}+0.5000\right)^2=(0.50)^2$$

$$-0.175\le\frac{x}{H_d}\le 0 \quad (3.)$$

The following equation can decide the downstream section (Imanian & Mohammadian, 2019):

$$\frac{z}{H_d}=-0.5\left(\frac{x}{H_d}\right)^{1.85} \quad (4.)$$

2.1.2 Discharge characteristics

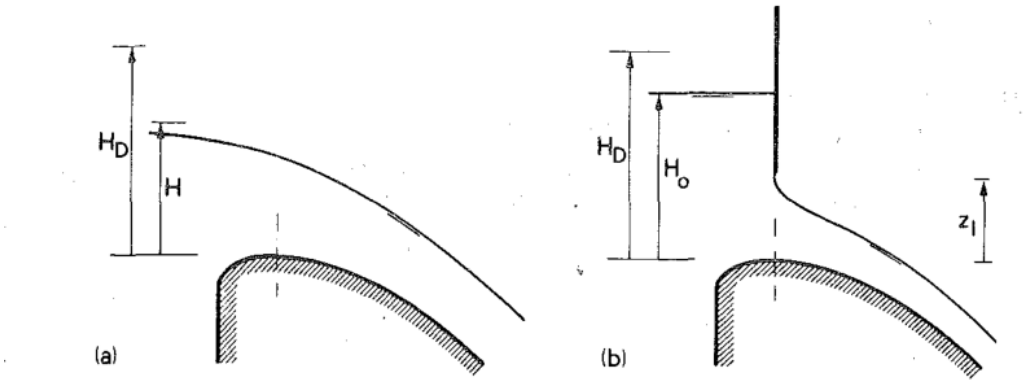

Figure 2-1 Schematical flow configuration for flow: (a) Ungated Flow; (b) Gated Spillway Flow (Hager & Bremen, 1988)

The determining factors of discharge are different between ungated spillways and gated spillways, and the critical geometric elements of the two types of spillways are shown in Figure 2-1.

For ungated spillway flow, a highly influential factor is the discharge coefficient C_d. C_d depends on the relative head $\chi=\frac{H}{H_D}$, which means the actual head on the spillway divided by the design head of the spillway (Hager & Bremen, 1988).

The ungated spillway discharge equation is outlined as follows (Hager & Bremen, 1988):

$$Q=C_d b(2gH^3)^{\frac{1}{2}} \quad (5.)$$

In the equation, C_d means discharge coefficient, H means the actual head on the spillway, and b means the spillway width (Hager & Bremen, 1988).

For gated spillways, the discharge characteristics are related to the design head H_D, the actual head H_0, and relative gate opening Z_l, which is the gate opening z_l divided by the design head H_D. According to Hager & Bremen (1988), the discharge Q_g over a gated standard spillway is related as follows:

$$Q_g = C_{dD} b (2g H_0^3)^{\frac{1}{2}} \left[1 - \left(1 - \frac{Z_l}{\chi_0}\right)^{\frac{3}{2}}\right] \left[\frac{1}{6} + Z_l\right]^{\frac{1}{9}} \quad (6.)$$

In this equation, $\chi_0 = \frac{H_0}{H_D}$, $C_{dD} = 0.495$, and $C_{dD} b (2g H_0^3)^{1/2}$ means the design discharge Q_D.

Hager & Bremen (1988) proposed a generalized discharge-head diagram to describe the relation of discharge and head for both gated spillways and ungated spillways, which is presented in Figure 2-2.

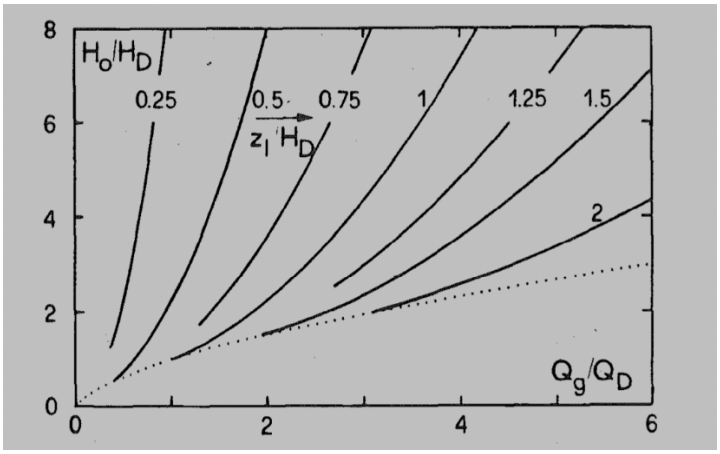

Figure 2-2 Generalized discharge-head relation for gated standard spillway; (...)=ungated spillway (Hager & Bremen, 1988)

2.1.3 Pressure

The pressure distribution over the spillway crest is highly relative to the actual head over spillways, and the minimum bottom pressure is influenced by the relative head (Hager, 1991). According to Hager (1991), the pressure over the spillway crest can be defined as follows:

$$\bar{P}_c = \frac{\Delta p_c}{\rho g H} \quad (7.)$$

For different spillway downstream slopes, the pressure distribution is different. Hager (1991) concluded that when the relative head is larger than one, the negative pressure zone occurs at the 45° spillway's crest. For the 30° spillway geometry, the minimum bottom pressure exists at the end of the upstream spillway when the relative head is large (Hager, 1991).

Hager (1991) also proposed an equation to describe the minimum crest pressure:

$$\bar{P}_{min} = \frac{\Delta p_{min}}{\rho g H} = \gamma(1 - \chi) \qquad (8.)$$

In which

$\gamma = 1.0$ for WES design and the 45° spillways geometry,

$\gamma = 0.9$ for the 30° spillways geometry,

$\chi = \frac{H}{H_D}$, which is the relative head or head ratio.

According to Khatsuria (2005), the increase in the crest velocity of the spillway is accompanied by a decrease in pressure. Likewise, when the actual head of the spillway is greater than the design head (head ratio increases), the discharge coefficient increases, and the pressure at the crest of the spillway drops. Figures 2-3 and 2-4 show that when the head ratio gradually increases to a greater value, the discharge coefficient sharply falls because the flow separates from the spillway surface and produces changes in the pressure area (Imanian & Mohammadian, 2019).

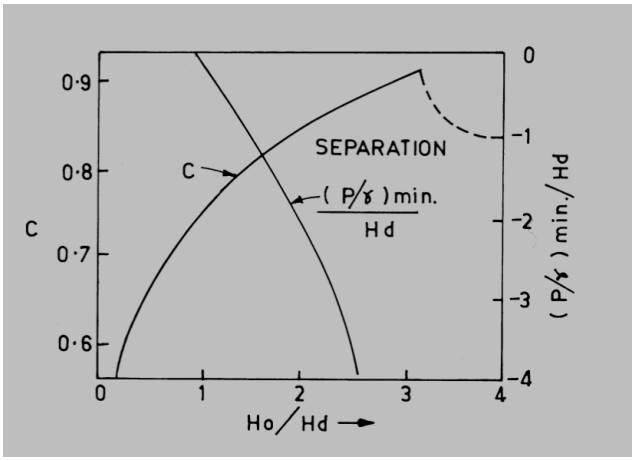

Figure 2-3 Discharge coefficient versus crest pressures (Khatsuria, 2005).

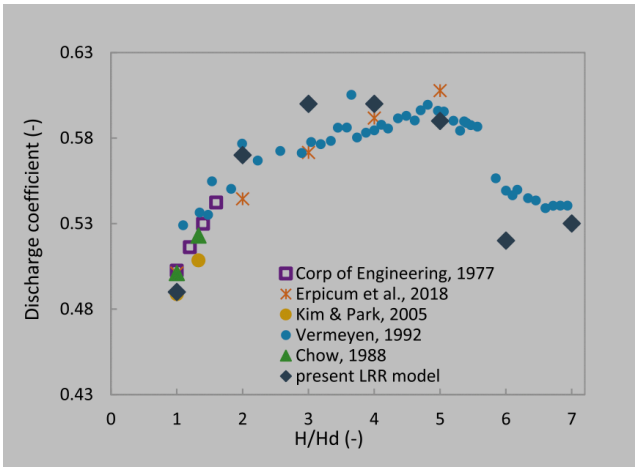

Figure 2-4 Discharge coefficient versus head ratio (results of LRR model) (Imanian & Mohammadian, 2019).

For the design of the spillway's energy dissipator, the dynamic pressure is an essential parameter. Aghaei et al. (2022) proposed two equations to calculate the bottom pressure and the maximum pressure in the curve of the flip bucket, which is the energy dissipation structure at the end of the spillways' bottom.

The general equation for bottom pressure can be defined as follows (Aghaei et al., 2022):

$$\frac{P_{\text{bottom}}}{\rho v_0^2} = 5.7\left(\frac{R}{h_0}\right)^{-0.58}(\tan\ \beta)^{-0.02}\left(\frac{1}{Fr_0^2}\right)^{0.604}(\tan\ \theta)^{0.046}(\tan\alpha)^{0.207} \quad (9.)$$

The maximum pressure equation can be described as follows (Aghaei et al., 2022):

$$\frac{P_{max}}{\rho v_0^2} = 7.9\left(\frac{R}{h_0}\right)^{-0.61}(\tan\ \beta)^{-0.1}\left(\frac{1}{Fr_0^2}\right)^{0.578}(\tan\ \theta)^{0.151}(\tan\alpha)^{0.34} \quad (10.)$$

In which α = chute slope angle

β = deflection angle

θ = takeoff angle

$\frac{R}{h_0}$ = relative curvature of the flip bucket

Fr_0 = Froude number

Another important phenomenon related to pressure is called cavitation. Cavitation is the static pressure altering from the liquid to the vapor state by reducing the local pressure while maintaining the temperature constant (Falvey, 1990). Cavitation can be caused by turbulence or vortices in the flowing water, creating bubbles or voids in the liquid. When the cavitation bubbles reach a place of high local pressure with the flow, the bubbles will collapse, thus creating cavitation damage to the hydraulic structures (Khatsuria, 2005).

According to Falvey (1990), cavitation damage can be predicted by considering the cavitation index, the flow velocity, the surface construction material, and the exposure time. The damage potential can be expressed as follows:

$$D_p \propto \left(\frac{1}{\sigma_s}\right)\left(\frac{\sigma_s}{\sigma_f} - 1\right)\left(\frac{V}{V_r}\right)^6 \quad (11.)$$

In this relation, D_p is damage potential, σ_s is cavitation index for the initiation of damage, σ_f is the cavitation index for the flow, V_r is the reference velocity, and V is flow velocity (Khatsuria, 2005).

According to Falvey (1990), the damage severity can be defined by the damage index D_i, which can be expressed as follow:

$$D_i = D_p \ln(t - t_o) \quad (12.)$$

$$t_o = t_c - e^{\left(\frac{D_i}{D_p}\right)} \quad (13.)$$

In which t_c is the cumulative time of operation.

2.1.4 Water surface profile

Hager (1991) proposed a linear equation to express the free water surface profile of the spillway, and it can be seen as follows:

$$S = 0 \cdot 75\left[\chi^{1\cdot1} - \left(\frac{1}{6}\right)X\right], -2 < X < +2 \quad (14.)$$

In which $X = \frac{x}{H_D}, x =$ horizontal coordinate, χ is the relative head, $S = \frac{s}{H_D}$. And when $x < 0$, on the upstream side of the spillway crest, s is the vertical water depth over the crest. When $x \geq 0$,

s is the vertical flow depth above the bottom (Hager, 1991). It can be concluded that the water surface profile is influenced by the relative head and the $\frac{x}{H_D}$.

2.1.5 Hydraulic head ratio

The hydraulic characteristics of the ogee spillways are highly dependent on the hydraulic head ratio, which is the ratio of the actual head to the design head. Most previous studies focused on the low hydraulic head ratio, and few considered the situation when the actual head is much larger than the design head.

According to Peltier et al. (2018), the high head ratio of spillways needs to be investigated more since the completed spillways may encounter extreme climate changes, which cause the actual heads to be significantly higher than their original design head.

Peltier et al. (2018) measured the velocity fields near the ogee spillways and the relative pressure along the spillways in the high head ratio from one to five. Imanian & Mohammadian (2019) proposed and evaluated numerical models to investigate the velocity and pressure fields over ogee spillways under the high head ratio, ranging from one to seven. It can be seen that recently the high hydraulic head ratio situation of the ogee spillways has attracted the attention of academics but still needs to be further studied.

2.2. Physical models of spillways

Building a successful physical model is complex and most important in the research of spillways since most of the empirical formulas for spillways are derived from experimental results from physical models, and physical models are the basis of all numerical models. To clearly perform the literature review of the physical models, this part will discuss the physical models in the free flow, the gated flow, the orifice flow, and the submergence flow conditions, respectively.

2.2.1 Free flow

Hager (1991) compared the three-arc crest shape spillway with the continuous upstream quadrant crest shape and found that the continuous upstream quadrant geometry had a better hydraulic performance. Hager & Bremen (1988) experimented with gated and ungated spillways and plotted the relation of discharge coefficient versus hydraulic head ratio for the ungated spillway in the free flow condition, which can be seen as follows.

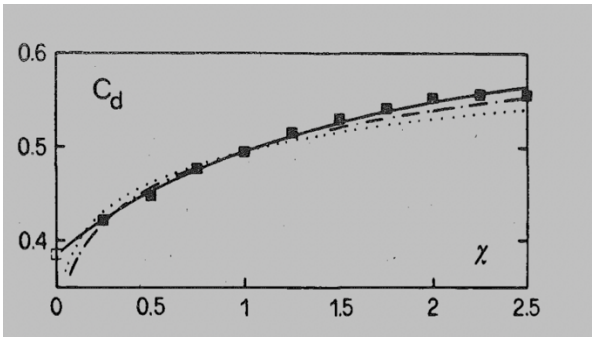

Figure 2-5 Discharge coefficient Cd as a function of the relative head for ungated spillway flow (Hager & Bremen, 1988)

Peltier et al. (2018) built two physical models to investigate the relative pressure and velocity over the crest of ogee spillways under the high hydraulic head ratios. To obtain accurate experimental results, they applied the Large Scale Particle Image Velocimetry (LSPIV) to measure the velocity field and used pressure sensors to measure the relative pressure along the ogee spillways.

Bernoulli's equation can be used to describe the relationship between pressure and velocity, which can be seen as follows:

$$\frac{P_{rel}(x,z)}{\rho g} = H - z - \frac{u^2(x,z) + w^2(x,z)}{2g} = H - z - \frac{v^2}{2g} \qquad (15.)$$

In which H is the upstream head, u(x, z) and w(x, z) are the longitudinal and vertical components of the local velocity, respectively, v is the norm of the velocity, ρ is the volume mass of water, and g is the gravity acceleration (Peltier et al., 2018).

Figure 2-6 compares velocity fields in the W1 and W2 setups. W1 and W2 are different in the design head, where the W1 is 0.15 m, and W2 is 0.1 m. The different setups aim to determine scale effects in the velocity field and the relative pressure zone (Peltier et al., 2018).

Figure 2-6 and Figure 2-7 present the velocity fields when the head ratio is 5. The velocity measurement results show that the scaled-velocity distributions of two different scale models have minor differences, which proves that in the velocity fields, the scale effect can be negligible (Peltier et al., 2018). Besides, Figure 2-7 indicates that when the velocity section is close to the

spillways, the velocity profile will increase slightly, which can be explained by the acceleration effect when it is close to the spillways (Peltier et al., 2018).

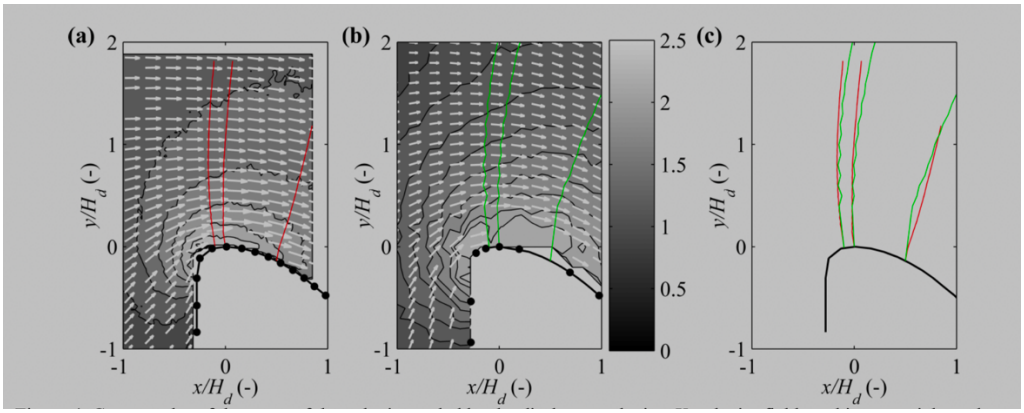

Figure 2-6 Contour plot of the norm of the velocity scaled by the discharge velocity, V, velocity fields, and isopotentials evaluated at three positions along the spillway (Black points = location of the pressure sensors). (a) W1, H/Hd = 5. (b) W2, H/Hd = 5. (c) (Peltier et al., 2018)

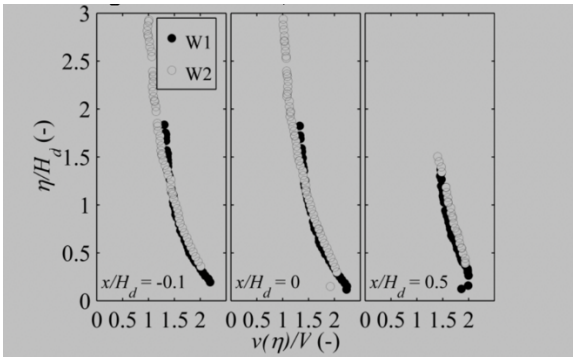

Figure 2-7 Distribution along the isopotentials displayed in Figure 8 of the velocity v(η) normalized by the discharge velocity V (Peltier et al., 2018).

Peltier et al. (2018) stated that the relative pressure over the crest decreases with the increase of the head ratio. It can be seen from Figure 2-8 that the relative pressure of the W1 setup is smaller than the W2 setup when the head ratio is higher than three. Peltier et al. (2018) stated that this phenomenon could be explained by the presence of the scale effect when the head ratio is up to three, or perhaps attributed to the different sizes of pressure sensors which are decided by the different sizes of spillways.

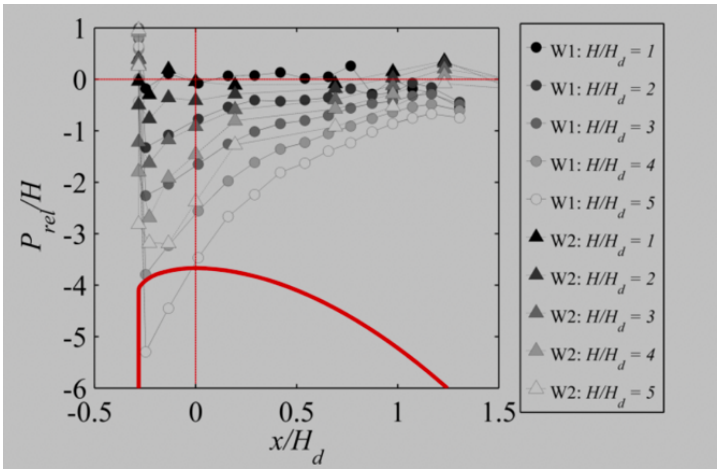

Figure 2-8 Relative pressure along the spillway crest (Peltier et al., 2018)

Karim & Mohammed (2020) employed a hybrid model, including a physical and numerical model, to examine the mean and vertical velocity profile over the ogee spillway crest. In the experimental model, Karim & Mohammed (2020) applied Particle Image Velocimetry (PIV) camera to obtain the velocity distribution measurement and used MATLAB to process the data.

2.2.2 Gated flow

As previously discussed, Hager & Bremen (1988) experimented with the vertical plane gate and proposed a discharge equation for the gated spillways based on a semi-empirical approach. And they also illustrated a generalized discharge and head relation for gated and ungated spillways. The gated spillway flow under a plane vertical gate can be seen in Figure 2-9 and it can be seen that for the gated spillway, the relative opening of the gate contributes significantly to the flow pattern (Hager & Bremen, 1988).

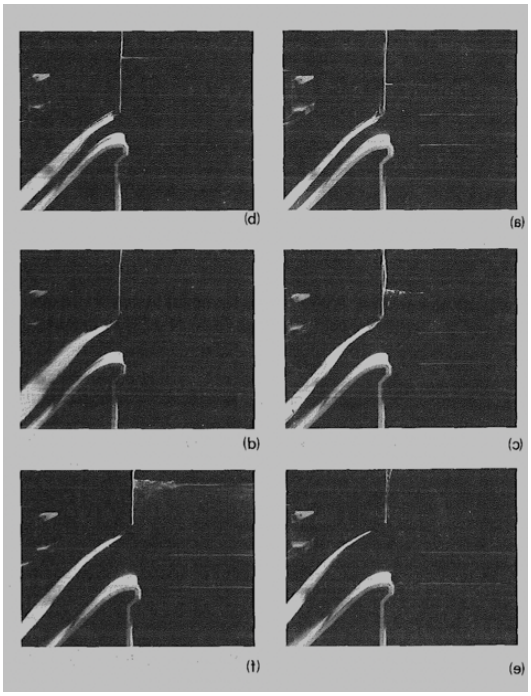

Figure 2-9 Patterns of Gated Spillway Flow: (a) Z_l = 1, χ= 1.5; (b) Z_l = 1, χ = 1.75; (C) Z_l = 1.5, χ = 2;(d) Z_l = 1.5, χ = 2.5;(e) Z_l = 2, χ = 2.5;(f) Z_l = 2, χ = 2.75 (Hager & Bremen, 1988)

Based on the Tennessee Valley Authority (TVA) models, Schohl (2016) investigated the discharge correlations and the submergence flow effect for radial gated spillways.

According to Schohl (2016), the general discharge equation for the free flow of TVA or other similar models can be defined as a weir-type equation:

$$Q_f = S_f C_f L_c H_c^{\frac{3}{2}} \qquad (16.)$$

Where S_f is the tailwater submergence factor, which can be obtained from Figure 2-13. C_f is the discharge coefficient, H_c is the actual head over the flow crest, and L_c is the width of the spillway bay. All the spillway geometry and the hydraulics parameters are described in Figure 2-10.

For gated flow, the discharge equation depends on the relation between the value of the tailwater submergence *d* and the transition value of tailwater submergence d_1. Schohl (2016) stated that when *d* is smaller than d_1, the gated discharge can be calculated using the following formula:

$$Q_{g1} = C_{g1} S_{g1} G L_c \sqrt{2g\left(H_c - H_{mp}\right)} \qquad (17.)$$

In which G is the gate opening. C_{g1} is the discharge coefficient, which can be seen in Figure 2-11. S_{g1} is the tailwater submergence factor and the Sg1 value for two different spillways are plotted in Figure 2-14. H_{mp} is the elevation of the midpoint of gate opening minus the crest elevation (Schohl, 2016).

When d is larger than d_1, Schohl (2016) explained that the tailwater submergence effects will have an influence on the gated discharge, and the discharge need to use the following equation to calculate:

$$Q_{g2} = C_{g2} G L_c \sqrt{2g(H_c - d)} \qquad (18.)$$

In which the C_{g2} is the discharge coefficient which can be obtained from Figure 2-12.

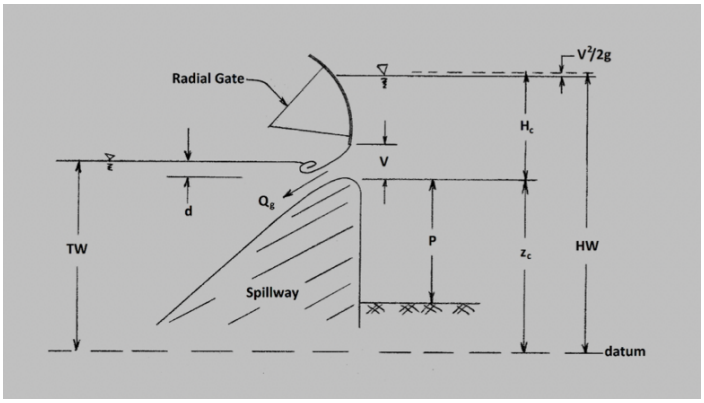

Figure 2-10 Gated Discharge under Spillway Gate (Schohl, 2016)

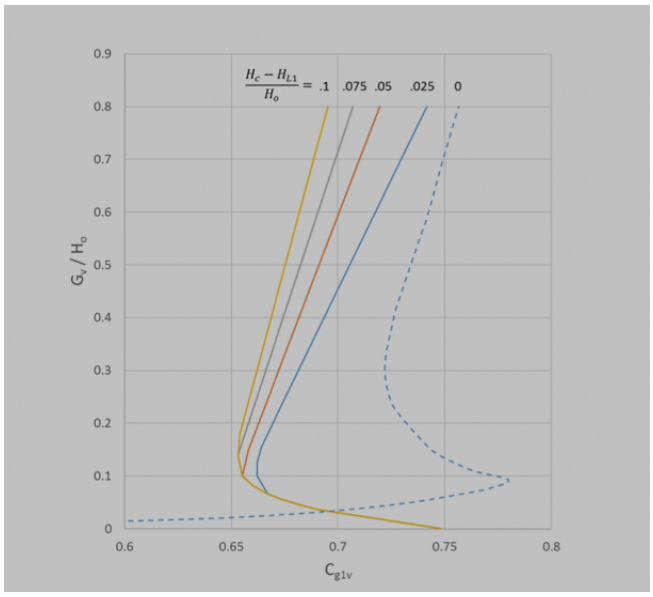

Figure 2-11 General Correlation for Discharge Coefficient, C_{g1v} (Schohl, 2016)

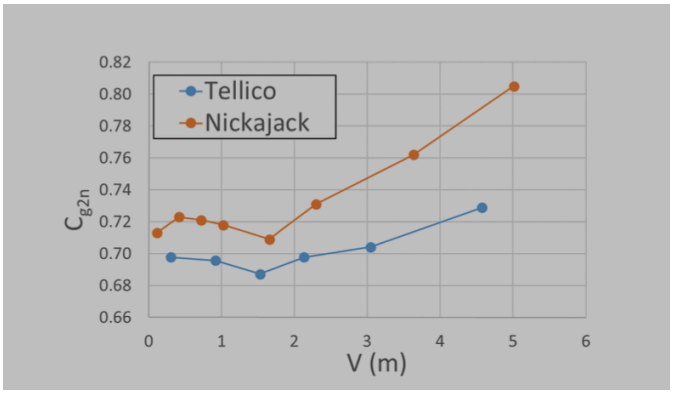

Figure 2-12 Variation of C_{g2n} with gate opening V (Schohl, 2016)

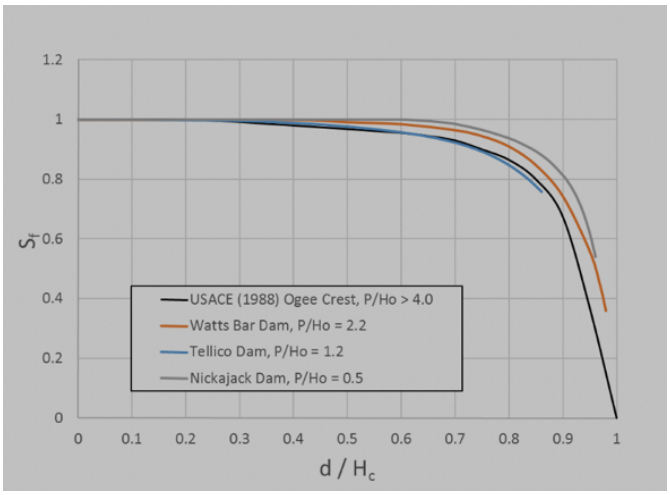

Figure 2-13 Submergence Factor Relationships (Schohl, 2016)

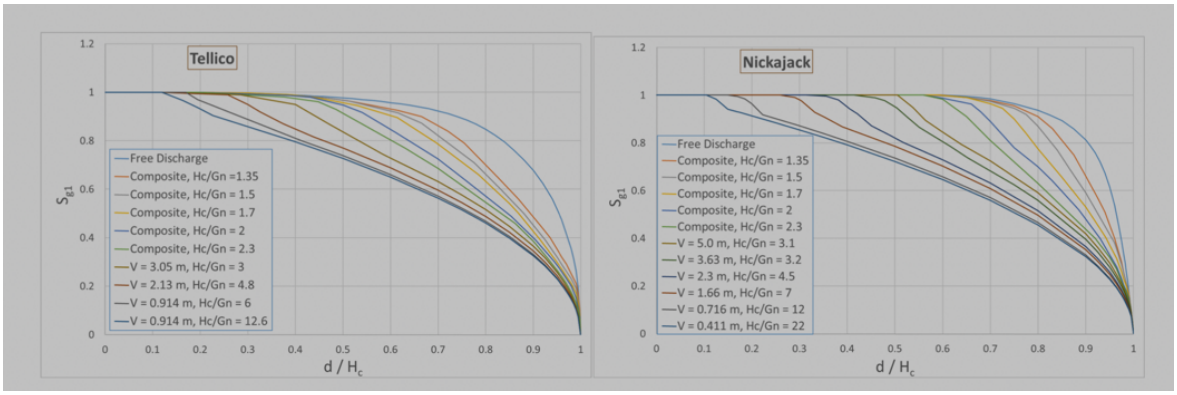

Figure 2-14 *S_{g1} for Tellico and Nickajack Spillways (Schohl, 2016)*

2.2.3 Orifice flow

For orifice flow conditions, Mazumdar & Roy (1997) prototyped Salal Dam Spillway to experiment with radial gate and to verify the accuracy of two gated spillways discharge equations.

U.S.B.R. equation for gated spillway:

$$Q = C\sqrt{2g}L[H_1^{1.5} - H_2^{1.5}] \quad (19.)$$

In which C=coefficient of discharge from U.S.B.R. curves, L=effective length of the spillway, H_1=head over the crest in m, H_2=head over the bottom of gate in m.

Sinniger's formula for gated spillway:

$$Q_s = C_{dg}b(GH_d)\sqrt{2gH_e} \quad (20.)$$

Q_s=discharge (Sinniger's formula), C_{dg}=Sinniger's discharge coefficient, b=width of a single bay, H_e=actual energy head, H_d=design head, g=gravitational acceleration, G= gate opening.

According to Mazumdar & Roy (1997), the discharge calculation of orifice flow is determined by the gate seat location. When the gate seat is downstream of the crest, the discharge should be calculated by Sinniger's equation. On the other hand, the discharge should be computed by the USBR equation.

Mazumdar & Roy (1997) found that the errors of two equations increase when the gate opening and hydraulic head drop, which is caused by the suction effect and pressure distribution changes. To modify the formulas, they proposed a pressure correction factor, which is related to the gate opening and hydraulic head ratio.

Pressure correction factor (C_p) is obtained from the following equation:

$$C_p = \left(\frac{H}{H_D}\right)^a \left(\frac{G}{H_D}\right)^b \tag{21.}$$

In which $C_p=Q_{measured}/Q_{computed}$ and a, b are constants. In Sinniger equation, a=-0.0157, b=-0.121249. In USBR equations, a=-0.01087, b=-0.158909 (Mazumdar & Roy, 1997). The errors were reduced by applying the C_p values and correcting the computed discharge. It should be mentioned here that when the free flow suddenly converts to orifice flow, a transient zone occurs (Mazumdar & Roy, 1997).

Orifice spillways are commonly used for irrigation and hydropower purposes. The breast wall spillway is a type of orifice spillway which has been less studied. Nguyen et al. (2015) conducted an experiment to examine the mean pressure distribution as well as the discharge capacity of the breast wall spillway.

Many hydraulic factors determine the discharge capacity of the breast wall spillway. The general discharge capacity of a spillway with a breast wall can be defined as (Nguyen et al., 2015):

$$Q = VA = C_{od} A \sqrt{2gZ_o} = \frac{bD}{\sqrt{\alpha\left(1 + f\frac{L_h}{D_h} + \sum K\right)}} \cdot \sqrt{2g\left[H_o - \frac{\int_0^D \left(z + \frac{p}{\gamma}\right) \mathrm{d}z}{D}\right]} \tag{22.}$$

In which, H_0= total head, D= the orifice opening, $\frac{p}{\gamma}$ = the mean pressure distribution, C_{od} = discharge coefficient, $A = bD$ which is the area of the orifice corresponding to the orifice opening.

From this general formula, Nguyen et al. (2015) concluded that the mean pressure distribution is essential to the discharge calculation. A schematic of the experimental setup, which aims to study the mean distribution and the discharge capacity, can be seen in Figure 2-15.

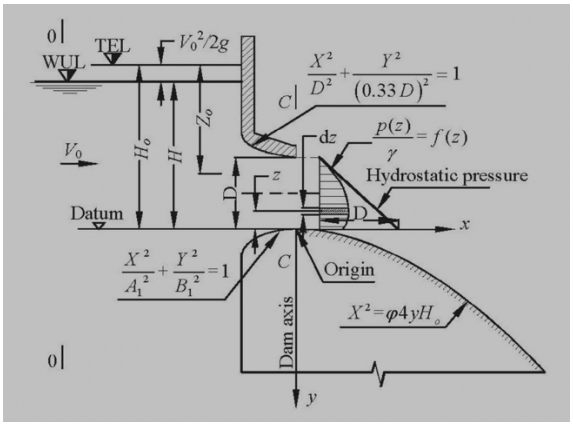

Figure 2-15 The scheme to determine the discharge capacity and the mean pressure distribution at the outlet section of the free breast wall spillway (Nguyen et al., 2015)

Nguyen et al. (2015) concluded that the mean vertical pressure distribution depends on the orifice opening, the outlet discharge, and the total head H_0.

Predicting the water head effect Z0 of the flow through the breast wall spillway is necessary to calculate the discharge. Z_0 is a function that involves the mean vertical pressure distribution. Nguyen et al. (2015) applied the regression analysis method to propose an equation to calculate the water head effect Z_0, which can be seen as follows:

$$\frac{Z_o}{H_o} = 1.0688 - 0.7455\frac{D}{H_o} - 0.0592\frac{H_d}{H_o} - 0.0273\frac{P_s}{H_o} \qquad (23.)$$

In which, H_d = design head, D = orifice opening, H_o = total head, P_s = the spillway height.

From this proposed equation, it can be easily seen that the orifice opening plays the most prominent role in determining the water head effect. In contrast, the design head and the spillway height show minor importance (Nguyen et al., 2015).

Exerting the multi-linear regression and the least squares method, Nguyen et al. (2015) proposed an accurate discharge formula for the breast wall spillways as:

$$\mathrm{Q} = C_Z C_{od} A\sqrt{2gH_0} \tag{24.}$$

$$C_Z = \sqrt{1.0688 - 0.7455\frac{D}{H_o} - 0.0592\frac{H_d}{H_o} - 0.0273\frac{P_s}{H_o}} = \sqrt{\frac{Z_0}{H_0}} \tag{25.}$$

C_z is the proposed water head effect coefficient, which can be used to demonstrate that the mean pressure distribution can influence the discharge capacity (Nguyen et al., 2015).

2.2.4 Submergence flow

The submerged weir flow is a challenging topic to study. Villemonte (1947) proposed a reduction factor for the free weir equation as follows:

$$Q = \frac{2}{3} C_{dfw} L\sqrt{2g} H^{\frac{3}{2}} \cdot \mathrm{S_c} \tag{26.}$$

$$S_c = k\left[1 - \left(\frac{h}{H}\right)^{1.5}\right]^{\mathrm{m}} \tag{27.}$$

In which C_{dfw} = the free-weir discharge coefficient, S_c = reduction factor or submergence coefficient.

Wu & Rajaratnam (1996) proposed another reduction factor to the same free weir equation:

$$S_c = 1.0 + 1.162\left(\frac{h}{H}\right) - 1.331\sin^{-1}\left(\frac{h}{H}\right) \tag{28.}$$

For the ogee gated spillway, Ansar & Gonzalez-Castro (2003) used an Acoustic Doppler Current Profiler (ADCP) to conduct experiments and applied dimensional analysis to propose an equation for the submerged weir flow condition, which can be seen as:

$$\frac{y_c}{h} = a\left(\frac{h}{H}\right)^b \tag{29.}$$

Where a and b are constants that need to be determined from experiments. y_c is the critical depth over the still crest. The prototype gated spillways can be seen in Figure 2-16. According to Ansar & Gonzalez-Castro (2003), when the submergence depth is less than 20% of the current

hydraulic head depth, the gates of the spillway exert little effect on the flow of the submerged weir.

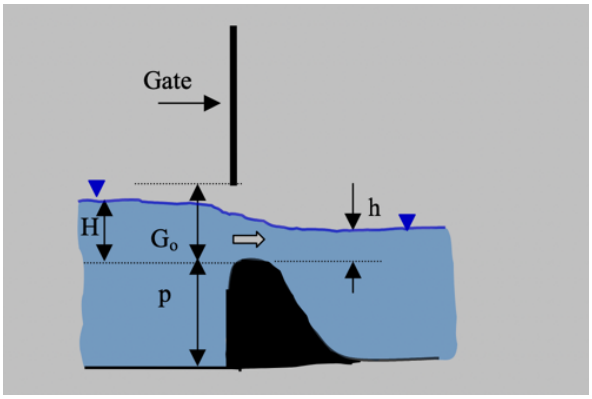

Figure 2-16 Submerged weir flow at prototype gated spillways (Ansar & Gonzalez-Castro, 2003)

2.3. Numerical models of spillways

Empirical design formulas for spillways have been obtained based on experimental tests. These formulas usually have their particular case/ limitations to be applied. To develop these formulas, numerous experiments are required. After the trial-and-error process, the final design and formulas can be developed. This traditional modeling method is useful and classic, but it will cost a lot of time and reduce working efficiency. In addition, physical modeling needs construction resources, which will cost a lot. To improve the modeling from various aspects such as required time, construction resources, and the analysis of the results, numerical modeling is typically applied. (Salazar et al., 2013). It should be noted that 3D numerical codes can be divided into two categories: (1) the Lagrangian approach and meshless techniques, such as the particle finite element method (PFEM) (Saunders et al., 2014); (2) the Eulerian approach, such as the finite element method (Salazar et al., 2013) and (3) the Finite Volume Method (Bhajantri et al., 2007).

2.3.1 Numerical models based on the Lagrangian approach

Saunders et al. (2014) investigated a particle-based method, Smoothed Particle Hydrodynamics (SPH), to simulate the flow characteristics near gated spillways and examined the ski jump further downstream by comparing them with the physical model results. According to Saunders et al. (2014), compared with the grid-based model, the SPH model is more capable of detecting splashing and flowing debris. Unlike the mesh-based model, the particle-based model uses particles to denote the volume of a liquid, and each particle is composed of the properties of mass, density, velocity, and position (Saunders et al., 2014). Figure 2-17 shows the simulation of spillway flow, the velocity magnitude, as well as the ski jump.

Equation 30 is the continuity equation of the SPH method, where W_{ab} is the interpolation kernel, ρ_a is the density of particle a, m_b is the mass of particle b, v_a and v_b are the velocity of particles a and b (Saunders et al., 2014).

$$\frac{d\rho_a}{dt} = \sum_b m_b(v_a - v_b)\nabla W_{ab} \qquad (30.)$$

Equation 31 is the momentum equation of particle motion, where the P and μ are the pressure and viscosity of particles, $\mathbf{r}_{ab}$ is the position distance between particle a and b, $\mathbf{v}_{ab}$ is the

difference in velocity between particles a and b, η is the smoothing parameter and ξ is viscous term parameter (Saunders et al., 2014).

$$\frac{d\mathbf{v}_a}{dt} = \mathbf{g} - \sum_b m_b \left[\left(\frac{P_b}{\rho_b^2} + \frac{P_a}{\rho_a^2} \right) - \frac{\xi}{\rho_a \rho_b} \frac{4\mu_a \mu_b}{(\mu_a + \mu_b)} \frac{\mathbf{v}_{ab} \mathbf{r}_{ab}}{\mathbf{r}_{ab}^2 + \eta^2} \right] \nabla_a W_{ab} \qquad (31.)$$

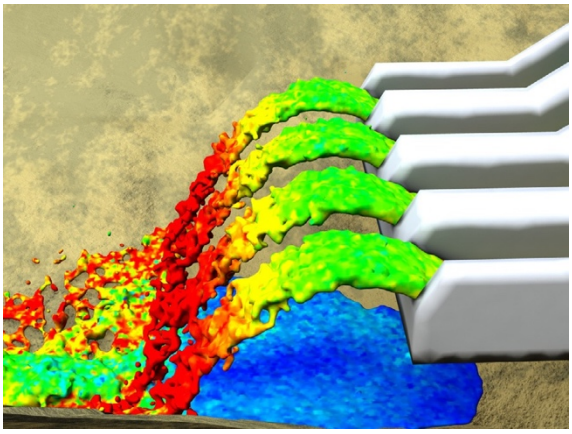

Figure 2-17 Visualisation of steady-state flow in side profile showing the trajectory of water off the ski-jump and point of impact of water on the terrain. The shading on the water surface represents speed, with blue being 0 m/s, green intermediate, and red being 2.5 m/s (Saunders et al., 2014).

Another meshless particle method, the weakly compressible moving particle semi-implicit (WC-MPS) method was applied to predict the flow characteristics such as water surface profile, velocity, and pressure over ogee spillways by Jafari-Nodoushan et al. (2016). According to Jafari-Nodoushan et al. (2016), the WC-MPS model can be employed in other kinds of spillways.

The governing equations for a weakly compressible flow can be described using Equation 32, where $\boldsymbol{u}$ is the velocity vector, t is time, ρ is the density of the fluid, p is the pressure, and $\boldsymbol{g}$ is the gravitational acceleration, $\boldsymbol{r}$ is the position vector, μ is the fluid viscosity (Shakibaeinia & Jin, 2009):

$$\begin{cases} \dfrac{1}{\rho}\dfrac{\mathrm{D}\rho}{\mathrm{D}t} + \nabla \cdot \boldsymbol{u} = 0 & \text{mass conservation} \\ \rho \dfrac{\mathrm{D}\boldsymbol{u}}{\mathrm{D}t} = -\nabla p + \mu \nabla^2 \boldsymbol{u} + \boldsymbol{g} & \text{momentum conservation} \\ p = f(\rho) & \text{equation of state} \\ \dfrac{\boldsymbol{Dr}}{\boldsymbol{Dt}} = \boldsymbol{u} & \text{lagrangian motion} \end{cases} \qquad (32.)$$

The positioning scheme of initial particles, including fluid particles, ghost particles, and wall particles, can be seen in Figure 2-18.

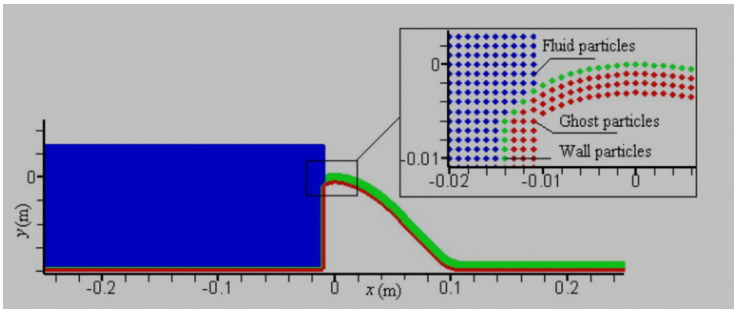

Figure 2-18 Initial position of particles for ogee spillway of Case I (fluid-type, ghost-type, and wall-type particles) (Jafari-Nodoushan et al., 2016)

2.3.2 Numerical models based on the Eulerian equation

Bhajantri et al. (2007) developed two numerical models based on the finite volume method (FVM). They used the weakly compressible flow equations to simulate hydraulic characteristics in terms of the weakly compressible flow, such as the velocity distribution, pressure distribution, and discharge coefficient.

According to Bhajantri et al. (2007), the weakly compressible flow can be solved by equations 33 and 34. Equation 33 is the continuity equation, in which ρ is the density of the fluid, $\vec{V}$ is the velocity vector, t is the time, a is the sound of speed, and p is pressure.

$$\frac{\partial p}{\partial t} + \rho_o a_o^2 \nabla \cdot \vec{V} = 0 \qquad (33.)$$

Equation 34 is the Euler equation which is used to present the equation of motion (Bhajantri et al., 2007).

$$\frac{\partial \vec{V}}{\partial t} + \vec{V} \cdot \nabla \vec{V} + \frac{1}{\rho_0} \nabla (p + g\rho_o y) = 0 \qquad (34.)$$

The governing equation for the Finite Volume Method can be seen as equation 35, in which G includes the flow variables, and F is the flux vector:

$$\frac{\partial G}{\partial t} + \nabla \cdot \vec{F} = 0 \qquad (35.)$$

Kazemzadeh-Parsi (2014) employed Smoothed Fixed Grid Finite Element method (SFGFEM) to solve the water surface simulation of radial gated spillways under free flow. According to Kazemzadeh-Parsi (2014), the SFGFEM is developed on the non-boundary-fitted meshes, which are a kind of unstructured mesh method. They applied SFGFEM to three gated hydraulic structures, and the results illustrated that the SFGFEM is applicable to the gated hydraulic structures in free surface flow problems. Figure 2-19 explains the intersection of non-boundary-fitted mesh and the free surface, containing three domains: internal, external, and boundary intersecting elements (Kazemzadeh-Parsi, 2014). Figure 2-20 shows the mesh solution of the gated spillway.

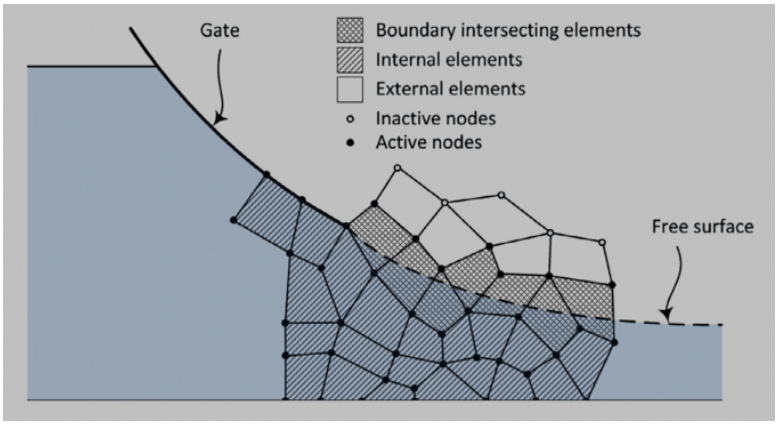

Figure 2-19 A schematic representation of a non-boundary-fitted mesh intersecting by the free surface (Kazemzadeh-Parsi, 2014).

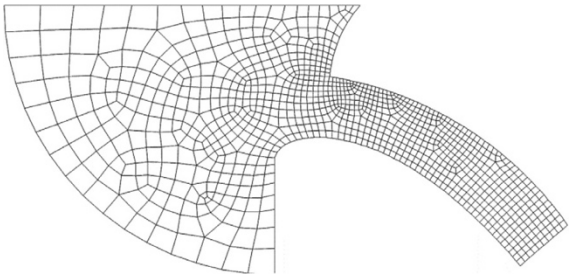

Figure 2-20 Non-boundary-fitted mesh used in the solution of the gated spillway (Kazemzadeh-Parsi, 2014).

Savage & Johnson (2001) applied FLOW-3D to solve the Reynolds-averaged Navier-Stokes (RANS) equations and compared the results with the physical model to investigate the discharge and pressure over ogee spillways. In FLOW-3D, they used Fractional Area/ Volume Obstacle Representation (FAVOR) method to develop the ogee spillway and implemented the Volume-of-Fluid (VOF) method to simulate the free surface (Savage & Johnson, 2001).

According to Savage & Johnson (2001), applying Reynolds Averaging can lessen the impact of rapid fluctuations. However, the fluctuations related to crest pressure problems still need to be solved by combining the physical and numerical models. They stated that the FLOW-3D using the finite volume method to solve the RANS equation could successfully simulate the discharge over the ogee spillway and the pressure on the tangent line. However, the problems in crest pressure and the flow transition from supercritical to subcritical still need to be further studied (Savage & Johnson, 2001).

Zawawi et al. (2018) analyzed the effect of gate opening area on water volume friction and the velocity upstream and downstream using the finite element model ANSYS. When the gate opening area increases, the discharge volume increases to cause a significant impact force of impact to the spillway and downstream. The impact risk poses damage to the downstream hydraulic structures. Therefore, in the practical flood control operation, the gate opening area needs to be operated with extra care to avoid dam failure (Zawawi et al., 2018).

Chatila & Tabbara (2004) employed the *k-ε* model through the finite element method software ADINA to solve the turbulent flow problems and simulate the free surface and flow field under different hydraulic head ratios over ogee spillways. The *k-ε* model is one of the RANS models, which applies the time-averaged method to solve turbulent flows. To obtain accurate results, Chatila & Tabbara (2004) considered the unstructured grid in the finite element model and compared the performance with laboratory measurements. The investigation indicated that the ADINA could predict the free surface profiles over ogee spillways with high accuracy. According to Chatila & Tabbara (2004), the ADINA can be considered in future research related to the prediction of the flow over stepped spillways and the energy dissipators application.

Morales et al. (2012) employed the standard k-ω model as the turbulence closure model and combined the VOF method and k-ε model to simulate the free water surface over the ogee spillway.

The k-ε model is one of the most commonly used turbulence models. The standard k-ε model can be defined by the following equations (Imanian & Mohammadian, 2019):

$$\frac{\partial \mathrm{k}}{\partial \mathrm{t}} + \frac{\partial k u_i}{\partial x_i} = \frac{\partial}{\partial x}\left[\left(v + \frac{v_T}{\sigma_k}\right)\frac{\partial k}{\partial x_i}\right] + G_k - \varepsilon \qquad (36.)$$

$$\frac{\partial \varepsilon}{\partial \mathrm{t}}+\frac{\partial \varepsilon u_i}{\partial x_i}=\frac{\partial}{\partial x}\left[\left(v+\frac{v_T}{\sigma_\varepsilon}\right)\frac{\partial \varepsilon}{\partial x_i}\right]+C_{1\varepsilon}\frac{\varepsilon}{k}G_k-C_{2\varepsilon}\frac{\varepsilon^2}{k} \quad (37.)$$

$$v_T=C_\mu\frac{k^2}{\varepsilon} \quad (38.)$$

Where k is the turbulent kinetic energy and ε is the turbulent kinetic energy dissipation rate.

According to Menter (1993), the standard k-ε model is commonly used in most boundary layers and the free shear layers away from surfaces. Although the standard k-ε model can be successfully used in some flows, some disadvantages still exist. For example, the standard k-ε model cannot simulate the separated flow, which needs to consider a good analysis of adverse pressure gradients (Menter, 1993). According to Shaheed et al. (2019), the k-ε model shows less accuracy in some complex turbulent flows, such as unconfined flows, rotating flows, and flows over curved boundary layers, which may equip the flows with high strains.

The realizable k-ε model outperforms the standard k-ε model in modeling the dissipation rate distribution of flat and round jets as well as the boundary layer in large pressure gradient, separated, and recirculating flows (Shaheed et al., 2019). According to Shaheed et al. (2019), the improvements in the realizable k-ε model make it perform better than the standard k-ε model in simulating the secondary flows.

The transport equations in the realizable k-ε model can be defined as Equations 39-40, and the strain-rate tensor can be seen in Equation 41 (Shaheed et al., 2019). Equation 42 is used to calculate the turbulent viscosity, and Equations 43-45 can compute the dynamic viscosity coefficient C_μ (Shaheed et al., 2019).

$$\frac{\partial \mathrm{k}}{\partial \mathrm{t}}+\frac{\partial k u_i}{\partial x_i}=\frac{\partial}{\partial x}\left[\left(v+\frac{v_t}{\sigma_k}\right)\frac{\partial k}{\partial x_i}\right]+G_k-\varepsilon \quad (39.)$$

$$\frac{\partial \varepsilon}{\partial \mathrm{t}}+\frac{\partial \varepsilon u_i}{\partial x_i}=\frac{\partial}{\partial x}\left[\left(v+\frac{v_t}{\sigma_\varepsilon}\right)\frac{\partial \varepsilon}{\partial x_i}\right]+\sqrt{2}C_{1\varepsilon}S_{ij}\varepsilon-C_{2\varepsilon}\frac{\varepsilon^2}{k+\sqrt{v\varepsilon}} \quad (40.)$$

$$S_{ij}=0.5\left(\frac{\partial u_j}{\partial x_i}+\frac{\partial u_i}{\partial x_j}\right) \quad (41.)$$

$$v_t=C_\mu\frac{k^2}{\varepsilon} \quad (42.)$$

$$C_\mu = \frac{1}{A_0 + A_s \frac{kU^*}{\varepsilon}} \quad (43.)$$

$$U^* = \sqrt{S_{ij}S_{ij} + \widetilde{\Omega_{ij}}\widetilde{\Omega_{ij}}} \quad (44.)$$

$$\widetilde{\Omega_{ij}} = \overline{\Omega_{ij}} - \varepsilon_{ijk}\omega_k - 2\varepsilon_{ijk}\omega_k \quad (45.)$$

Kim & Park (2005) used FLOW-3D to analyze the influence of model scale and surface roughness on flow characteristics over the ogee spillway. In FLOW-3D, the water surface was defined by the VOF function, and the ogee spillway was developed as an obstacle by FAVOR method. The RANS equations were solved by the finite-volume method and the turbulence model is developed by the renormalized group (RNG) theory, which can be applied to high-Reynolds-number turbulent flows (Yakhot et al., 1992).

According to Kim & Park (2005), the discharge, velocity, and crest pressure on the ogee spillway will be affected by the changes in model scale and surface roughness, while the two features do not influence the vertical pressure distribution. The discharge flow rate and maximum velocity will slightly reduce when the surface roughness or model length scale increase (Kim & Park, 2005).

Rubinstein & Barton (1992) argued that the renormalization group shows the effect of small scales of turbulence on the large-scale features, such as boundaries and initial conditions (Yakhot et al., 1992). Equations 46-49 can be used to describe the RNG models (Yakhot et al., 1992).

$$\frac{\partial \mathrm{v}_i}{\partial \mathrm{t}} + v_j \nabla_j v_i = -\nabla_i p + v_0 \nabla^2 v_i + f_i \quad (46.)$$

$$\nabla_i v_i = 0 \quad (47.)$$

$$\frac{\partial \mathrm{K}}{\partial \mathrm{t}} + v_i \nabla_i K = -\varepsilon + v_0 \nabla^2 K - \nabla_i (v_i p) + v_i f_i \quad (48.)$$

$$\frac{\partial \varepsilon}{\partial \mathrm{t}} + v_i \nabla_i \varepsilon = 2v_0 (\nabla_j v_i)(\nabla_j f_j) - 2v_0 (\nabla_j v_i)(\nabla_j v_l)(\nabla_l v_i) - 2v_0^2 (\nabla_j \nabla_l v_i)^2 - 2v_0 (\nabla_j v_i)(\nabla_i \nabla_j p) + v_0 \nabla^2 \varepsilon \quad (49.)$$

In which f_i is the Gaussian force, $K \equiv \frac{1}{2} v_i v_i$ is the total kinetic energy, $\varepsilon \equiv v_0 \left(\nabla_j v_i\right)^2$ is the energy dissipation (Yakhot et al., 1992).

Chanel & Doering (2008) also employed the RNG model through FLOW-3D to simulate the flow discharge over ogee spillways and compared results regarding the ratio of spillway height over the design head to find the influence on accuracy. According to Chanel & Doering (2008), when the ratio of spillway height over the design head is increased, the discharge simulation results would gradually be lower than the physical models' results. In their study, when the ratio of spillway height to design head was between 1.4 and 1.6, the numerical model had satisfying accuracy (Chanel & Doering, 2008).

Imanian & Mohammadian (2019) used OpenFOAM to apply five turbulence closures to simulate the flow with high hydraulic head ratios over the ogee spillway. The five turbulence models are standard k–ε, realizable k–ε, RNG k–ε, shear-stress transport (SST) k-ω model, and Launder-Reece-Rodi (LRR) model. According to Imanian & Mohammadian (2019), the LRR model performs accurately with the increase of head ratio. When the head ratio increases to five, the discharge coefficient will decrease because the negative pressure zone appears in the crest area. Figure 2-21 shows that the negative pressure zone grows linearly with the increase of head ratio, which can explain the discharge coefficient reduction in the high head ratio (Imanian & Mohammadian, 2019).

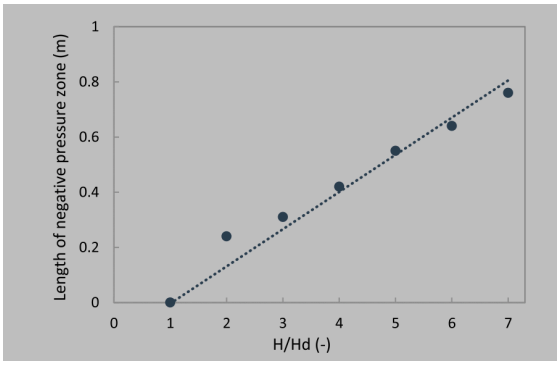

Figure 2-21 Length of negative pressure zone versus head ratio (Imanian & Mohammadian, 2019)

The LRR (Launder-Reece-Rodi) model is a turbulence model proposed by Launder et al. (1975), which can be defined using Equation 50 (Imanian & Mohammadian, 2019).

$$\frac{\partial}{\partial \mathrm{t}}\left(\rho\overline{\acute{u}_\iota\acute{u}_J}\right)+\frac{\partial}{\partial x_k}\left(\rho u_k\overline{\acute{u}_\iota\acute{u}_j}\right)=$$
$$-\frac{\partial}{\partial x_k}\left[\rho\overline{\acute{u}_\iota\acute{u}_j\acute{u}_k}+\overline{\acute{p}\left(\delta_{kJ}\acute{u}_\iota+\delta_{k\iota}\acute{u}_j\right)}\right]+\frac{\partial}{\partial x_k}\left[\mu\frac{\partial}{\partial x_k}\left(\overline{\acute{u}_\iota\acute{u}_j}\right)\right]$$
$$-\rho\left(\overline{\acute{u}_\iota\acute{u}_J}\frac{\partial u_j}{\partial x_k}+\overline{\acute{u}_j\acute{u}_k}\frac{\partial u_i}{\partial x_k}\right)+\overline{\acute{p}\left(\frac{\partial\acute{u}_\iota}{\partial x_J}+\frac{\partial\acute{u}_J}{\partial x_\iota}\right)}$$
$$-2\mu\overline{\frac{\partial\acute{u}_\iota}{\partial x_k}\frac{\partial\acute{u}_J}{\partial x_k}}-2\rho\Omega_k\left(\overline{\acute{u}_J\acute{u}_m}\epsilon_{ikm}+\overline{\acute{u}_\iota\acute{u}_m}\epsilon_{jkm}\right) \quad (50.)$$

The LRR model can be successfully used in strained homogeneous shear flows and two-dimensional inhomogeneous shear flows (Launder et al., 1975). Although the LRR model can solve the transport equations to decide the turbulent stresses avoiding the eddy viscosity approach (Imanian & Mohammadian, 2019), it still has some limitations. According to Novkovic et al. (2018), the LRR turbulence model might perform poorly in the zones of low Reynolds stress values in shear-flow fields.

To investigate the hydraulic characteristics of flow over ogee spillways and compare the performance of two numerical models, Kocaer & Yarar (2020) used ANSYS-Fluent to solve the standard k–ε model and employed OpenFOAM to simulate the k-ω SST model. According to Kocaer & Yarar (2020), the k-ω SST model in OpenFOAM has satisfying performance in the flow that is not a turbulent region, and the k–ε model in ANSYS-Fluent performs more accurately in the open channel turbulent flows.

To overcome the limitations of the k-ε models, the k-ω models were developed, which solve one equation for kinetic energy and the second equation for the turbulent dissipation rate (Menter, 1993).

The original k-ω model can be defined as follows (Devolder et al., 2018):

$$\frac{\partial \mathrm{k}}{\partial \mathrm{t}}+\frac{\partial \mathrm{u}_j k}{\partial \mathrm{x}_j}-\frac{\partial}{\partial \mathrm{x}_j}\left[(v+\sigma_k v_t)\frac{\partial k}{\partial x_j}\right]=P_k-\beta^* k\omega \quad (51.)$$

$$\frac{\partial \omega}{\partial \mathrm{t}}+\frac{\partial u_j\omega}{\partial \mathrm{x}_j}-\frac{\partial}{\partial \mathrm{x}_j}\left[(v+\sigma_\omega v_t)\frac{\partial \omega}{\partial x_j}\right]=\gamma\frac{\omega}{k}P_k-\beta\omega^2 \quad (52.)$$

$$P_k=v_t\frac{\partial u_i}{\partial x_j}\left(\frac{\partial u_i}{\partial x_j}+\frac{\partial u_j}{\partial x_i}\right) \quad (53.)$$

$$v_t = \frac{k}{\omega} \tag{54.}$$

where k is the turbulent kinetic energy, P_k is the production term of k, ν is the kinematic viscosity, ν_t is the turbulent kinematic viscosity, ω is the specific dissipation rate, $\sigma_k=\sigma_\omega=0.5$, $\beta^*=0.09$, $\beta = 0.072$ and $\gamma=0.52$ (Devolder et al., 2018).

Due to the characteristics of the k-ω model, it can be applied in the near wall turbulent flows, and the logarithmic region in adverse pressure gradient flows (Menter, 1994). However, although the k-ω model can perform well under adverse pressure gradient conditions, it still has some significant limitations. The original k-ω models lack the optimal dependency on free flow and cannot accurately simulate the free shear layers (Menter, 1993).

The shear-stress transport (SST) k-ω model is a two-equation viscosity model (Menter, 1994). This model is a modification based on the baseline (BSL) model (Menter, 1994), which considers the effect of the principal turbulent shear stress transport. It should be mentioned here that the new baseline model already combines the advantages of the original k-ω model and the standard k-ε model. However, it still cannot accurately predict separated flows from smooth surfaces because the BSL model did not consider the transport of turbulent shear stress (Menter, 1994). The SST k-ω model is based on a k-ω formulation, with the original k-ω model activated in the near wall region and the standard k-ε model activated in the outer wake region and free shear layers. By applying the viscosity limiter, the SST k-ω model attempts to give better separation prediction and improve adverse pressure prediction (Menter, 1994).

In the SST k-ω model, k and ω are defined by the following equations (Lee, 2018):

$$\frac{\partial \mathrm{k}}{\partial \mathrm{t}} + \nabla \cdot (uk) = P_k - \beta^* k\omega + \nabla \cdot (v + \sigma_k v_t)\nabla k \tag{55.}$$

$$\frac{\partial \omega}{\partial \mathrm{t}} + \nabla \cdot (u\omega) = \alpha D^2 - \beta\omega^2 + \nabla \cdot (v + \sigma_\omega v_t)\nabla\omega + 2(1 - F_1)\sigma_{\omega 2}\frac{1}{\omega}\nabla k \cdot \nabla\omega \tag{56.}$$

$$v_t = \min\left(\frac{k}{\omega}, \frac{a_1 k}{\Omega F_2}\right) \tag{57.}$$

Where u is velocity, $P_k = \min(G, 10\beta^* k\omega)$, and other parameters can be found in the following Figure 2-22 (Lee, 2018).

a_1	0.31
β^*	0.09
F_1	$\tanh\left\{\left\{\min\left[\max\left(\frac{\sqrt{k}}{\beta^*\omega y}, \frac{500\nu}{y^2\omega}\right), \frac{4\sigma_{\omega 2}k}{CD_{k\omega}y^2}\right]\right\}^4\right\}$
F_2	$\tanh\left\{\left[\max\left(\frac{2\sqrt{k}}{\beta^*\omega y}, \frac{500\nu}{y^2\omega}\right)\right]\right\}$
$CD_{k\omega}$	$2\sigma_{\omega 2}\frac{1}{\omega}\nabla k \cdot \nabla\omega$
α	$\alpha_1 F_1 + \alpha_2(1 - F_1)$ with $\alpha_1 = 5/9$ and $\alpha_2 = 0.44$
β	$\beta_1 F_1 + \beta_2(1 - F_1)$ with $\beta_1 = 3/40$ and $\beta_2 = 0.0828$
σ_k	$\sigma_{k1} F_1 + \sigma_{k2}(1 - F_1)$ with $\sigma_{k1} = 0.85$ and $\sigma_{k2} = 1$
σ_ω	$\sigma_{\omega 1} F_1 + \sigma_{\omega 2}(1 - F_1)$ with $\sigma_{\omega 1} = 0.5$ and $\sigma_{\omega 2} = 0.856$

Figure 2-22 Coefficients in SST k-ω model (Lee, 2018).

According to Menter (1994), the SST k-ω model can give a better near-wall behavior than the k-ε model. Furthermore, compared with the k-ω model, the SST k-ω model does not show the dependency of the freestream values. In addition, due to the viscosity limiter, the SST k-ω model can better predict adverse pressure gradient flows and better separation than the k-ω model and k-ε model (Menter, 1994).

Artificial intelligence algorithms can be applied to the optimization of numerical models of spillways. Salazar et al. (2013) employed the finite element method (FEM) and artificial neural network (ANN) to simulate the underflow discharge curves of the Oliana Dam gated spillway. According to them, the 2D FE models can successfully compute the discharge capacity and discharge curves of radial gated spillways. Salazar et al. (2013) stated that the results of FEM could be used to build and train the ANN, which provides the models with more accurate and precise results for prediction and performs quasi-real-time simulations. Developing the ANN aims to save the calculation cost of numerical models and accurately calculate the actual discharge for operational situations of the dam. In this case, the ANN took the practical operation parameters, such as the gate opening and the upstream hydraulic head, as input and used the multilayer perceptron (MLP) to compute the outflow discharge (Salazar et al., 2013).

2.4. Discussion

To date, ungated spillways operating under high head ratios, as well as the gated spillways, have been investigated through a limited number of research studies, using both experimental and numerical models. Based on the extensive literature review conducted in the current section, the following points are important considerations for evaluating spillways with gated spillways and ungated spillways with high head ratios.

- Even though various numerical models were developed for spillway studies, it does not mean that their accuracy and performance are similar for every practical situation. Therefore, a specific scenario requires a particular numerical model to compare with the physical model and determine the accuracy of the numerical prediction.
- The pressure area emerging at the crest of the ungated spillway under high head ratios should be taken into account, as this leads to a reduction in the spillway discharge coefficient (Imanian & Mohammadian, 2019).
- The pattern of the spillway flow has a tremendous influence on the choice of the design equations. In this study, the free flow and the gated flow are primarily considered. Therefore, the two most important independent variables in this research are the relative head ratio and the relative gate opening.
- Regarding the comparison of physical and numerical models, numerical models can more economically allow more information on velocity and pressure details than experimental ones. However, the physical models are still useful and continued to be used as they often provide more accurate results than numerical models (Karim & Mohammed, 2020).
- The numerical models using Lagrangian approach, such as the SPH model, which is particle-based (Saunders et al., 2014), and the models using Euler approach, such as the Finite Element Method (Salazar et al., 2013), can be widely considered for the simulation of spillways.
- A mesh-based model, VOF is usually used to find the free water surface, and FAVOR is applied to define the obstacles with structured grids (Savage & Johnson, 2001; Kim & Park, 2005; Imanian & Mohammadian, 2019; Karim & Mohammed, 2020; Kocaer & Yarar, 2020).

- Artificial intelligence applications, such as ANN, can be trained with the result data of developed numerical models. By providing quasi-real-time simulations, the applications of ANN are able to take the practical operation parameters, such as gate opening and the head ratio, as input, and compute the discharge as output accurately and in quasi-real-time (Salazar et al., 2013).

Chapter 3 Experimental and numerical study of the gated and ungated Ogee spillway

Abstract

This study was carried out by combining numerical modeling and experimental measurements to investigate the hydraulic characteristics of ungated and gated ogee spillways with high head ratios. The primary objective was to validate the use of a numerical model as a complementary approach to the experimental model for simulating the hydraulic behavior of these spillways, providing a more comprehensive understanding of their hydraulic properties under varying conditions of head ratios and relative gate openings. An Acoustic Doppler Velocimeter (ADV) was used to measure the vertical flow velocity distributions, and ultrasonic sensor wave gauges were used to obtain the time history of the water level. The results of the measurements were compared with the simulation results using a model fitted with three different turbulence models (realizable k-ε, RNG k-ε, k-ω SST). The numerical model was developed using OpenFOAM. With respect to the ungated spillway, three different head ratios ranging from 1.4 to 4.6, which correspond to high head ratios, were investigated. Similarly, three different relative gate openings ranging from 0.5 to 2 were investigated for the gated spillway. The results of water surface profiles and velocity profiles suggest that the numerical and experimental models achieve a good agreement for sections located further away from the spillway. For the ungated spillway, the simulation results for the near-spillway sections are enhanced when the head ratio increases. Considering the velocity profiles and error analysis, the realizable k–ε model was found to best predict the results of the experimental model. A discussion about the discharge equation, velocity fields, pressure fields, and the corner separation zone is also included in this study.

Keywords

Numerical modeling; Experimental study; Ogee spillway; Gated spillway; Ungated spillway; High head ratio; Relative gate opening; Turbulence models; OpenFOAM

3.1. Introduction

The spillway is a safety structure for a dam, which enables the discharge excess water from the reservoir in a safe and effective manner into the downstream channel and prevent dam overtopping. Since a large number of dam failures are caused by deficient spillway design, the discharge capacity and hydraulic characteristics of the spillways play vital roles in the maintenance and safe operation of the dam. According to the control structure, spillways can be divided into gated and ungated. A gated spillway can regulate flooding by controlling the opening of the gates, while an ungated spillway uses the height of the dam to control the upstream water level. Therefore, compared with an ungated spillway, a gated spillway can relatively reduce the height of the crest of the dam. Previous research on spillways employed experimental tests and numerical models.

Extensive research on spillways has shown that experimental models are useful and suitable for most cases. Hager & Bremen (1988) used physical models to propose the equations using the relative gate openings in order to compute the discharge over plane-gated spillways. They also suggested the equations for ungated spillways, which involve the hydraulic head ratio. Schohl (2016) investigated the discharge correlations of radial gated spillways based on the test data which was obtained from two physical models developed for the Tennessee Valley Authority spillways. Considering orifice flow, Mazumdar & Roy (1997) conducted an experimental model to propose a pressure correction factor, which is related to the gate opening and hydraulic head, in order to modify the discharge equations of gated spillways with radial gates. Nguyen et al. (2015) constructed an experimental model to examine the influence of a curved downstream profile on the mean flow pressure distribution as well as the discharge capacity of the breast wall spillway. Ansar & Gonzalez-Castro (2003) established a prototype gated spillway for analyzing the equation of gated spillways under the submerged weir flow. To measure the velocity and pressure distribution of ogee spillways crest under the high head ratio, Peltier et al. (2018) designed two experimental models scales of ogee spillways, to validate the velocity and relative pressure by employing the large-scale particle image velocimetry (LSPIV) and pressure sensors located along the spillway crest.

Even though the application of experimental models is important in terms of studying hydraulic characteristics of spillways and it is still used to propose new and improve existing formulas, it

requires considerable financial, material, and human resources, while also being time-consuming. Therefore, numerical models, which can reduce these costs, are more and more employed in this field of research. Previous investigation demonstrated that numerical models can provide reasonably accurate applications for the study of spillway hydraulic characteristics, in terms of velocity, pressure, and discharge.

FLOW-3D, a computational fluid dynamics (CFD) package, can simulate, with reasonable accuracy, the hydraulic characteristics of spillways, such as pressure, free surface profile, velocity distribution, as well as discharge of the flow over ogee spillways. The Finite Volume Method was applied to solve the RANS equations (Savage & Johnson, 2001; Kim & Park, 2005; Morales et al., 2012; Karim & Mohammed, 2020). Chatila & Tabbara (2004) modeled the free surface profiles over spillways by applying the CFD software ADINA, based on the Finite Element Method. Bhajantri et al. (2007) performed a simulation of the hydraulic characteristics of spillways, such as velocity and pressure profile by utilizing the Finite Volume Method based on weakly compressible equations. Kazemzadeh-Parsi (2014) presented the application of smoothed fixed grid Finite Element Method to simulate the free surface over the radial gated spillway. Fleit et al. (2017) successfully investigated the head-discharge relationships under free flow and the velocity under submerged flow conditions by employing the CFD software REEF3D.

Another well-known CFD software, OpenFOAM can also be applied to predict the velocity, pressure, and discharge coefficient of the flow over ogee spillways by solving the turbulence models. Imanian & Mohammadian (2019) applied the OpenFOAM using standard k–ε, realizable k–ε, RNG k–ε, shear-stress transport (SST) k-ω model and Launder-Reece-Rodi (LRR) model to simulate the velocity profile, pressure field, and discharge coefficient of ogee spillway under high head ratios. Kocaer & Yarar (2020) compared the two turbulence models, k–ε and k-ω model of ANSYS-Fluent and OpenFOAM, to predict the water depth and free surface profile over ogee spillways. Salazar et al. (2013) used the finite element method to compute the discharge of the Oliana Dam and obtained the results of FEM models to train the artificial neural networks (ANN) for the quasi-real-time calculation, which considered particular situations such as the energy head and gate opening. The up-to-date particle-based methods, such as the Smoothed Particle Hydrodynamics (SPH) and the weakly compressible moving particle semi-

implicit formulation (WC-MPS) are able to give satisfactory simulations of hydraulic characteristics over spillways (Saunders et al., 2014; Jafari-Nodoushan et al., 2016).

Various climatic changes in recent years have caused led to changes in the flow regime of river inflows into reservoirs. As such, the head upstream of the spillway is often much higher than the initial design head under extreme climate conditions, resulting thus in a high head ratio situation (Peltier et al., 2018). Up to now, most studies have focused on low head ratio spillways, and little attention has been paid to observing the high hydraulic head ratios. Therefore, the situation when the actual head is highly larger than the design head needs extensive attention as well as research in various aspects.

Furthermore, regarding the study of gated spillways, past studies either applied only the experimental model or applied only a numerical model. To the authors' knowledge, no previous study has investigated the hybrid approach, which considers at the same time both physical and numerical modeling for gated ogee spillways. Besides, most of the studies have focused on radial gates and much fewer on plane gates. To optimize the investigation of the plane gate spillways, the simultaneous application of physical and numerical models is important.

This is the first study to consider both experimental and numerical models for gated ogee spillways. In the case of the ungated spillway, the models focus on the high hydraulic head ratios study, and in the case of the gated spillway, the study of the different relative gate openings has been performed. In the experimental tests, flow velocity distribution was measured using an Acoustic Doppler Velocimeter (ADV), while the time history of the water surface elevation was monitored using an ultrasonic wave gauge. Meanwhile, the CFD software package OpenFOAM has been applied in combination with three turbulence closures models, namely the realizable k–ε, the k-ω SST model, and the RNG k–ε model. The performance of the numerical simulations was evaluated by comparing the results of the experimental tests with those of the numerical models in terms of the velocity distribution and water surface profiles.

The overall structure of the paper includes five sections: the introduction, methodology, results, discussion, and summary of this paper. The methodology part presents the setup of the experiment, the governing equations, and other features of numerical models, such as boundary conditions, initial conditions, mesh sensitivity, model algorithm, and so on. The third part

presents the results of this study and evaluates the performance of the numerical simulations. The discussion of the results and concluding remarks complete this paper.

3.2. Methodology

3.2.1 Experimental setup

The experiments were carried out in a flume at the Water Resources Laboratory at the University of Ottawa, Canada. The flume is 12.10 m long, 0.39 m wide, and 0.60 m deep. The ogee spillway profile was designed and calculated by Equations 1- 4 of chapter 2, where Equations 1-3 were applied to the upstream quadrant, while Equation 4 was applied to the downstream section.

$$\left(\frac{x}{H_d}+0.2418\right)^2+\left(\frac{z}{H_d}+0.1360\right)^2=(0.04)^2$$

$$-0.2818\le\frac{x}{H_d}\le-0.2760 \qquad (1.)$$

$$\left(\frac{x}{H_d}+0.1050\right)^2+\left(\frac{z}{H_d}+0.2190\right)^2=(0.2)^2$$

$$-0.276\le\frac{x}{H_d}\le-0.175 \qquad (2.)$$

$$\left(\frac{x}{H_d}\right)^2+\left(\frac{z}{H_d}+0.5000\right)^2=(0.50)^2$$

$$-0.175\le\frac{x}{H_d}\le 0 \qquad (3.)$$

$$\frac{z}{H_d}=-0.5\left(\frac{x}{H_d}\right)^{1.85} \qquad (4.)$$

The laboratory-scale model, which was custom-designed for this specific research needs, was manufactured with acrylic plexiglass. Since the maximum water level of the flume in the lab is 52 cm, the design head was set to 4 cm, and the height of the model was set to 25 cm to achieve the professed purpose of investigating the high head ratios in the flume. The width of the spillway is 38.50 cm, its base length is 30.63 cm, and the downstream slope of the chute is 1:1 (Khatsuria, 2005).

To regulate the discharge easily and accurately, the flow rate was provided by a controlled pump. Although in reality, most flows are unsteady, the flow was considered steady in the present study to facilitate the investigation. In order to achieve head ratios as high as possible in this experimental setting for the ungated spillway, the selected inlet flow rates were 0.012 m^3/s, 0.052 m^3/s, and 0.082 m^3/s.

For the gated spillway, the flow rates of 0.012 m^3/s, 0.027 m^3/s, and 0.053 m^3/s were selected to test three gate openings. The gate was designed with a height of 40 cm, a width of 38.5 cm, and a plate thickness of 1.1 cm. An angle of 11 degrees was chosen for the bottom edge of the gate to facilitate smooth flow separation at the bottom of the gate and reduce gate vibration. The vertical plane gate was opened and closed manually, which was mounted at the spillway crest.

Figure 3-1 shows the images of the flume in the laboratory, as well as the setup of spillway models. Figure 3-2 presents the brief schematic diagrams of the experimental setup, in which (a) is for the ungated spillway, and (b) is for the gated spillway.

For the ungated spillway, high head ratios of 1.4, 3.7, and 4.6 were used, while the relative gate openings for the gated spillway were 0.5, 1, and 2. The upstream water level was recorded using a MassaSonic M-5000 Smart Ultrasonic Sensor wave gauge with an accuracy of +/- 1mm. Regarding the velocity distribution, an Acoustic Doppler Velocimeter (ADV) made by Nortek was employed to measure the velocity in the centerline of three upstream sections. For the ungated spillway, these measurement sections were selected 5, 10, and 20 cm upstream from the spillway. For the gated spillway, the measurement sections were selected at 10, 15, and 20 cm upstream from the spillway. The velocity data of each section was collected along the water depth at 6-8 depths. The correlation was up to 97%, and the signal-to-noise ratio was between 30 to 40 for all tests. Regarding the setting of the Vectrino Profiler, the sampling rate was 50 Hz, the velocity range was 1.0 m/s, and the number of cells was seven. Each measurement point was measured for two minutes to effectively collect the data. The collected data were processed and filtered by the 1-D median filtering using MATLAB. To ensure the accuracy of the experiments, the experimental data were acquired through a minimum of three independent trials.

a) b)

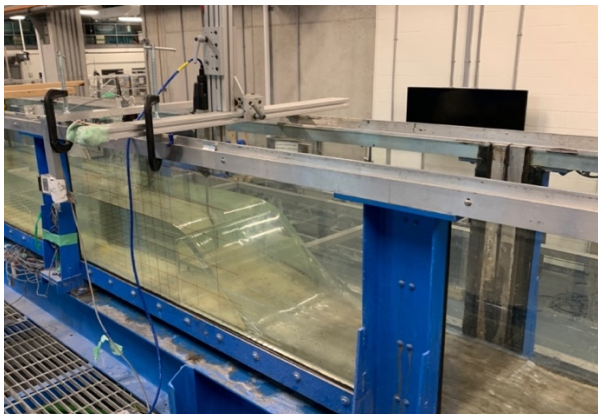

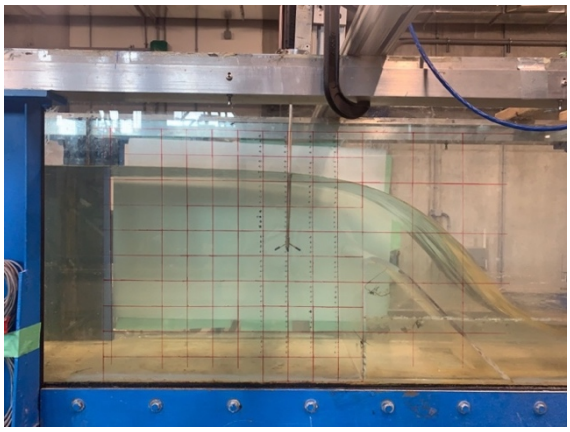

c)

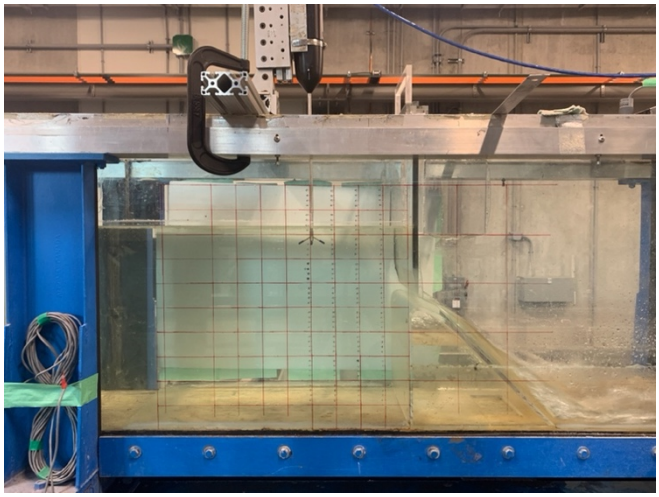

Figure 3-1 Image of the flume in the laboratory (a). the overview of the flume (b). the image example of an ungated spillway case (c). the image example of a gated spillway case.

a).

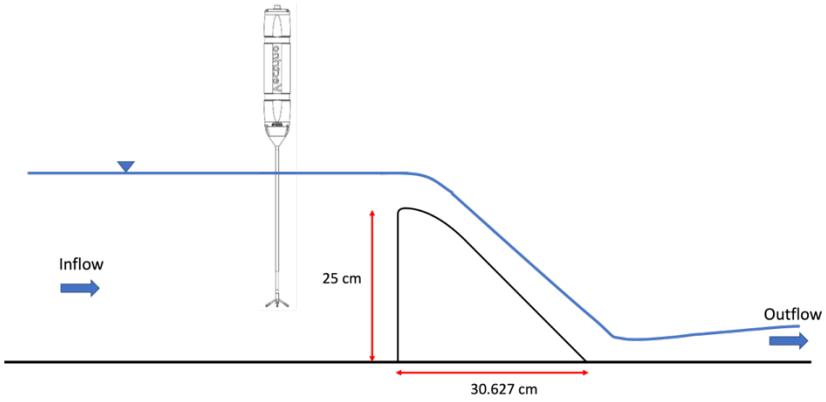

b).

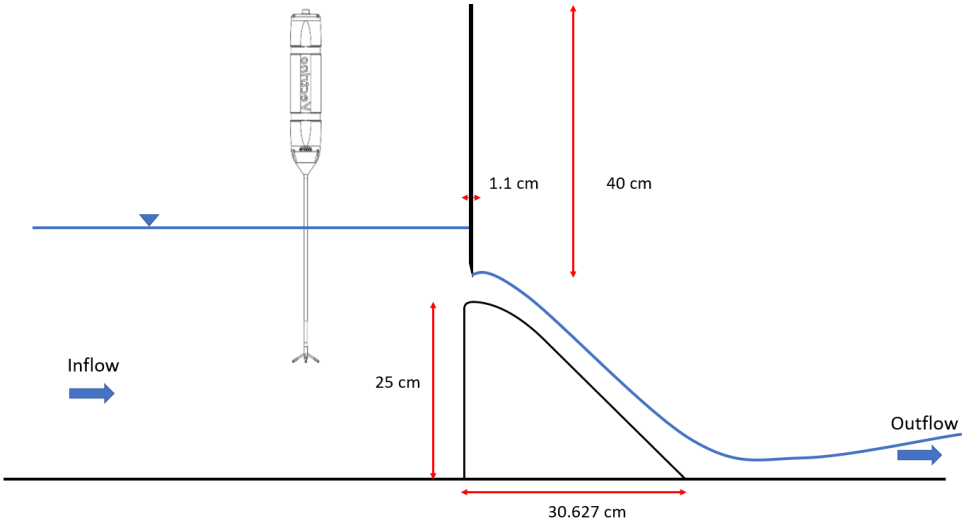

Figure 3-2 A brief schematic diagram of the experiment setup (a). ungated spillway (b) gated spillway.

3.2.2 Governing equations

For incompressible flows, the governing equations for continuity and momentum conservation can be described using Equations 58-59 (Savage & Johnson, 2001; Ferziger & Perić, 2002; Imanian & Mohammadian, 2019).

Continuity equation:

$$\frac{\partial}{\partial x}(uA_x) + \frac{\partial}{\partial y}(vA_y) + \frac{\partial}{\partial z}(wA_z) = 0 \qquad (58.)$$

where u, v, and w represent the velocity variables in the x-, y-, and z- directions, respectively. A_x, A_y, A_z are the fractional areas of open flow area in the *x*-, *y*-, and *z*- directions, respectively (Savage & Johnson, 2001).

Momentum equation:

$$\frac{\partial \bar{u}_i}{\partial t} + \bar{u}_j \frac{\partial \bar{u}_i}{\partial x_j} = -\frac{1}{\rho}\frac{\partial \bar{p}}{\partial x_i} + g_i + f_i \qquad (59.)$$

where $\bar{u}_i$ is the average flow velocity, g_i is the gravitational acceleration, and f_i is the Reynolds stresses required by the turbulence closure (Savage & Johnson, 2001; Imanian & Mohammadian, 2019).

3.2.3 Turbulence models

Some of the most well-known models for simulating the hydraulic characteristics of spillways are based on the Reynolds-Averaged Navier-Stokes (RANS) equations, which consider Reynolds averaging to reduce the effect of the rapid fluctuations (Savage & Johnson, 2001). In this study, three well-known RANS models, the realizable k-ε, k-ω SST, and RNG k-ε, have been used.

The realizable k-ε model, which is based on the standard k-ε model, improves on the dissipation rate equation and accounts for the influence of mean rotation on turbulent stresses, allowing the model to accurately predict complex turbulence, such as flows with a high mean shear rate or a considerable separation (Shih et al., 1995).

The equations of the realizable k-ε model can be defined as Equations 60-61 (Shaheed et al., 2019).

$$\frac{\partial \mathrm{k}}{\partial \mathrm{t}} + \frac{\partial k u_i}{\partial x_i} = \frac{\partial}{\partial x}\left[\left(v + \frac{v_t}{\sigma_k}\right)\frac{\partial k}{\partial x_i}\right] + G_k - \varepsilon \qquad (60.)$$

$$\frac{\partial \varepsilon}{\partial \mathrm{t}} + \frac{\partial \varepsilon u_i}{\partial x_i} = \frac{\partial}{\partial x_i}\left[\left(v + \frac{v_t}{\sigma_\varepsilon}\right)\frac{\partial \varepsilon}{\partial x_i}\right] + \sqrt{2}C_{1\varepsilon}S_{ij}\varepsilon - C_{2\varepsilon}\frac{\varepsilon^2}{k + \sqrt{v\varepsilon}} \qquad (61.)$$

The strain-rate tensor S_{ij} in the transport equations is shown in Equation 62 (Shaheed et al., 2019).

$$S_{ij} = 0.5\left(\frac{\partial u_j}{\partial x_i} + \frac{\partial u_i}{\partial x_j}\right) \qquad (62.)$$

Equation 63 is used to calculate the turbulent viscosity (Shaheed et al., 2019).

$$v_t = C_\mu \frac{k^2}{\varepsilon} \tag{63.}$$

Equations 64-66 can be used to compute the dynamic viscosity coefficient C_μ (Shaheed et al., 2019).

$$C_\mu = \frac{1}{A_0 + A_s \frac{kU^*}{\varepsilon}} \tag{64.}$$

$$U^* = \sqrt{S_{ij}S_{ij} + \widetilde{\Omega_{ij}}\widetilde{\Omega_{ij}}} \tag{65.}$$

$$\widetilde{\Omega_{ij}} = \overline{\Omega_{ij}} - \varepsilon_{ijk}\omega_k - 2\varepsilon_{ijk}\omega_k \tag{66.}$$

The shear-stress transport (SST) k-ω model is a two-equations viscosity model, which combines the advantages of the original k-ω model and the standard k-ε model, considering the transport of turbulent shear stress and enabling the better separation prediction and adverse pressure prediction (Menter, 1994). According to Menter (1994), the SST k-ω model can better predict adverse pressure gradient flows and provide a better near-wall flow behavior than the k-ω and k-ε models.

In the SST k-ω model, k and ω are defined by the following equations (Lee, 2018):

$$\frac{\partial \mathrm{k}}{\partial \mathrm{t}} + \nabla \cdot (uk) = P_k - \beta^* k\omega + \nabla \cdot (v + \sigma_k v_t)\nabla k \tag{67.}$$

$$\frac{\partial \omega}{\partial \mathrm{t}} + \nabla \cdot (u\omega) = \alpha D^2 - \beta\omega^2 + \nabla \cdot (v + \sigma_\omega v_t)\nabla\omega + 2(1 - F_1)\sigma_{\omega 2}\frac{1}{\omega}\nabla k \cdot \nabla\omega \tag{68.}$$

$$v_t = \min\left(\frac{k}{\omega}, \frac{a_1 k}{\Omega F_2}\right) \tag{69.}$$

where u is velocity, $P_k = \min(G, 10\beta^* k\omega)$, while the other parameters can be found in Figure 3-3 (Lee, 2018).

a_1	0.31
β^*	0.09
F_1	$\tanh\left\{\left\{\min\left[\max\left(\frac{\sqrt{k}}{\beta^*\omega y}, \frac{500\nu}{y^2\omega}\right), \frac{4\sigma_{\omega 2}k}{CD_{k\omega}y^2}\right]\right\}^4\right\}$
F_2	$\tanh\left\{\left[\max\left(\frac{2\sqrt{k}}{\beta^*\omega y}, \frac{500\nu}{y^2\omega}\right)\right]\right\}$
$CD_{k\omega}$	$2\sigma_{\omega 2}\frac{1}{\omega}\nabla k \cdot \nabla\omega$
α	$\alpha_1 F_1 + \alpha_2(1 - F_1)$ with $\alpha_1 = 5/9$ and $\alpha_2 = 0.44$
β	$\beta_1 F_1 + \beta_2(1 - F_1)$ with $\beta_1 = 3/40$ and $\beta_2 = 0.0828$
σ_k	$\sigma_{k1} F_1 + \sigma_{k2}(1 - F_1)$ with $\sigma_{k1} = 0.85$ and $\sigma_{k2} = 1$
σ_ω	$\sigma_{\omega 1} F_1 + \sigma_{\omega 2}(1 - F_1)$ with $\sigma_{\omega 1} = 0.5$ and $\sigma_{\omega 2} = 0.856$

Figure 3-3 Coefficients in SST k-ω model (Lee, 2018).

The RNG k-ε model (Renormalization Group) improves the standard k-ε model by incorporating renormalization theory to calculate small-scale eddies and to demonstrate the effect of small-scale turbulence on large-scale characteristics (Yakhot et al., 1992; Darmawan & Tanujaya, 2019). According to Speziale & Thangam (1992), the RNG k-ε model can handle high strain rates when generating the dissipation term, which leads to better prediction for the backstep problem. The transport equations of the RNG models are described by Equations 70-71 (Imanian et al., 2021).

$$\frac{\partial k}{\partial t} + \frac{\partial k u_i}{\partial x_i} = \frac{\partial}{\partial x_i}\left[\left(\nu + \frac{\nu_T}{\sigma_k}\right)\frac{\partial k}{\partial x_i}\right] + G_k - \varepsilon \qquad (70.)$$

$$\frac{\partial \varepsilon}{\partial t} + \frac{\partial \varepsilon x_i}{\partial x_i} = \frac{\partial}{\partial x_i}\left[\left(\nu + \frac{\nu_T}{\sigma_\varepsilon}\right)\frac{\partial \varepsilon}{\partial x_i}\right] + C_{1\varepsilon}\frac{\varepsilon}{k}G_k - \left(C_{2\varepsilon} + \frac{C_\mu \eta^3(1 - \eta/\eta_o)}{1 + \beta\eta^3}\right)\frac{\varepsilon^2}{k} \qquad (71.)$$

3.2.4 Numerical model features

This research employed OpenFOAM (Open Field Operation And Manipulation), which is implemented in C++ and is one of the most well-known open-source CFD tools for hydraulic engineering (Jacobsen et al., 2012; Imanian & Mohammadian, 2019). To successfully simulate the flow over ogee spillways, the interFoam solver, which is a VOF (Volume of Fluid) model solver in OpenFOAM, was implemented.

The finite volume method (FVM) was applied, containing time and space discretization. The Euler implicit time scheme was used as a temporal scheme. The space discretization included the gradient, divergence, interpolation, and wall distance calculation schemes. The Gauss linear was applied for the gradient scheme to solve the cell gradient. As OpenFOAM supports a wide range

of divergence approaches, the divergence scheme with the best simulation results was finally chosen after much trial and error. The divergence schemes for both gated and ungated spillways simulations included linear scheme and limited linear scheme with a coefficient of one. The linear scheme was used for the interpolation, and the mesh wave scheme calculated the wall distance. For the pressure field, with a tolerance of 10^{-10}, the Preconditioned Conjugate Gradient (PCG) solver and the Diagonal Incomplete Cholesky (DIC) pre-conditioner were adopted. For all the cases, the maximum Courant number is 0.5, and the under-relaxation factors were 0.8. With the time step of 0.005 s, the simulation time of the ungated spillway was set to 30 s. On the other hand, the gated spillway models need more running time to simulate, so the time step is 0.01 s, and the running time is up to 150 s.

The numerical models were developed based on the setup of the physical model described previously. The total length of the numerical model was 7.506 m and with a height of 0.6 m. As discussed earlier, the height of the spillway was 0.25 m, and the length was 0.306 m. For the gated spillway, Figure 3-4 (b) explains the geometry of the flume and the setup in the numerical simulation, equipping a gate with a thickness of 0.011 m. The geometry of the ungated spillway is demonstrated using Figure 3-4 (d).

The boundary conditions are different between the gated and ungated spillways. For the gated spillway, the boundaries are presented in Figure 3-4 (a). The upper part of the boundary is divided into two domains: a top wall defined as a wall; and an atmosphere defined as a patch. The left boundary is defined as water inflow, and the right boundary is the flow outlet. The bottom of the upstream channel is wall 1, the spillway is wall 2, and the downstream channel is wall 3.

The velocity boundary condition (BC) for the water inflow patch was considered to be *variable Height Flow Rate Inlet Velocity*, which is a suitable boundary condition for multiphase flow with a given flow rate. The velocity boundary condition of the outflow patch was *zero Gradient*, and for all the wall-type boundaries, *no slip* was set for the boundary conditions. A BC named *pressure Inlet Outlet Velocity* was applied for the atmosphere patch which applied the pressure while allowing for flow through the boundary. The initial inlet flow rate was specified as 0.012 m^3/s, 0.027 m^3/s, and 0.053 m^3/s.

Figure 3-4 (c) shows the boundary domains for the ungated spillway model. Unlike the gated spillway simulation, the upper area was defined as an atmosphere patch. The velocity BC for the atmosphere patch was considered to be *pressure Inlet Outlet Velocity*. The *fixed value* was set as the BC of the water inlet. The rest of the boundary condition settings are identical to the simulation of the spillway with gates. The initial inlet velocity was determined as 0.1 m/s, 0.348 m/s, and 0.49 m/s.

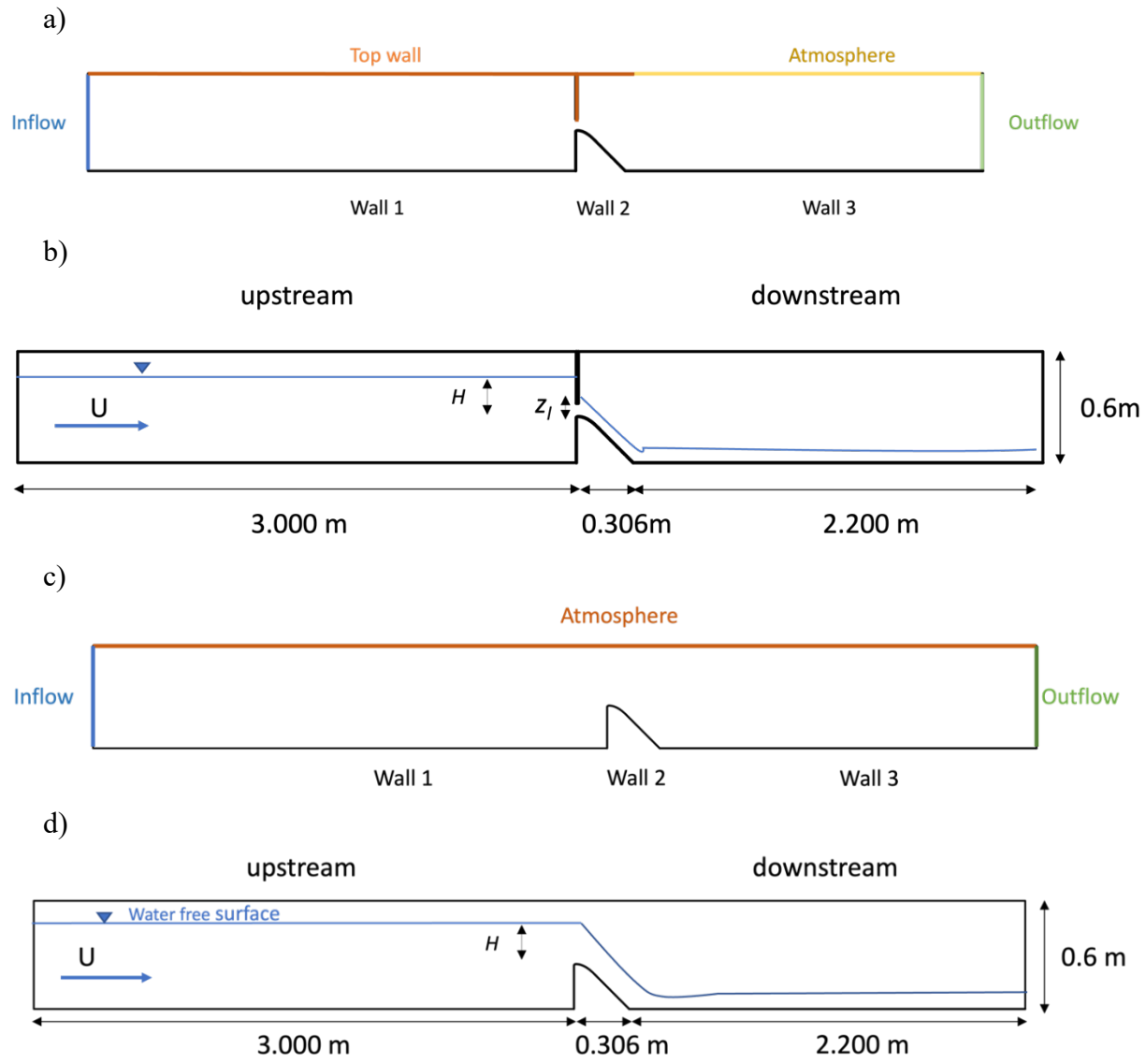

Figure 3-4 The boundary conditions and the geometry of the simulation (a). boundary conditions of the gated spillway in numerical simulation (b). geometry of the flume and the gated spillway in the numerical model (c). boundary conditions in the ungated spillway (d). geometry of the flume and the ungated spillway in the numerical model.

The structured grid was used in the simulation of the ungated spillway and the gated spillway. For the ungated spillway, Figure 3-5 depicts the layout of the computational grid, and Figure 3-6 shows the example of water and air phases under a head ratio of 3.7. The computational mesh of the gated spillway is illustrated in Figure 3-7, and the example of water and air phases under a relative gate opening of 1 is presented in Figure 3-8. Considering the upstream and downstream channels of the spillway are excessively long, the computational cost would be prohibitively expensive if the uniform-size grid was used. As a result, this study employed a refined grid in the vicinity of the spillway, while adopting a coarser grid farther away from the spillway.

In the simulation of the ungated spillway, a grid sensitivity analysis was carried out for three grid sizes. Comparing the velocities simultaneously at the same section for different grid sizes of 6mm, 4mm, and 2.5mm, respectively, allowed for the mesh sensitivity analysis, which can be seen in Figure 3-9. The comparison of velocity results for grid sizes of 6 mm and 4 mm in Figure 3-9 (b) and (c) shows that the separation of the velocity distribution is substantial, indicating that the numerical model results are still sensitive to the mesh size and the accuracy of the result is dependent on the grid quality. While the velocity distribution results of 4 mm and 2.5 mm are practically identical, this demonstrates that the result of the 4 mm grid is no longer dependent on grid size. As a result, the mesh size of the ungated spillway model was set to 4 mm, and there are 110400 cells in total after modeling.

a)

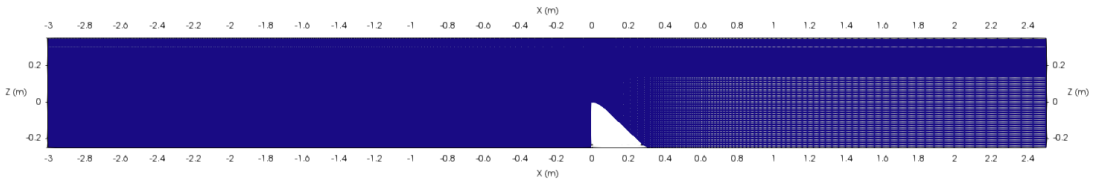

b)

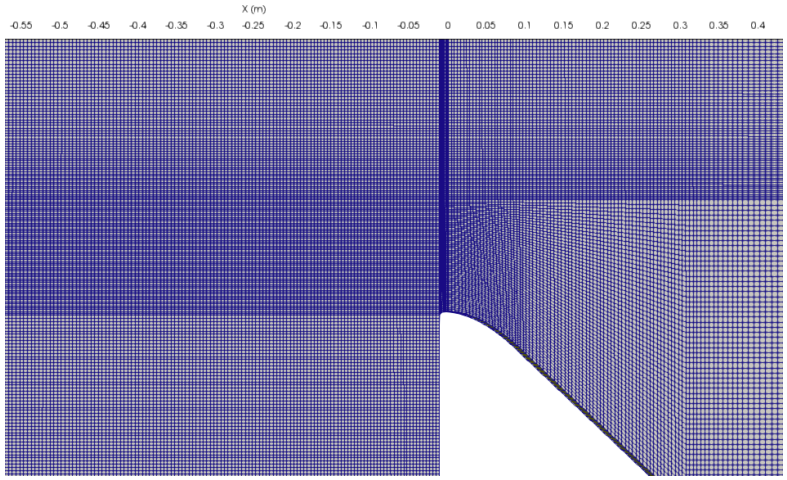

Figure 3-5 Computational grid domain of the ungated spillway simulation of (a). overall view (b). closer view.

a)

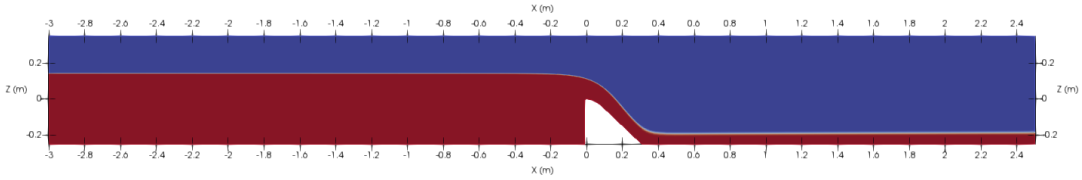

b)

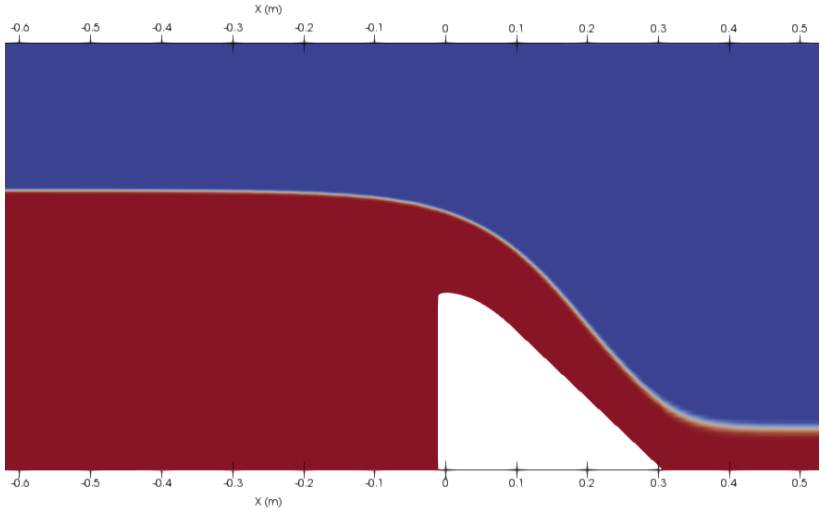

Figure 3-6 Water area in the ungated spillway simulation when head ratio is 3.7 (a) overall view (b) closer view.

a)

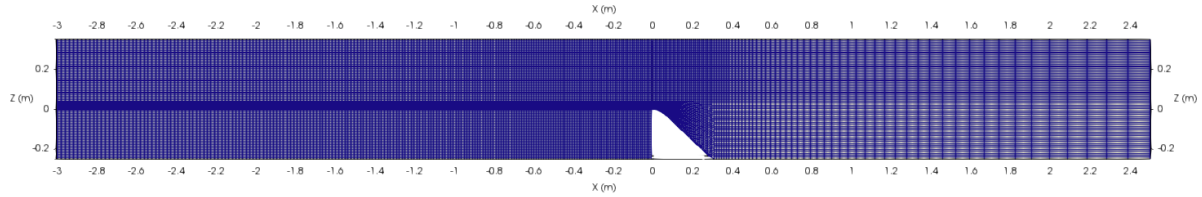

b)

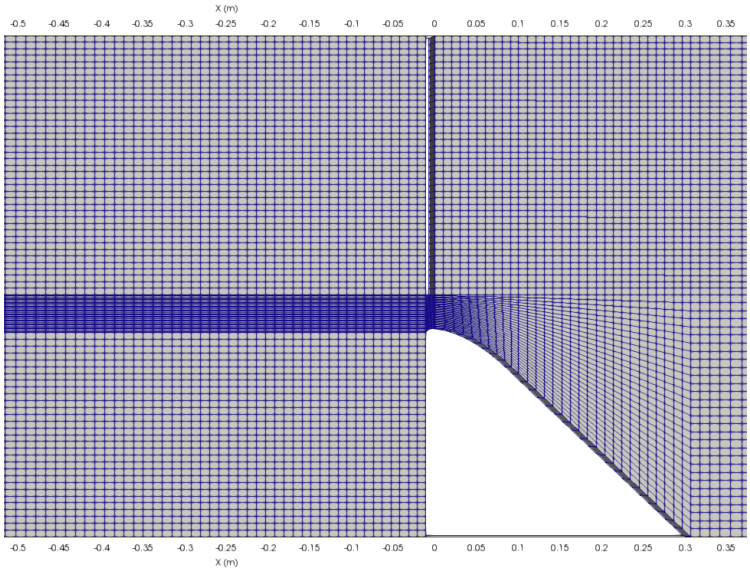

Figure 3-7 Computational grid domain of the gated spillway simulation (a). overall view (b). closer view.

a)

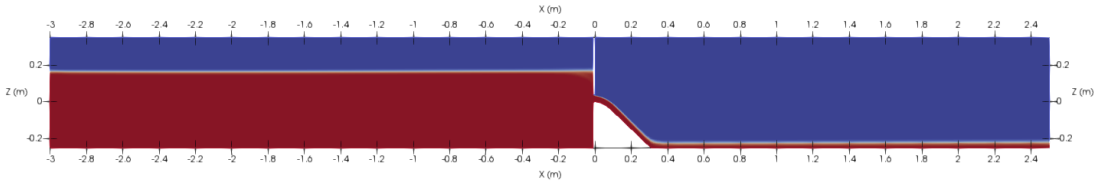

b)

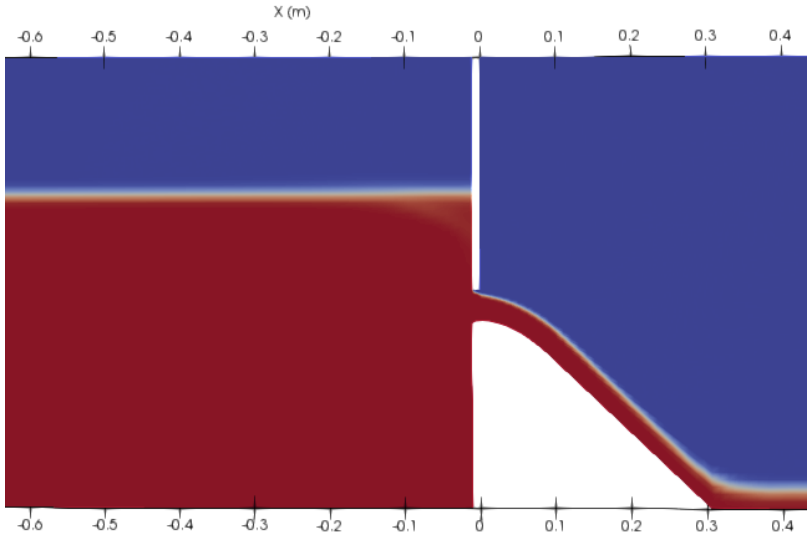

Figure 3-8 Water area in the gated spillway simulation when the relative gate opening is 1 (a) overall view (b) closer view.

a)

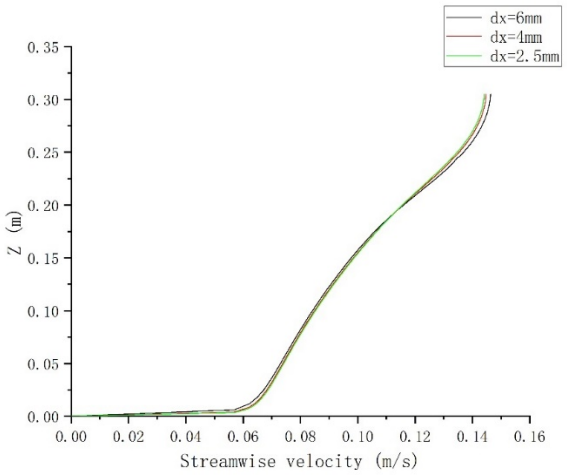

b)

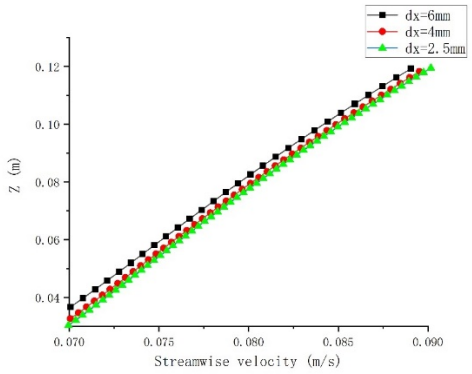

c)

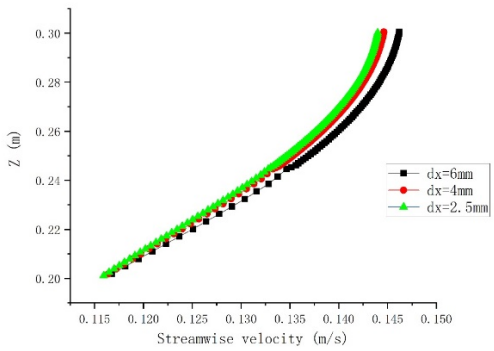

Figure 3-9 Mesh sensitivity analysis in the ungated spillway simulation (a). compare by velocity results (b). close view in the range of 0.06m~0.15m (c). close view in the range of 0.2m~0.3m.

a) b)

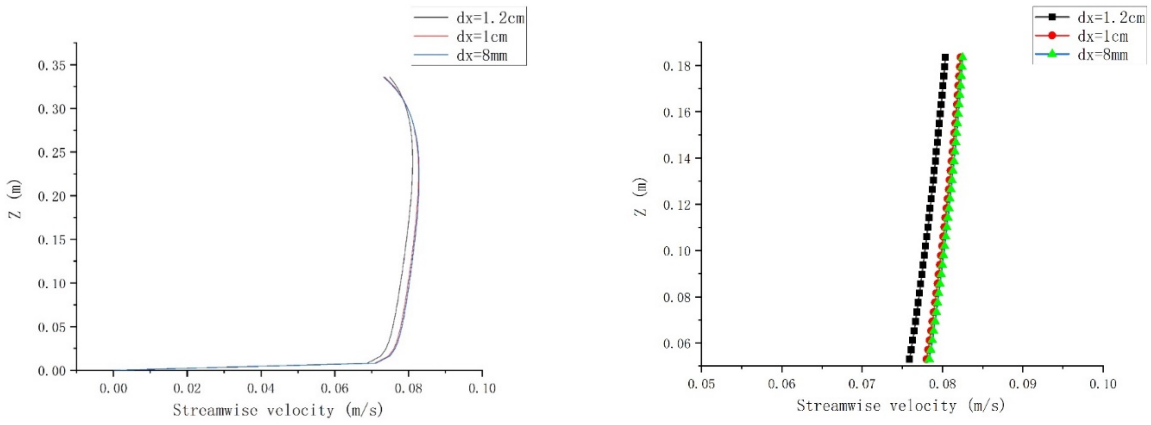

Figure 3-10 Mesh sensitivity analysis in the gated spillway simulation (a). compare by velocity result (b). close view in the range of 0.05m~0.185m

The mesh sensitivity analysis for the gated spillway is similar to the analysis of the ungated spillway. In Figure 3-10, the comparison of velocity results in the same section shows that when the size of the cells changes from 1.2 cm to 1.0 cm, the velocity results consequently become different, which explains that the result is still sensitive to the mesh size. When the size changes from 1.0 cm to 8 mm, the minimal difference in velocity demonstrates that the result of the 1.0 cm grid is no longer dependent on the cell size. Therefore, to save the computational cost, the 1.0 cm grid size was chosen for the gated spillway simulation, and after modeling, the number of cells is 25900.

3.3. Results

The hydraulic head H of the ungated spillway, which can be determined by Equation 72, plays a significant role in investigating the high head ratios spillway.

$$H = h + \frac{V^2}{2g} = h + \frac{Q^2}{2gB^2(h + h_{uf})^2} \quad (72.)$$

In Equation 72, h is the water depth above the spillway crest, Q is the inflow at the inlet, B is the width of the spillway, g is gravitational acceleration, and h_{uf} is the height of the upstream spillway (Peltier et al., 2018; Imanian & Mohammadian, 2019). Figure 3-11 presents the schematic diagram of the ogee spillway.

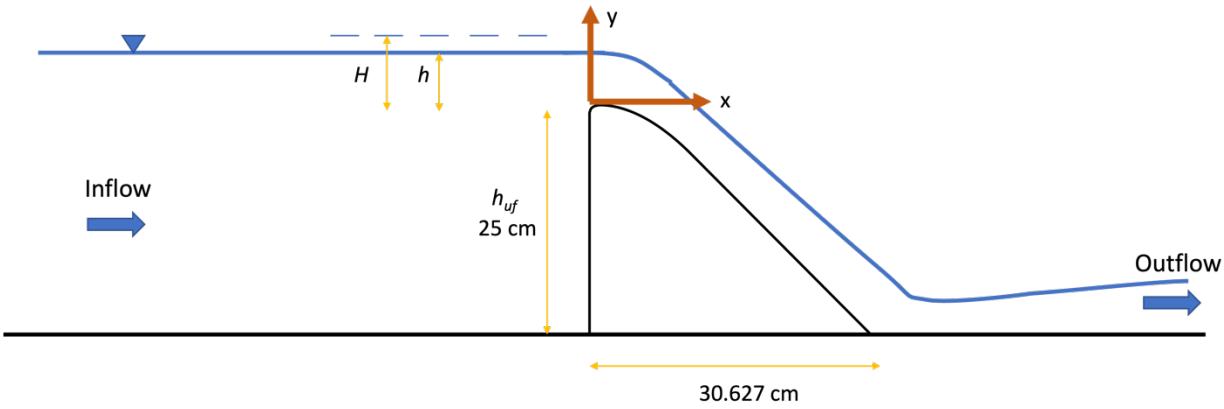

Figure 3-11Brief schematic diagram of the ogee spillway.

3.3.1 Free surface Validation

This research focuses on the hydraulic characteristics upstream of the spillway. To verify the accuracy of the numerical simulations, the water surface profiles of the three turbulence models (realizable k-ε, RNG k-ε, and k-ω SST models) were compared with the experimental results. Figure 3-12 shows that the water surface profiles predicted by the three turbulence models are essentially identical to experimental results when the head ratio is 3.7, where the water level is 0.39 m. The water surface profile upstream of the spillway starts to drop near the crest of the spillway.

The discharge coefficient C_d can be calculated as follows.

$$Q = C_d b(2gH^3)^{\frac{1}{2}} \quad (5.)$$

Figure 3-13 compares the discharge coefficients from literature (Vermeyen, 1992; Hager & Bremen, 1998) with the results of experimental and numerical models from this study. Figure 3-13 reveals that when the head ratio is less than 5, the discharge coefficients show the same increasing trend as the head ratio increases. As illustrated in Figure 3-13 and Figure 3-12 (b), the realizable k-ε and RNG k-ε models exhibited superior performance compared to the k-ω SST model in accurately simulating both the water surface profile and discharge coefficient.

To investigate the performance of the numerical simulations and determine the best performance of the three turbulence models, it is important to consider more complex hydraulic characteristics in addition to the water surface profiles and discharge coefficients. Therefore, the results of velocity profiles were investigated next.

a). b).

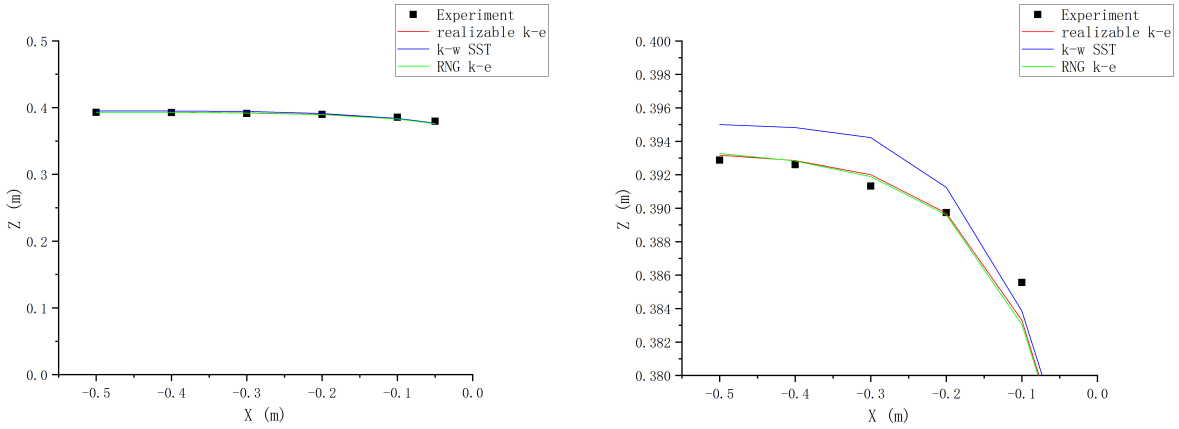

Figure 3-12 Water surface profile simulation of ungated spillway under the head ratio of 3.7 (a). Overview, (b). Closer view

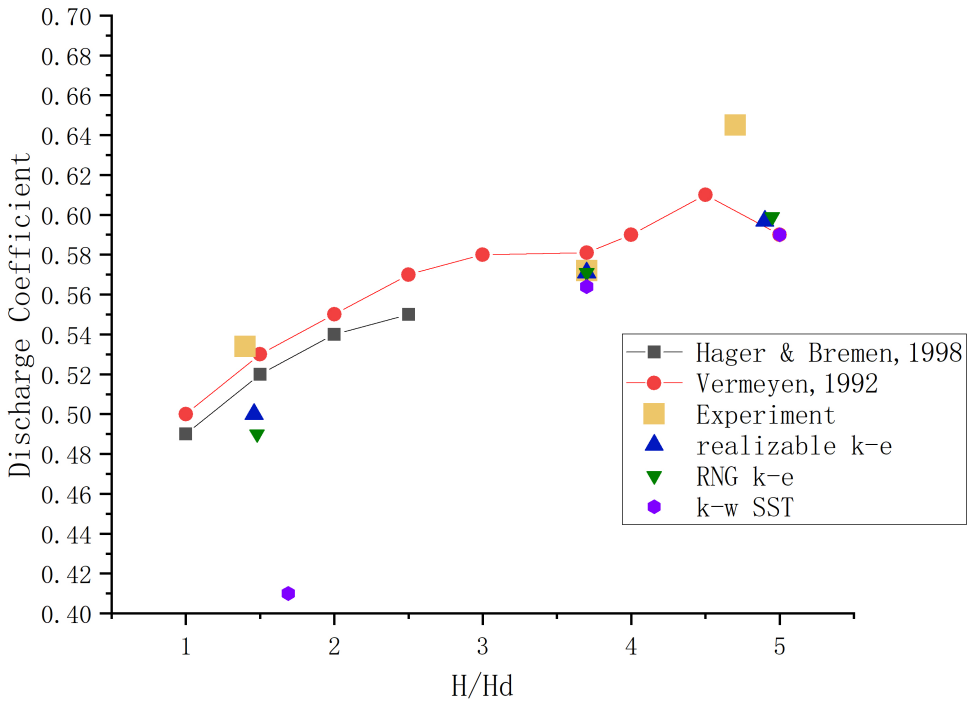

Figure 3-13 Discharge coefficient versus head ratio (comparison with the experimental models, numerical models, and previous research)

3.3.2 Velocity Validation

Velocity profiles obtained from the experimental runs are compared with the velocity distribution results of the numerical models using the corresponding sections for verification. Figure 3-14 shows the location of the velocity measurement sections for both ungated and gated spillways. For the ungated spillway, the measurement sections were taken at a distance of 0.05 m, 0.10 m, and 0.20 m upstream of the spillway crest. Since fewer measurement points are available for the section located at 0.05 m when the discharge is 0.082 m^3/s, a measurement section with a distance of 0.15 m was added at this flow rate. For the gated spillway, three measurement sections were taken at 0.10 m, 0.15 m, and 0.20 m upstream of the spillway.

Figures 3-15, 3-16, 3-17 demonstrate the velocity distribution of ungated spillways in the three sections under different head ratios (H_r=1.4, 3.7, and 4.6). The vertical axis represents the vertical distance from the bottom surface to the measurement point, and the horizontal axis indicates the dimensionless normalized velocity, which is the velocity value divided by the discharge velocity. Likewise, Figures 3-18, 3-19, 3-20 illustrate the velocity profiles of the gated spillways when relative gate openings are 0.5, 1, and 2, with the normalized velocity as the horizontal axis, and water depth measured perpendicularly from the surface as the vertical axis. The experimental measurements were performed three times, and the mean value was calculated to determine the results. The error bars, which indicate the standard deviation, were also included in the figure to provide a visual representation of the data variability.

a)

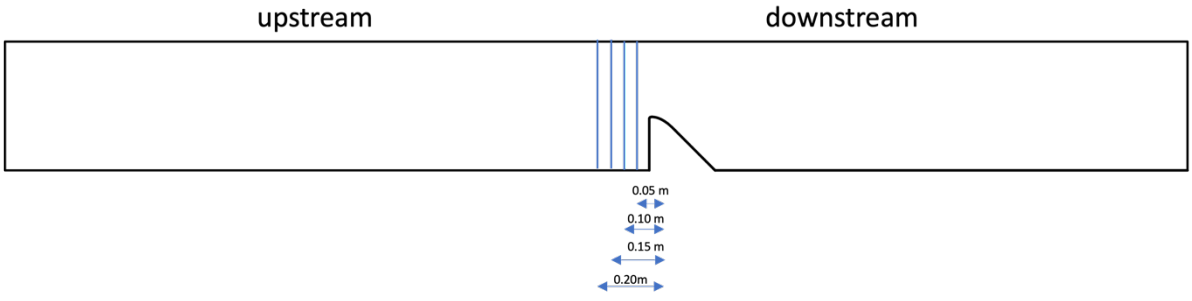

b)

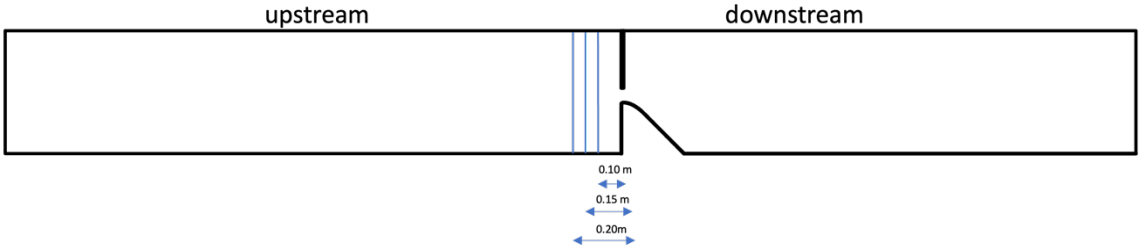

Figure 3-14 The location of the velocity measurement sections (a). ungated spillway (b). gated spillway

a)

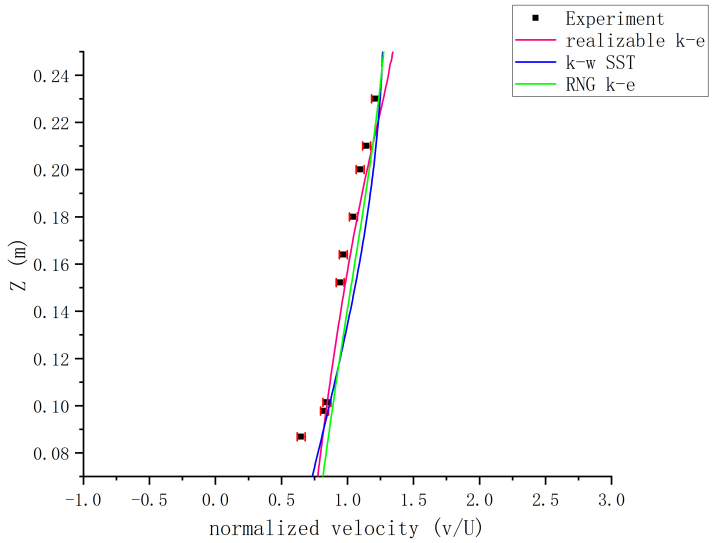

b)

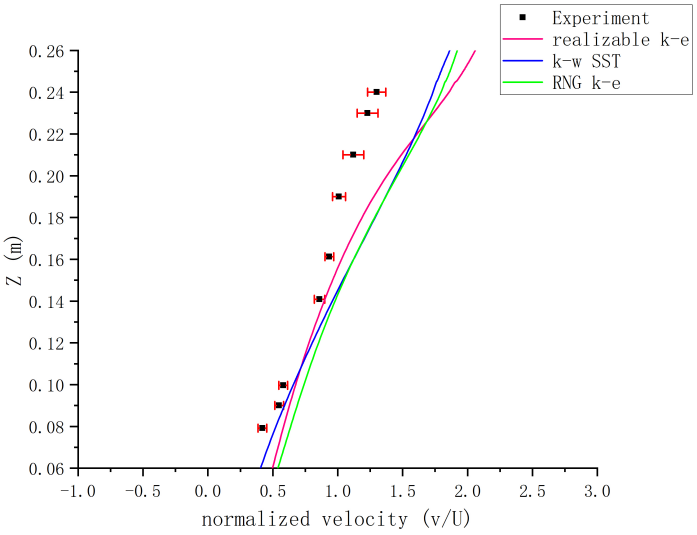

c)

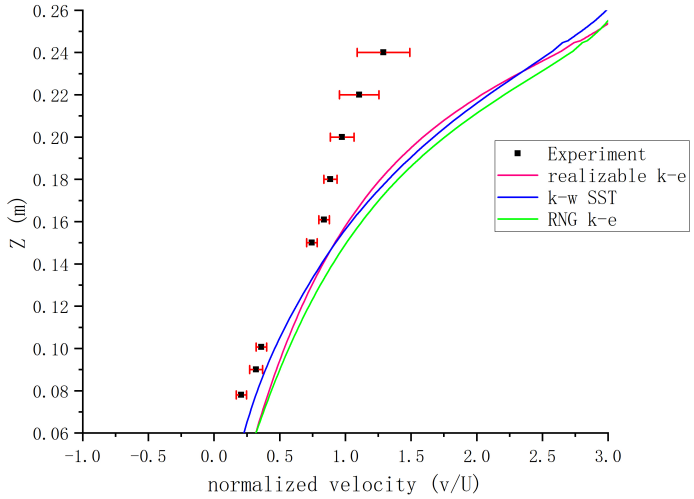

Figure 3-15 Comparison between experimental and numerical models results using the normalized velocity under the head ratio of 1.4 (a). Section 1 (x = -0.20 m) (b). Section 2 (x=-0.10 m) (c). Section 3 (x=-0.05 m).

a)

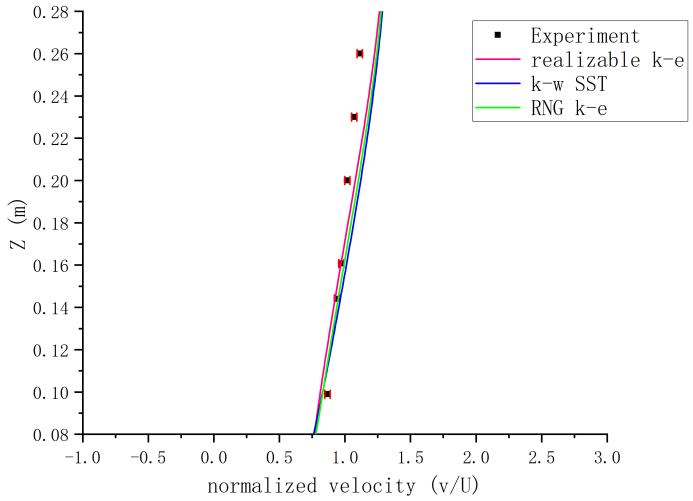

b)

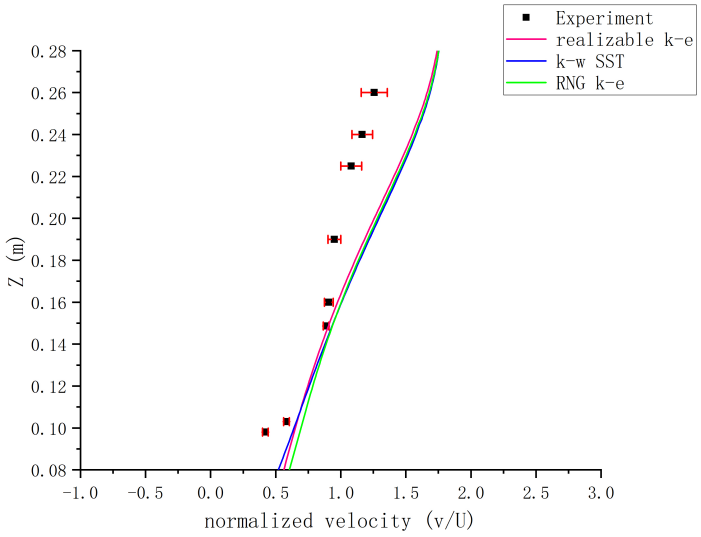

c)

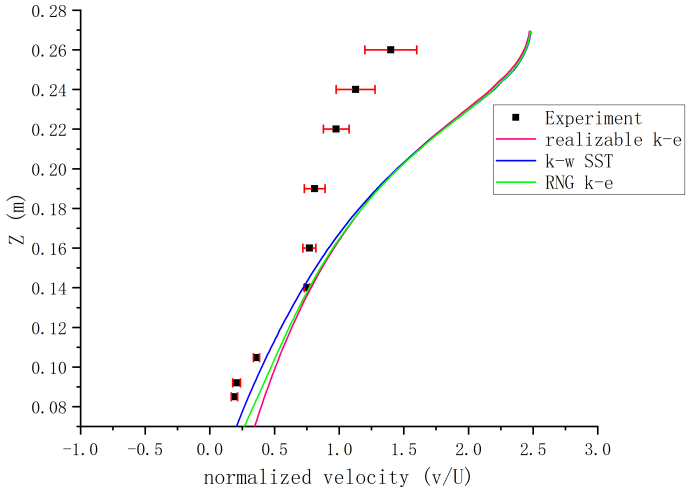

Figure 3-16 Comparison between experimental and numerical models results using the normalized velocity under the head ratio of 3.7 (a). Section 1 (x = -0.20 m) (b). Section 2 (x=-0.10 m) (c). Section 3 (x=-0.05 m).

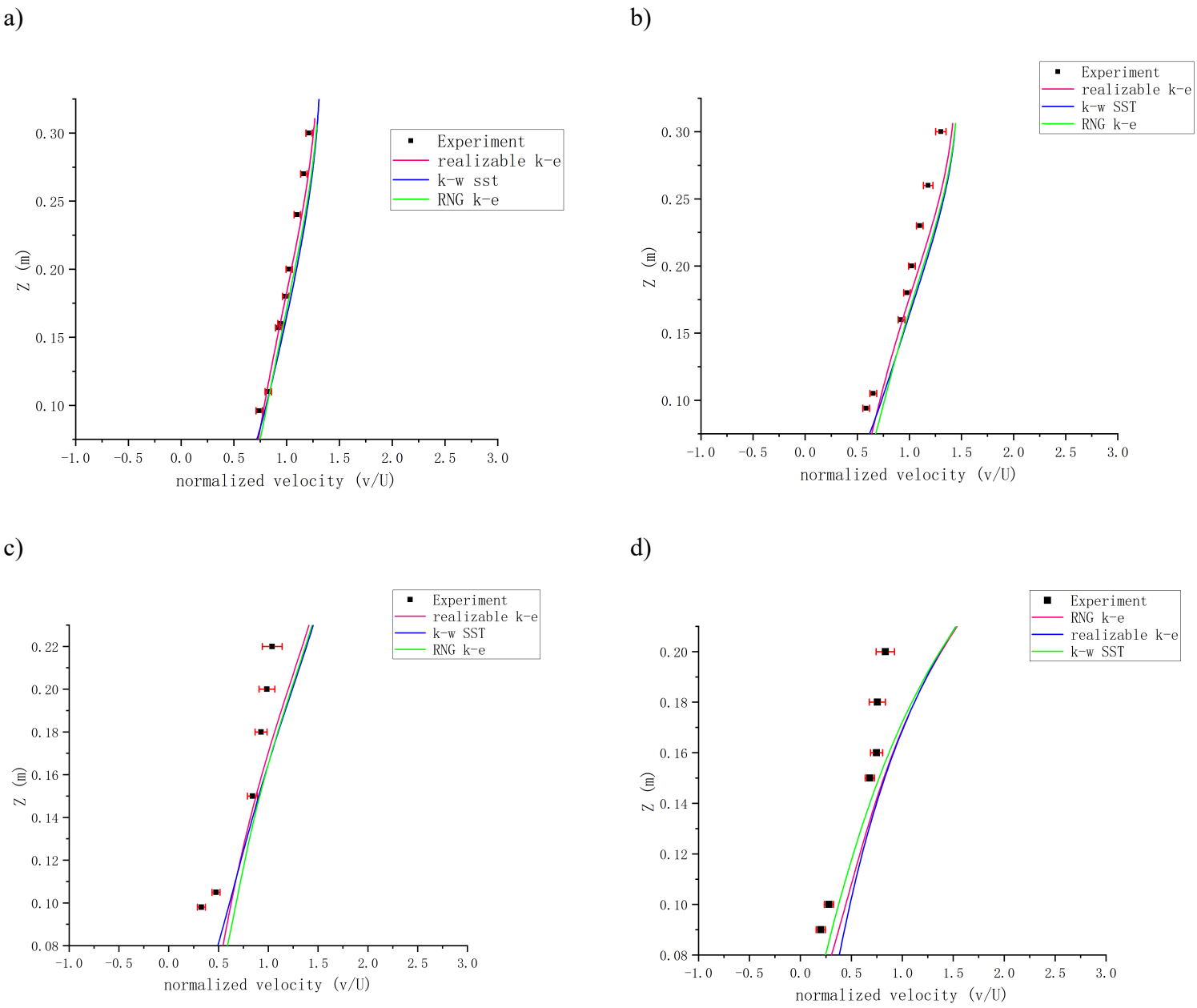

Figure 3-17 Comparison between experimental and numerical models results using the normalized velocity under the head ratio of 4.6 (a). Section 1 (x = -0.20 m) (b). Section 2 (x=-0.15 m) (c). Section 3 (x=-0.10 m) (d). Section 4(x=-0.05)

The velocity profiles in Figures 3-15, 3-16, 3-17 reveal that the results obtained with the realizable k-ε, RNG k-ε, and k-ω SST models are in good agreement with the laboratory measurement. What stands out in Figs 3-15, 3-16, 3-17 is that the numerical model results are strongly supported by the experimental data especially when for the section is x=-0.2 m, which is farthest from the spillway. In the simulation of the ungated spillway, the performance of three employed turbulence models gradually exhibits a uniform tendency with increasing head ratio values. It can be clearly seen from Figure 3-17 (d) the k-ω SST model slightly outperforms the other two turbulence models in the near-wall turbulent flow.

To quantify the accuracy of the model, an error analysis was performed for the vertical velocity distribution of different sections upstream of the spillway. The error analysis indicators are defined as Equations 73-78, and the results are presented in Table 1. Different error analysis indicators have different optimal values. For example, numerical models with R^2 values closer to one are considered that they are well-performed. On the other hand, other error indicators, such as RMSE, MAPE, etc, indicate that, when the values are close to zero, the simulation results exhibit minor errors.

$$RMSE = \sqrt{\frac{1}{N}\sum_{i=1}^{n} (\mathrm{Y} - \mathrm{D})^2} \tag{73.}$$

$$NRMSE = \frac{RMSE}{Ave(Y)} \tag{74.}$$

$$\mathrm{NMSE} = \frac{\mathrm{RMSE}^2}{\mathrm{Ave}(Y) \cdot \mathrm{Ave}(\mathrm{D})} \tag{75.}$$

$$MAE = \frac{1}{N}\sum_{i=1}^{n} |\mathrm{Y} - \mathrm{D}| \tag{76.}$$

$$MAPE = \frac{1}{N}\sum_{i=1}^{n} \frac{|\mathrm{Y} - \mathrm{D}|}{Y} \tag{77.}$$

$$R^2 = \left(\frac{sum\left(\left(\mathrm{D} - \mathrm{mean}(\mathrm{D})\right) * \left(\mathrm{Y} - \mathrm{mean}(\mathrm{Y})\right)\right)}{\sqrt{\mathrm{sum}\left(\left(\mathrm{D} - \mathrm{mean}(\mathrm{D})\right)^2\right) * \mathrm{sum}\left(\left(\mathrm{Y} - \mathrm{mean}(\mathrm{Y})\right)^2\right)}} \right)^2 \tag{78.}$$

where Y is the experimental model measured vector, D is the numerical model calculated vector, and N is the number of measured vectors.

Based on the error analysis results presented in Table 1, it can be inferred that the simulation results improve when the head ratio values rise in the near-spillway section (x=-0.05 m), as evidenced by the decrease in error indicators such as RMSE, NRMSE, NMSE, MAE, and MAPE. Similarly, for the other two sections (x=-0.1m and x=-0.2 m), the error indicators MAPE and NRMSE reduce when the head ratio increases, which indicates that the performance of the models is enhanced with an increase in head ratios.

From Figures 3-15, 3-16, 3-17 and the error analysis is shown in Table 1, it can be generally summarized that realizable k-ε, RNG k-ε, and k-ω SST models, have similar errors and provide comparable results. The difference observed in Section 3 (x=-0.05 m) could be due to measurement errors caused by the limitations of the measuring instrument in the area close to the block. The block may have affected the probe and caused inaccuracies in the measurements.

Table 1 Error analysis of ungated spillway simulation using three different turbulence models under three different head ratios.

Section Location	Head ratio (H/H_d)	Turbulence model	RMSE (m/s)	NRMSE (-)	NMSE (-)	MAE (m/s)	MAPE (-)	R^2 (-)
X= -0.20 m	1.4	realizable k-ε	0.007	0.07	0.000055	0.005	0.066	0.94
		RNG k-ε	0.009	0.09	0.000095	0.007	0.091	0.94
		k-ω SST	0.010	0.10	0.000119	0.009	0.102	0.93
X= -0.10 m		realizable k-ε	0.031	0.35	0.001240	0.025	0.261	0.95
		RNG k-ε	0.032	0.36	0.001380	0.028	0.322	0.97
		k-ω SST	0.029	0.33	0.001120	0.025	0.251	0.98
X= -0.05 m		realizable k-ε	0.062	0.82	0.006230	0.047	0.605	0.90
		RNG k-ε	0.070	0.93	0.008550	0.055	0.709	0.92
		k-ω SST	0.062	0.83	0.006290	0.046	0.528	0.93
X= -0.20 m	3.7	realizable k-ε	0.024	0.06	0.000590	0.019	0.054	0.99
		RNG k-ε	0.028	0.08	0.000830	0.023	0.064	0.99
		k-ω SST	0.033	0.09	0.001150	0.028	0.079	0.99
X= -0.10 m		realizable k-ε	0.087	0.27	0.009420	0.072	0.231	0.89
		RNG k-ε	0.095	0.30	0.011420	0.082	0.271	0.88
		k-ω SST	0.095	0.30	0.011460	0.080	0.253	0.91
X= -0.05 m		realizable k-ε	0.210	0.82	0.072880	0.165	0.708	0.90
		RNG k-ε	0.211	0.83	0.073360	0.162	0.647	0.91
		k-ω SST	0.210	0.83	0.070600	0.153	0.542	0.91
X= -0.20 m	4.6	realizable k-ε	0.021	0.04	0.001900	0.018	0.036	0.99
		RNG k-ε	0.031	0.06	0.004100	0.029	0.061	0.99
		k-ω SST	0.037	0.07	0.005700	0.035	0.074	0.99
X= -0.15 m		realizable k-ε	0.053	0.11	0.003200	0.050	0.113	0.98
		RNG k-ε	0.067	0.14	0.005200	0.065	0.150	0.98
		k-ω SST	0.070	0.15	0.005600	0.067	0.151	0.99
X= -0.10 m		realizable k-ε	0.111	0.30	0.015500	0.101	0.351	0.89
		RNG k-ε	0.125	0.34	0.020900	0.117	0.411	0.89
		k-ω SST	0.119	0.32	0.018700	0.111	0.366	0.91
X= -0.05 m		realizable k-ε	0.156	0.55	0.036600	0.140	0.608	0.86
		RNG k-ε	0.149	0.53	0.032600	0.130	0.525	0.88
		k-ω SST	0.138	0.49	0.026800	0.111	0.406	0.88

For the case of the gated spillway validation, Figures 3-18, 3-19, 3-20 show comparison of the physical and numerical models of the vertical velocity profiles. The employed quantitative error analysis approach is identical with the one used for the ungated spillway, which contains the statistical indicators and the R^2 value; calculation results are presented in Table 2.

Table 2 Error analysis of gated spillway simulation using three different turbulence models under three different relative gate-opening.

Section Location	Relative Gate Opening (Z_l/H_d)	Turbulence model	RMSE (m/s)	NRMSE (-)	NMSE (-)	MAE (m/s)	MAPE (-)	R^2 (-)
X= -0.20 m	0.5	realizable k-ε	0.005	0.056	0.000022	0.004	0.051	0.91
		RNG k-ε	0.004	0.050	0.000016	0.003	0.042	0.92
		k-ω SST	0.014	0.181	0.000248	0.137	0.179	0.68
X= -0.15 m		realizable k-ε	0.011	0.138	0.000136	0.010	0.129	0.94
		RNG k-ε	0.005	0.072	0.000034	0.004	0.061	0.97
		k-ω SST	0.021	0.268	0.000562	0.020	0.268	0.76
X= -0.10 m		realizable k-ε	0.028	0.364	0.001046	0.026	0.347	0.90
		RNG k-ε	0.024	0.309	0.000717	0.021	0.270	0.92
		k-ω SST	0.036	0.477	0.001938	0.034	0.476	0.72
X= -0.20 m	1.0	realizable k-ε	0.015	0.101	0.000270	0.014	0.096	0.92
		RNG k-ε	0.024	0.155	0.000674	0.023	0.153	0.93
		k-ω SST	0.041	0.266	0.002159	0.039	0.259	0.67
X= -0.15 m		realizable k-ε	0.031	0.197	0.001128	0.029	0.187	0.88
		RNG k-ε	0.033	0.211	0.001310	0.031	0.206	0.89
		k-ω SST	0.053	0.341	0.003771	0.051	0.333	0.79
X= -0.10 m		realizable k-ε	0.064	0.415	0.005766	0.058	0.388	0.73
		RNG k-ε	0.063	0.409	0.005572	0.056	0.383	0.68
		k-ω SST	0.081	0.521	0.009779	0.073	0.503	0.60

X= -0.20 m	2.0	realizable k-ε	0.041	0.136	0.001996	0.041	0.133	0.98
		RNG k-ε	0.036	0.119	0.001522	0.036	0.117	0.97
		k-ω SST	0.059	0.191	0.004145	0.057	0.187	0.95
X= -0.15 m		realizable k-ε	0.067	0.210	0.005430	0.067	0.205	0.91
		RNG k-ε	0.060	0.189	0.004304	0.059	0.182	0.88
		k-ω SST	0.080	0.253	0.008105	0.082	0.245	0.89
X= -0.10 m		realizable k-ε	0.130	0.390	0.023031	0.126	0.372	0.74
		RNG k-ε	0.122	0.368	0.020137	0.115	0.353	0.73
		k-ω SST	0.141	0.422	0.027568	0.139	0.397	0.75

Figures 3-18, 3-19, 3-20 illustrate that the realizable k-ε and RNG k-ε turbulence models reproduce well the experimental measurements, notably at the sections located further upstream of the gated spillway. Unlike the sections located further upstream of the spillway, simulation results in the near-spillway section (x=-0.10 m) are significantly different than the experimental ones. These differences grow significantly when the measurement height approaches the height of the spillway crest. When the measurement location is smaller than 25 cm, these differences are reduced. One possible explanation for these observations is the uncertainty errors in the observed measurements caused by measuring limitations of the Vectrino Profiler. Besides, according to Karim & Mohammed (2020), another possible reason why the difference between the physical and numerical models occurs is that the numerical simulation did not consider the surface roughness of the spillway. Furthermore, as discussed by Versteeg & Malalasekera (1995), the k-ε and related models are typically less accurate in the zone of highly curved flow.

Taking the RNG model in the section1 (x=-0.20 m) as an example, the velocity profiles in Figures 3-18, 3-19, 3-20 (a) and the error analysis in Table 2 indicate that as the relative gate-opening increases, the R^2 value increases and approaches 1, suggesting better agreement between the numerical model and the experimental results, and thus illustrating that the simulation performance improved. What is striking in Figures 3-18, 3-19, 3-20 is that the simulation performance of realizable k-ε and RNG k-ε turbulence models differs slightly when the relative gate opening is 0.5, while an almost uniform simulation trend between the two turbulence models is shown as the relative gate opening increases to 2.0.

a)

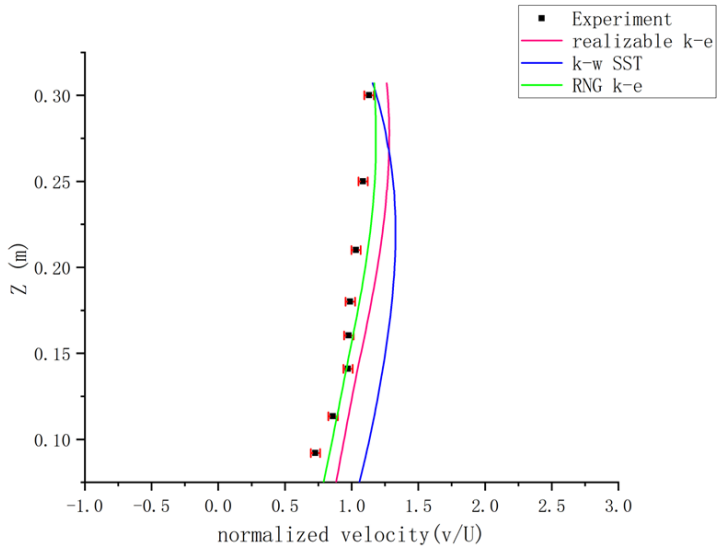

b)

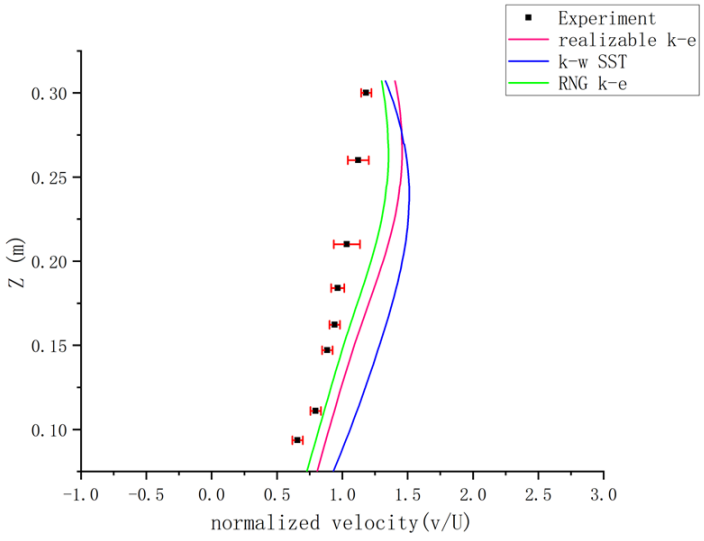

c)

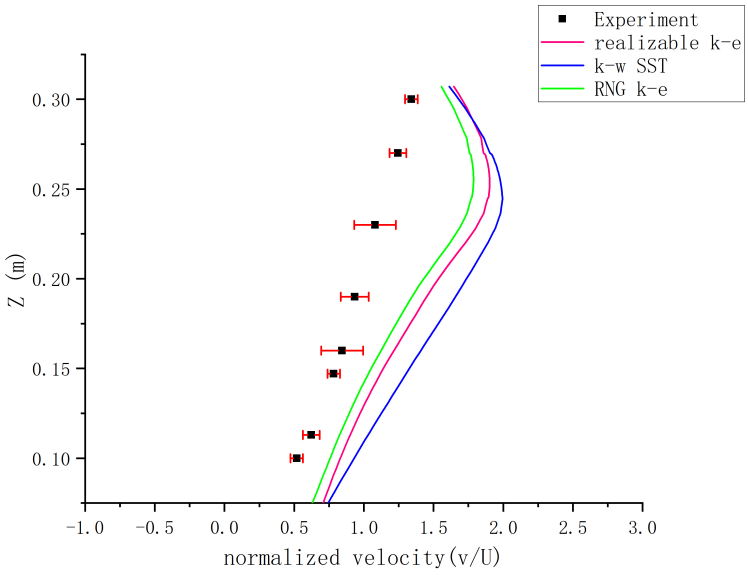

Figure 3-18 Comparison between experimental and numerical gated spillway models through the normalized velocity when relative gate opening is 0.5 (a). Section 1 (x = -0.20 m) (b). Section 2 (x=-0.15 m) (c). Section 3 (x=-0.10 m).

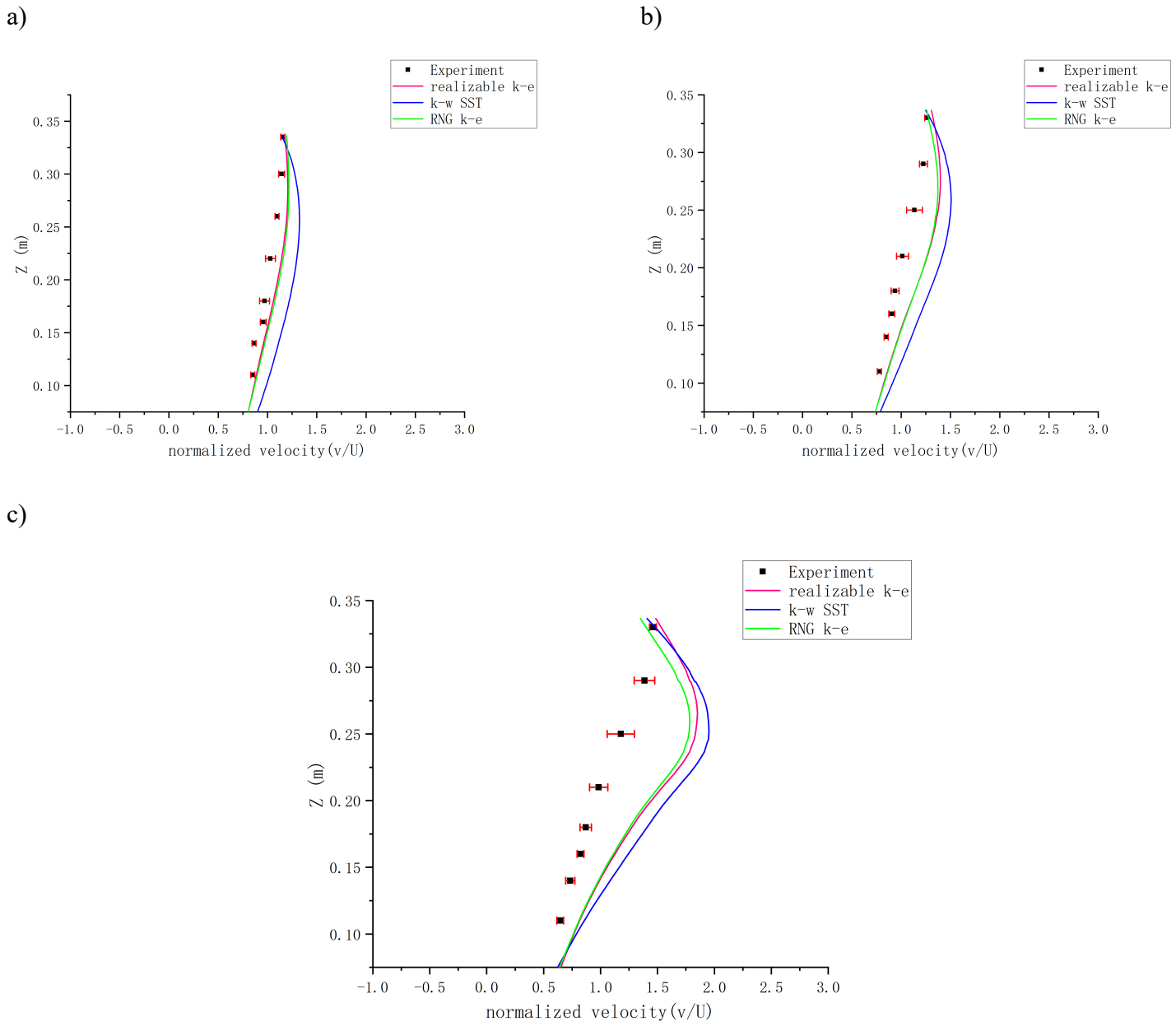

Figure 3-19 Comparison between experimental and numerical gated spillway models through the normalized velocity when relative gate opening is 1.0 (a). Section 1 (x = -0.20 m) (b). Section 2 (x=-0.15 m) (c). Section 3 (x=-0.10 m).

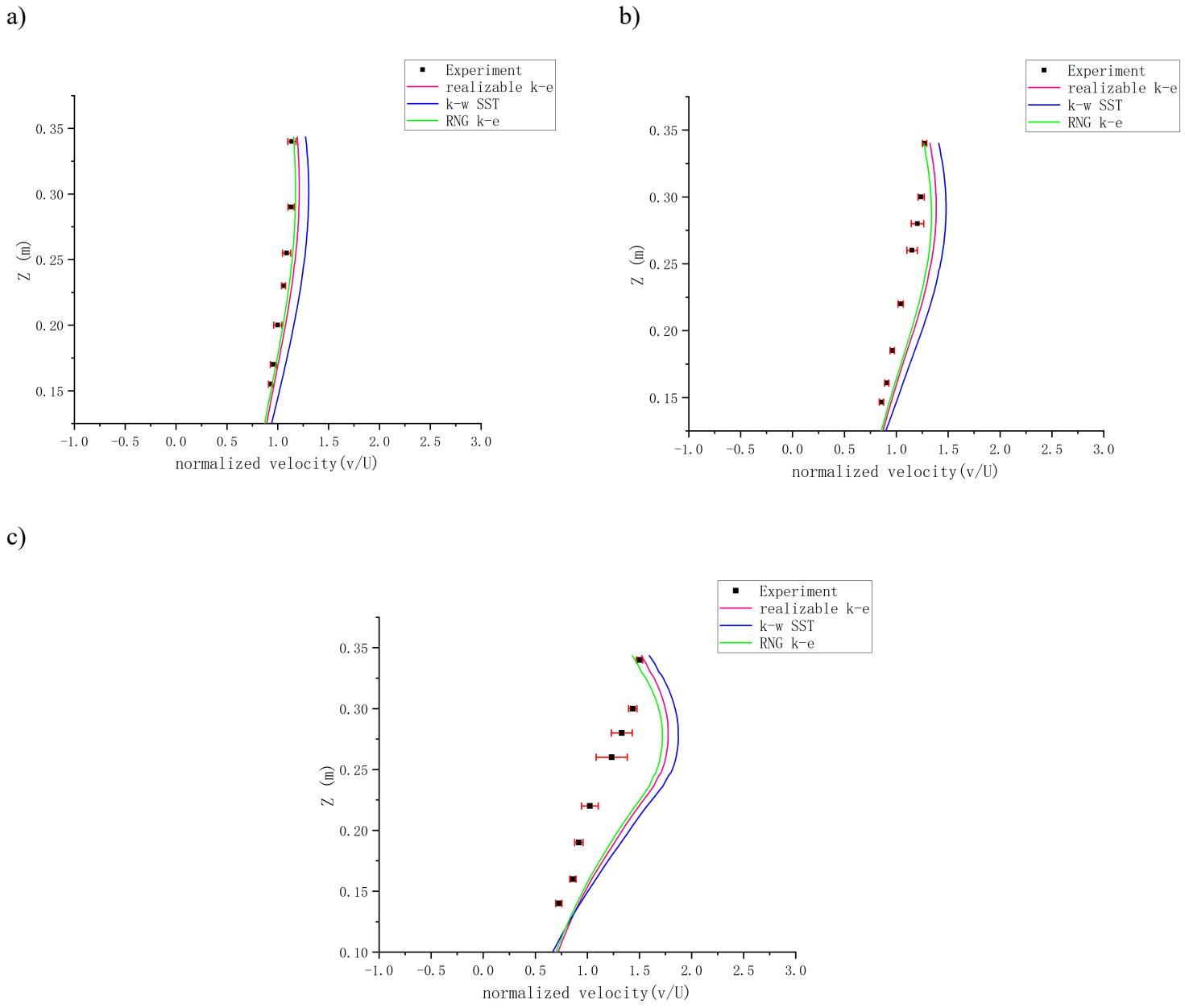

Figure 3-20 Comparison between experimental and numerical gated spillway models through the normalized velocity when relative gate opening is 2.0 (a). Section 1 (x = -0.20 m) (b). Section 2 (x=-0.15 m) (c). Section 3 (x=-0.10 m).

3.4.Discussion

3.4.1 Experimental results

3.4.1.1. Revised discharge equation of vertical plane gated spillway

Hager & Bremen (1988) proposed an equation to calculate the discharge for the vertical plane gated spillway, shown in Equation 6. According to Hager & Bremen (1988), the discharge of a vertical plane gated spillway involves the relative gate opening Z_l (Z_l = gate opening z_l/ design head H_D) and the normalized head x_0 (x_0 = actual head H_0/design head H_D).

$$Q_g = C_{dD} b (2g H_0^3)^{\frac{1}{2}} \left[1 - \left(1 - \frac{Z_l}{\chi_0}\right)^{\frac{3}{2}}\right] \left[\frac{1}{6} + Z_l\right]^{\frac{1}{9}} \quad (6.)$$

By using the experimental data obtained from this study to Equation 6, the calculated Q(g) is slightly different from the actual gated discharge Q(exp). This discrepancy may be caused by the scale limitations of the experimental models, knowing that the scale effects having a significant impact on the hydraulic characteristics of the ogee spillway. Another possible reason is that the maximum normalized head of Hager and Bremen's experiment is 4.11, while the three normalized heads from this research are 4.13, 4.75, and 5.35, respectively. Therefore, the discharge Q(exp) in this study can be used as a supplement to the high head ratios of Equation 6.

According to Hager & Bremen (1988), dimensionless geometric parameters, such as relative gate opening and normalized head, can determine the gated discharge. To amend Equation 6, a linear regression analysis was performed for the difference between Q(exp) and Q(g) in relation to relative gate opening and normalized head, which is presented in Figure 3-21. Equation 79 describes the relation in Figure 3-21, in which Z_l/x_0 takes into consideration both the relative gate opening and the relative head ratio. Notably, in Figure 3-21 is that the values of R^2 are greater than 0.96, illustrative of a strong correlation. Consequently, when the relative gate opening increases, the difference between the experimental discharge and the computed discharge using Equation 6 would decrease. On the other hand, when the value of the head ratio rises, the difference will increase accordingly.

$$\frac{Q_{exp}}{Q_g} = -0.7265 \frac{Z_l}{x_0} + 1.4077 \quad (79.)$$

Based on Equation 79, the revised discharge can be computed using Equation 80. Since the Z_l/x_0 can be specified as z_l/H_0, which is the gate opening over the actual head, it is used as the dimensionless parameter in Equation 80:

$$Q_{revised} = (-0.7265\frac{z_l}{H_0} + 1.4077) \times Q_g \quad (80.)$$

Table 3 Discharge under different relative gate openings.

Z_l	x_0	$\frac{Z_l}{x_0}$	Q(exp) (m^3/s)	Q(g) (m^3/s)	Q(revised) (m^3/s)
0.5	4.13	0.12	0.0126	0.0095	0.0125
1.0	4.75	0.21	0.0262	0.0212	0.0266
2.0	5.35	0.37	0.0525	0.0459	0.0522

Table 3 shows the different discharge values under three relative gate openings and normalized heads, which contains the discharge of experimental results, calculated results using Equation 6, and revised results. To provide a clearer representation of applying the revised equation 80, an error analysis of the Q(g) and the Q(revised) was carried out, and the results are shown in Table 4. According to the error analysis indicators, the Q(revised) shows good improvement to support the revised equation 80.

To evaluate the equation 80 critically, some limitations should be mentioned here. Firstly, due to the limited number sampling of measurement, this equation cannot be well proven to be a general equation. Further studies are required to validate the efficacy of the formula. Furthermore, the experimental results only demonstrate the validity for high normalized head values, while further investigations are necessary to verify for low normalized head situations to support the equation proposed here.

Table 4 Error analysis of the discharge calculated by Equation 6 and the revised discharge.

Q	RMSE	NRMSE	NMSE	MAE	MAPE	R^2
Q(g)	0.0051	0.167	0.00002176	0.0049	0.188	0.989
Q(revised)	0.0003	0.009	0.00000008	0.0002	0.009	0.999

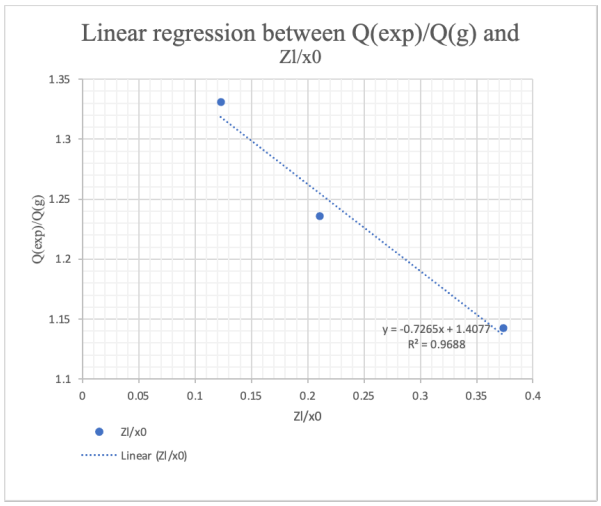

Figure 3-21 Linear regression between Q(exp)/Q(g) and the Zl/x0.

3.4.1.2. The comparison of velocity profiles between ungated and gated spillways

As the experiments were conducted under the discharge of 0.012 m^3/s and 0.053 m^3/s for both gated and ungated spillways, to study the influence of adding a vertical plane gate at the spillway crest, comparisons of velocity profiles between the ungated and gated spillways were examined to investigate the variation of velocity distribution after adding the gate.

Figure 3-22 reveals that the upstream velocity decreased after the gate was installed, and the velocity magnitudes were less than those in the case of the ungated spillway for the same water depth in section 1 (x=-0.20 m). One explanation for this variation is that the water depth increased due to the installation of the vertical gate. When the water level increases, the velocity profiles will decrease accordingly to maintain the same inlet discharge.

With this observation limited to the sections located relatively far upstream from the spillway, a general conclusion would require more research to further investigate the sections near the gate.

a) b)

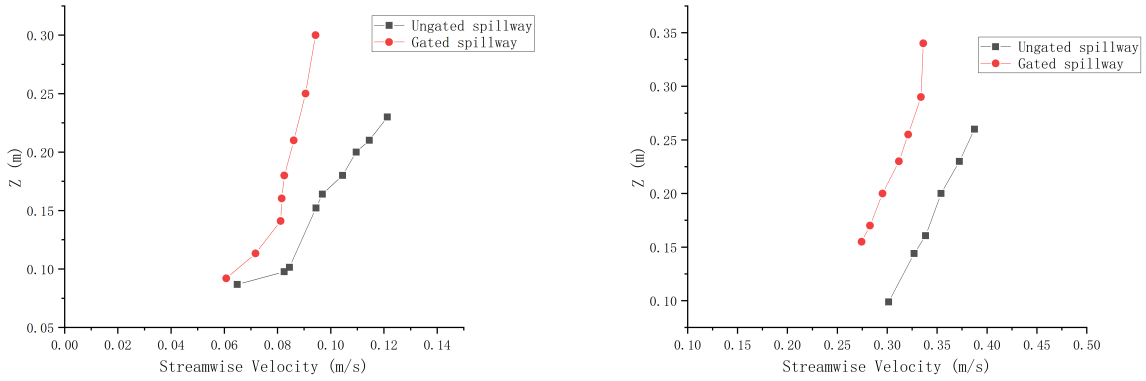

Figure 3-22 Comparison of velocity profiles between the ungated and gated spillways at section 1 (x=-0.20m) (a) Q=0.012 m^3/s, (b) Q=0.053 m^3/s.

3.4.2 Numerical simulation

Based on the velocity profile results and the error analysis, the realizable k-ε, RNG k-ε, and k-ω SST models were used to simulate the ungated and gated spillways. Considering the accuracy for both ungated and gated spillways, the realizable k-ε model generally performs better in the numerical simulation. Detailed discussions regarding the velocity field, the corner eddy zone behind the spillway, and the pressure field of numerical simulations is presented based on the predicted results of the realizable k-ε model.

3.4.2.1. Velocity Field and Maximum Velocity Location

The predicted velocity fields of the ungated spillway under different head ratios are shown in Figure 3-23. What can be seen in Figure 3-23 is that the maximum velocity at the crest will increase with the increasing head ratios. When the head ratio was 4.6, the maximum velocity at the crest of the ungated spillway was 2.1 m/s.

To investigate the maximum velocity over the crest of the spillway in more detail, the vertical location of the maximum velocity was analyzed and shown in Figure 3-24. The vertical axis takes the position of the maximum velocity *dm* over the upstream actual head H_0, which is dimensionless. Similarly, the horizontal axis is dimensionless, which uses the ratio of the distance x from the spillway axis to the designed head *Hd*.

To assess the accuracy of the ungated spillway numerical simulation, Figure 3-24 (b) considers the vertical location of the maximum velocity near the crest between the realizable k-ε model results in this study, and Figure 3-24 (a) is the experimental results obtained from Karim & Mohammed (2020).

According to Karim & Mohammed (2020), the vertical location of the maximum velocity tends to be linearly distributed. Besides, the vertical location where the maximum velocity occurs is presented at a lower position with the increase in the head ratio (Karim & Mohammed, 2020). Figure 3-24 indicates that the vertical location of the maximum velocity, *dm,* follows almost the same trend in both the numerical model results of this study and those of Karim & Mohammed (2020). The trend shows that *dm* linearly increases along the horizontal direction and decreases when the head ratios rise. Figure 3-24 (b) depicts the linear regression analysis, including the

linear equations and the R^2 values, demonstrating a robust linear relationship for all R^2 values reaching more than 0.87.

a)

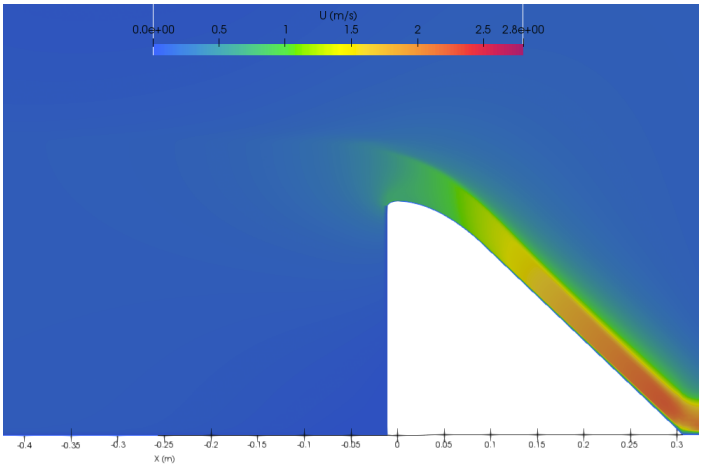

b)

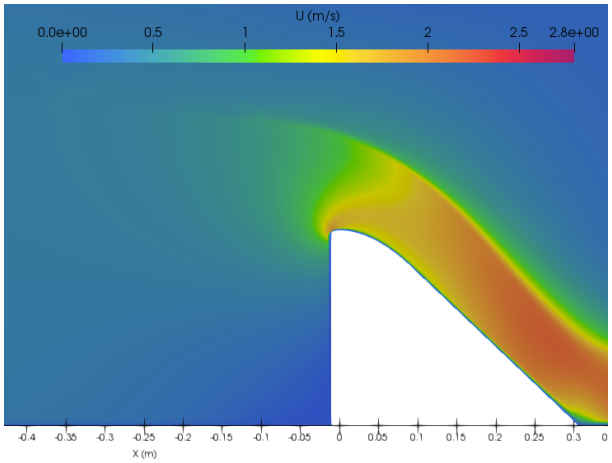

c)

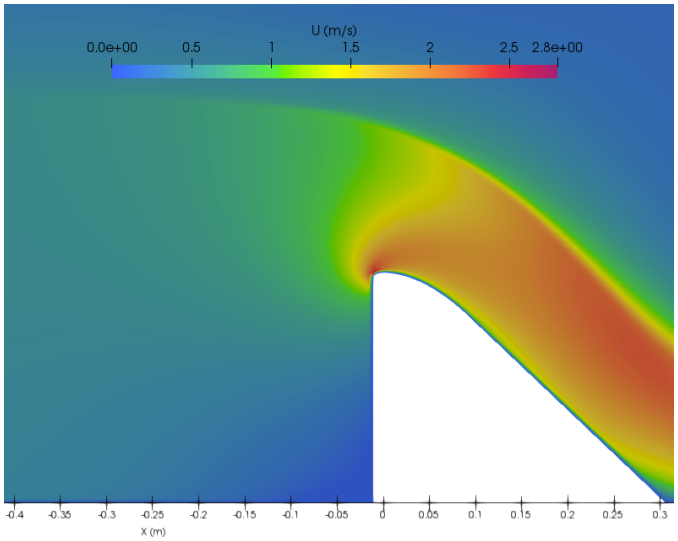

Figure 3-23 Predicted velocity field of the ungated spillway for different head ratios (a). Hr=1.4 (b). Hr=3.7 (c) Hr=4.6

a)

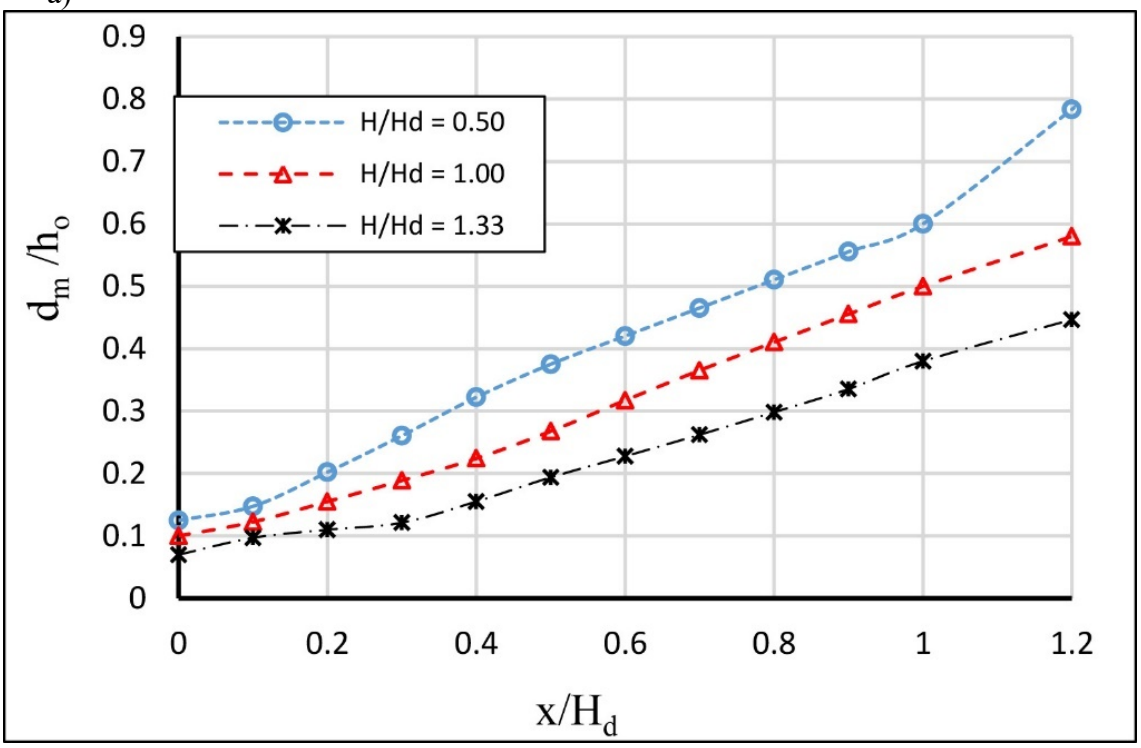

b)

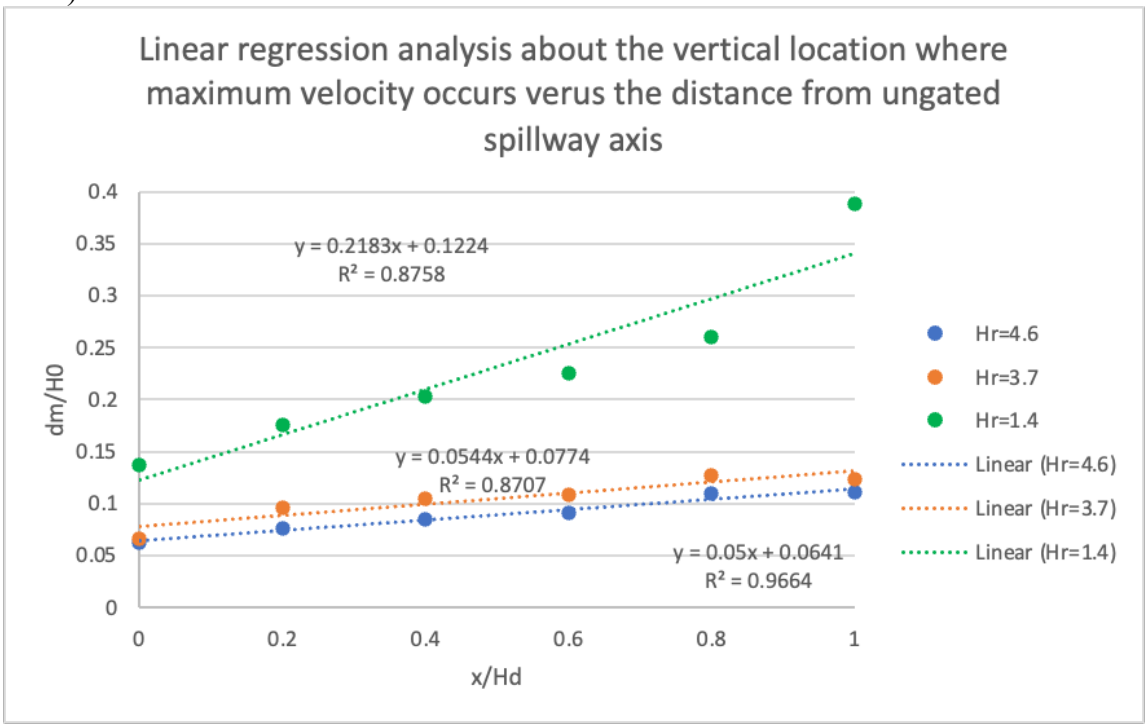

Figure 3-24 Vertical location of the maximum velocity of the ungated spillway (a) the experimental results from Karim & Mohammed (2020) (b) the linear regression analysis in this study using the results of numerical models.

a)

b)

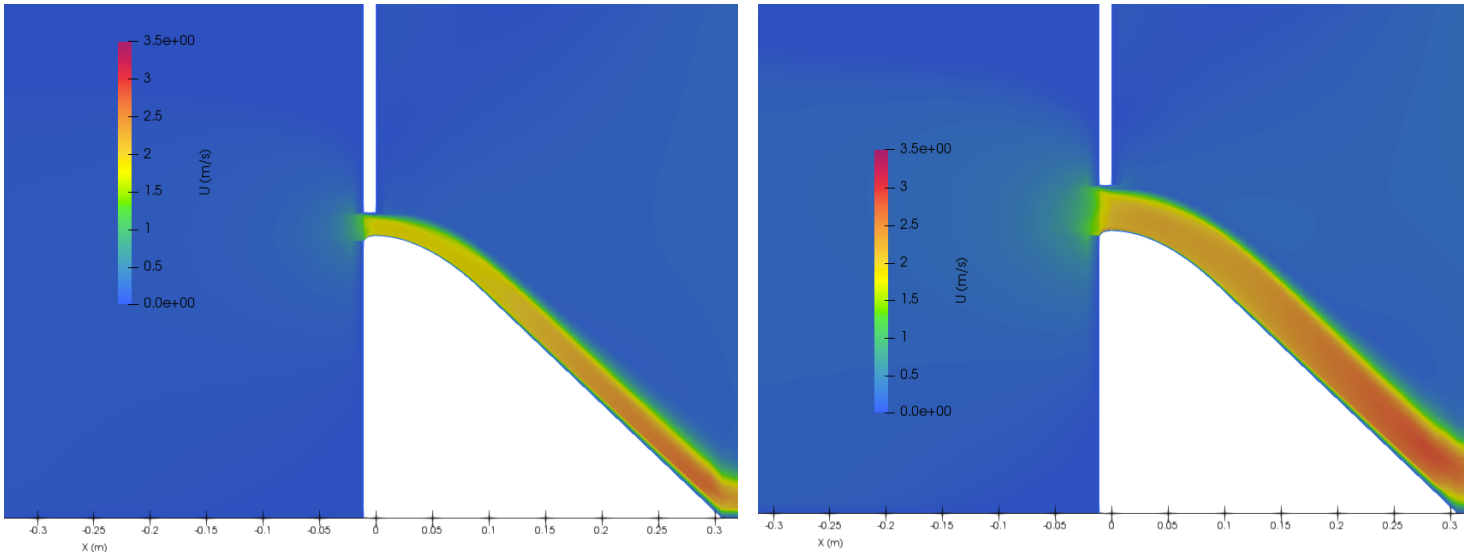

c)

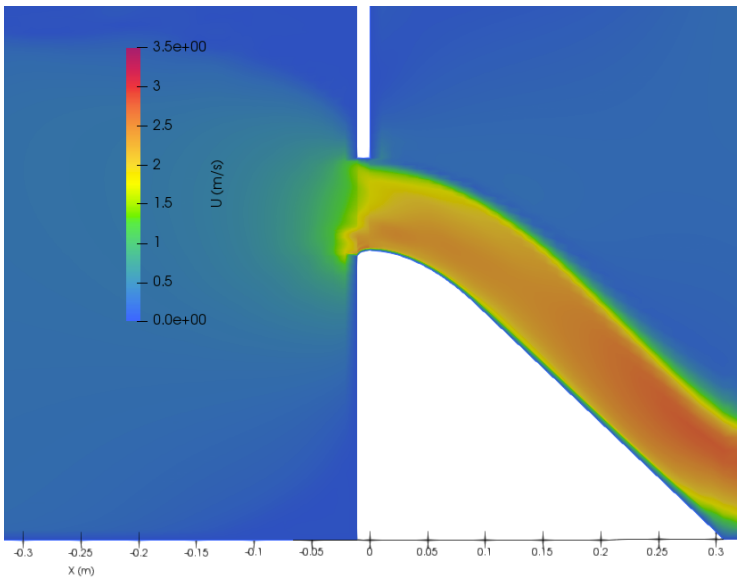

Figure 3-25 The predicted velocity field of the gated spillway for different relative gate openings (a). Z_l=0.5 (b). Z_l=1.0 (c) Z_l=2.

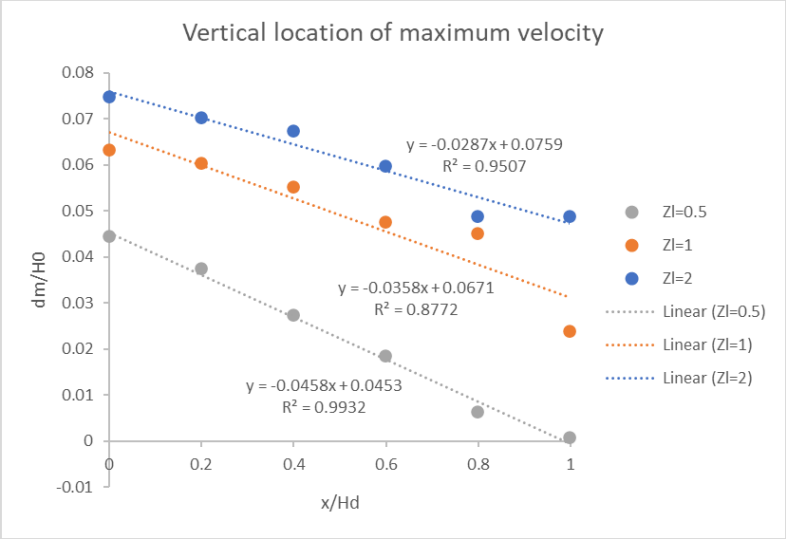

Figure 3-26 Vertical location of maximum velocity and the linear regression analysis of the gated spillway investigated by the realizable k-ε models.

Figure 3-25 shows the predicted velocity field of the gated spillway under different relative gate openings. Since the inlet discharge is the same for Figure 3-25 (a) and Figure 3-23 (a), Figure 3-25 (a) and Figure 3-23 (a) can be compared as an example to examine the difference in the velocity field of the ungated spillway and the gated spillway. After adding the gate, the maximum velocity at the spillway crest is 1.90 m/s, while the maximum velocity at the same location in the ungated spillway is 0.74 m/s. As mentioned earlier, the velocity of the gated spillway is smaller than the ungated spillway when the measured section is far from the spillway. However, the velocity at the crest of the gated spillway is significantly higher than that observed for the ungated spillway case since the cross-sectional area of the overflow is reduced after the gate is installed.

Similar to the analysis of the vertical location of maximum velocity *dm* in the ungated spillway, Figure 3-26 demonstrates the same analysis under the gated spillway. What stands out in this figure is the declining trend of the linear relationship between *dm* and the horizontal distance *x,* with the R^2 values. Unlike the ungated spillway, when the relative gate opening increases, the vertical location on which the maximum velocity occurs in the gated spillway is located at a higher position as a consequence of the intensifying high-velocity zone caused by the gate.

3.4.2.2. Corner Separation Zone

Aiming to examine the turbulent flow regime of the numerical simulation, an investigation of the corner separation zone is carried out. Figure 3-27 shows the example of where the corner separation zone occurs under head ratio of 4.6 using realizable k-ε model.

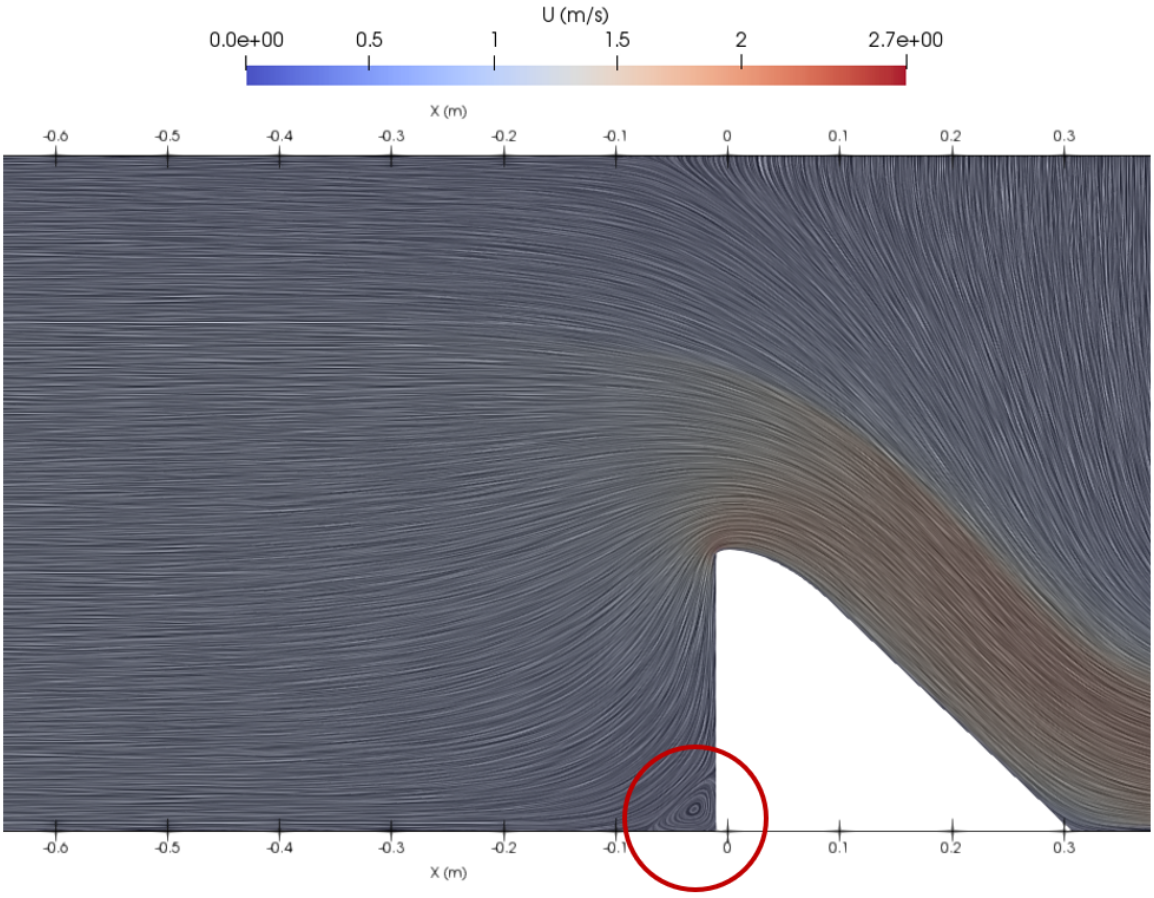

Figure 3-27 The predicted separation zone behind the spillway under head ratio of 4.6 using realizable k-ε model.

As described in the parts of the results, in this study, the k-ε turbulence models (realizable k-ε, RNG k-ε) provide better performance in simulating the hydraulic characteristics of the spillway than k-ω SST models, with the realizable k-ε model achieving the best results. With the purpose of evaluating the accuracy of the model results regarding the size of the corner separation zone behind the spillway, the significant streamline curvatures predicted and visualized by the three turbulence models were compared in the case of an ungated spillway with a head ratio of 1.4; the results are illustrated in Figure 3-28.

The size of the corner separation zone varies with different turbulence models, as shown in Figure 3-28. Table 5 presents the predicted size of the corner eddy, including its height (Lz) and length (Lx). It is well known that excessive numerical diffusion can lead to reduced eddy size in numerical simulations. In this study, the model with the largest eddy size is the one with the lowest numerical diffusion and, thus, can be considered the most accurate one.

According to Figure 3-28 and Table 5, the corner eddy predicted by the realizable k-ε model exhibits the largest size. Therefore, the size of the separation zone confirms the previous statement that, in this study, the realizable k-ε model provides the best simulation performance.

To evaluate the impact of the head ratio on the eddy size, the predicted corner separation zone, which employs the realizable k-ε model with three different head ratios, is shown for comparison in Figure 3-29 as well as Table 6. It is observed from Figure 3-29, as well as the length and height of the eddy in Table 6, that when the head ratio increases, the size of the corner eddy becomes larger. This observation supports the previous statement which indicated that as the head ratio increase, the simulation performance improves in this study.

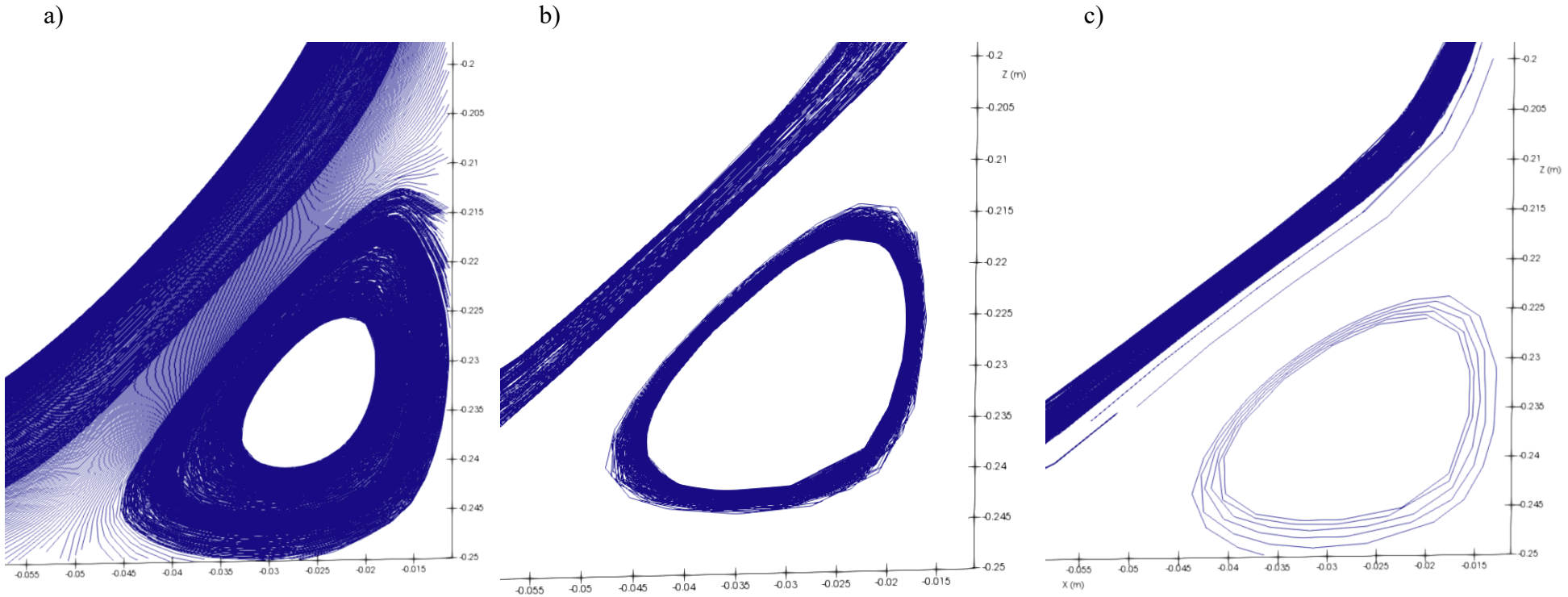

Figure 3-28 The predicted corner separation zone of the ungated spillway with hr=1.4 using (a) realizable k-ε (b) RNG (c) k-ω SST model.

Table 5 The size of the corner separation zone using different turbulence models.

Turbulence model	Height of the corner eddy *Lz* (m)	Length of the corner eddy *Lx* (m)
realizable k-ε	0.038	0.045
RNG k-ε	0.030	0.030
k-ω SST	0.025	0.033

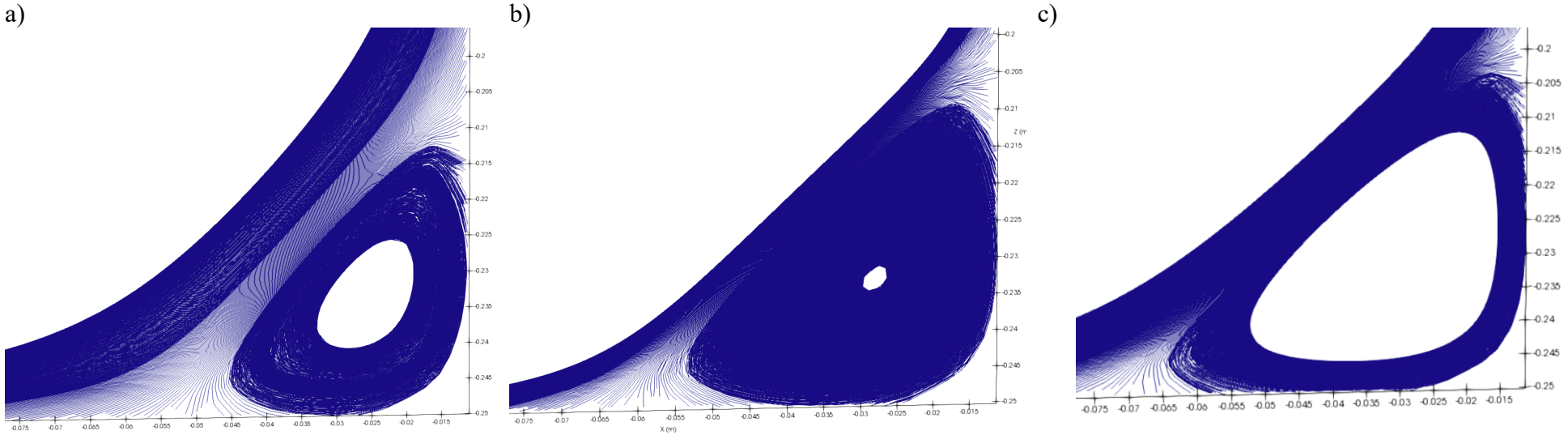

Figure 3-29 The predicted corner separation zone using the realizable k-ε model under different head ratios (a) hr=1.4 (b) hr=3.7 (c) hr=4.6.

Table 6 The size of the corner separation zone using realizable k-ε model under different head ratios.

Head ratio	Height of the corner eddy *Lz* (m)	Length of the corner eddy *Lx* (m)
1.4	0.038	0.045
3.7	0.040	0.054
4.6	0.045	0.065

3.4.2.3. Pressure field

Previous research shows that when the head ratio is less than or equal to 1, the relative pressure at the spillway crest is positive (Erpicum et al., 2018). At the same time, when the head ratio is greater than 1, which means the actual head is greater than the design head, negative pressures occur (Erpicum et al., 2018; Imanian & Mohammadian, 2019). Since the negative pressure may cause cavitation, which can damage the structure and stability of the spillway, it is necessary to research the negative pressure zone of the ogee spillway with high head ratios.

Figure 3-30 depicts the estimated pressure domain for the ungated and gated spillway using the realizable k-ε model. It can be clearly observed in Figures 3-30 (a)-(c) that when the head ratio increases, the negative pressure zone at the spillway crest becomes larger. Furthermore, Figures 3-30 (d)-(f) depict that the negative pressure zone at the spillway crest enlarges as the relative gate opening increases, which means that the absolute value of the minimum pressure becomes larger.

As mentioned before, the ungated and gated spillways employed in this research share the same inlet discharge of 0.012 m^3/s and 0.053 m^3/s. To examine the hydraulic characteristic of two different spillways, a comparison of the minimum pressure at the crest under the same discharge is conducted and presented in Table 7, which reveals that, after adding the gate, the minimum pressure at the spillway crest decreases and is negative. In other words, the absolute value of the pressure increases.

One explanation is that increasing the head leads to the sub-atmospheric or negative pressure developing along the crest at the interface between the flow and the spillway crest. In this study, increasing discharge and installing gates both caused higher heads and, therefore, higher absolute sub-atmospheric pressure.

Table 7 Comparison of the minimum pressure at the crest between the ungated and gated spillway

Q (m^3/s)	Spillway type	Minimum pressure at the crest (Pa)
0.012	Ungated spillway	-32
	Gated spillway	-425
0.053	Ungated spillway	-1140
	Gated spillway	-1870

The negative pressure at the gated spillway crest is smaller than that observed for the case of the ungated spillway with the same inlet discharge. This motivates further investigation of the minimum pressure for the gated spillway. Therefore, the vertical location of the minimum pressure of the gated spillway is analyzed next.

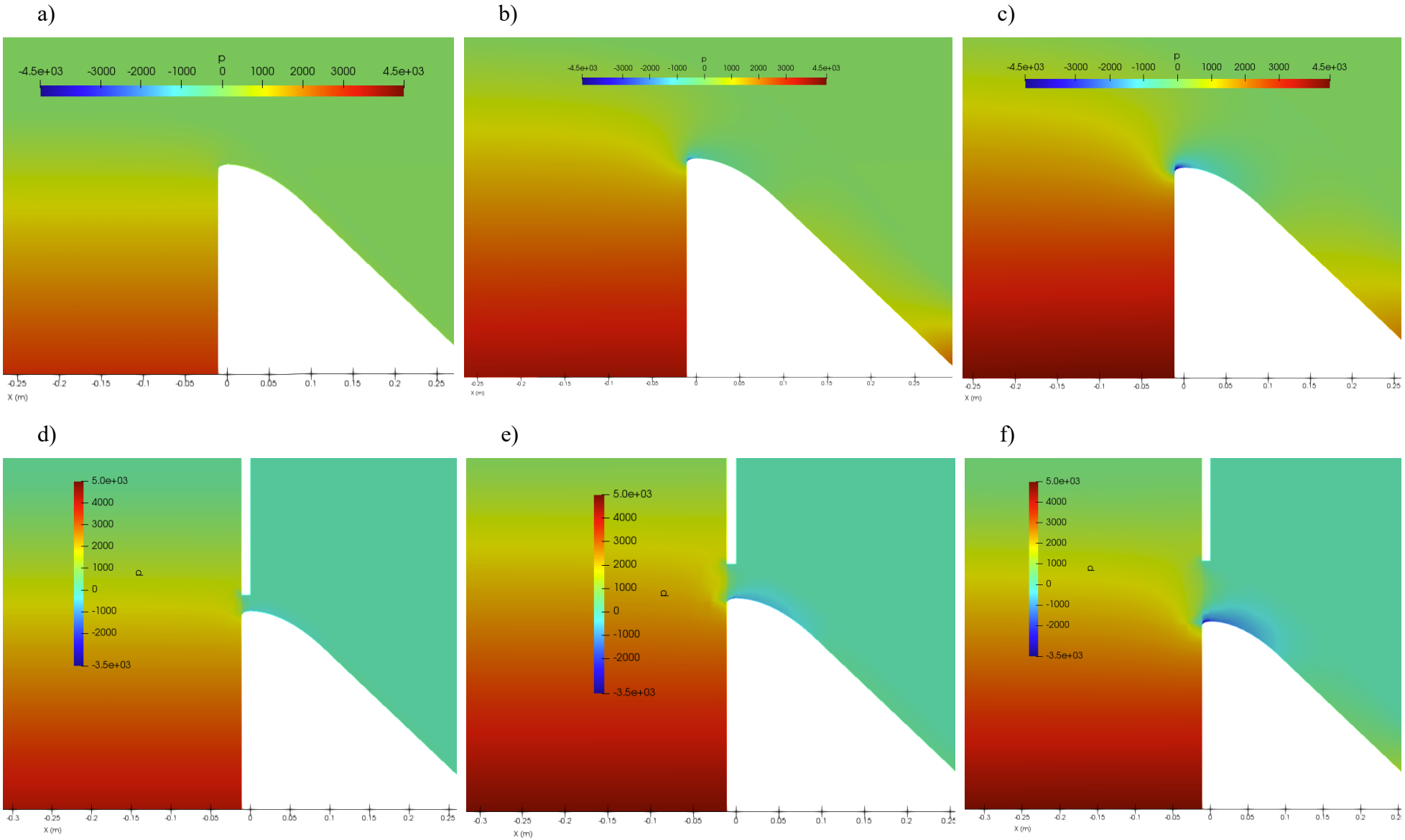

Figure 3-30 Predicted pressure field using realizable k-ε model of (a). Ungated spillway Hr=1.4 (b) Ungated spillway Hr=3.7 (c) Ungated spillway Hr=4.6 (d) Gated spillway Zl=0.5 (e) Gated spillway Zl=1.0 (f) Gated spillway Zl=2.0.

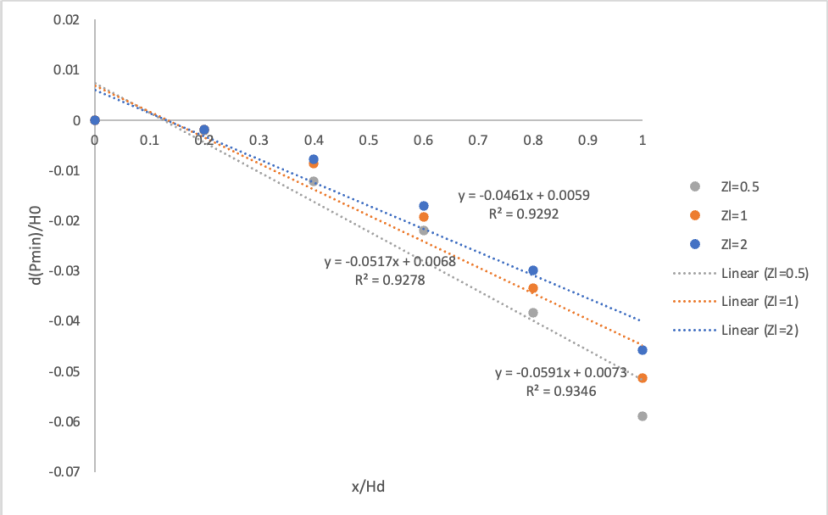

Figure 3-31 Vertical location of the minimum pressure

Figure 3-31 demonstrates the vertical location of where the minimum pressure occurs along the gated spillway. The vertical axis is dimensionless, which takes the depth where minimum pressure occurs *d(pmin)* divided by the actual hydraulic head H_0. The horizontal axis is calculated by dividing the distance to crest *x* of the design head H_d, which is dimensionless as well.

According to Figure 3-31, the vertical location of the minimum negative pressure slightly shifts upward with the increasing relative gate opening. Furthermore, the minimum pressure occurrence location and the horizontal spillway distance show a linear relationship, with R^2 greater than 0.92. In other words, as the distance to the crest increases, the location of the minimum negative pressure gradually and linearly moves downstream.

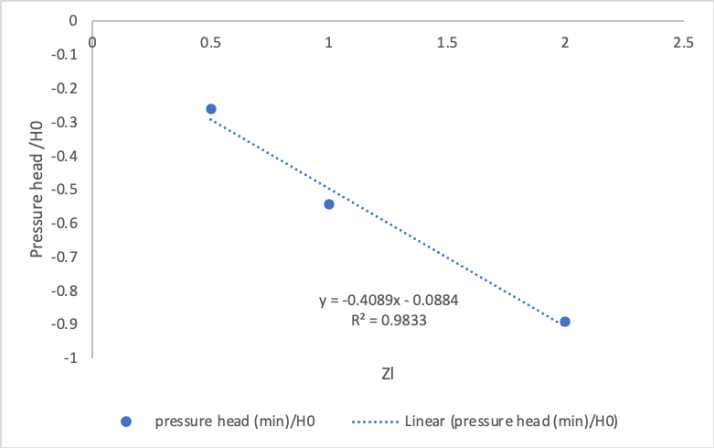

Figure 3-32 Minimum pressure head versus relative gate opening Zl.

To visualize the effect of increasing the relative gate opening on the pressure, Figure 3-32 presents the minimum pressure heads for different relative gate opening in a dimensionless form. The vertical axis takes the pressure head over the actual upstream head.

With an R^2 value greater than 0.98, Figure 3-32 shows a strong linear relationship between the relative gate opening and the minimum pressure head amplitude. According to Figure 3-32, the minimum pressure head reduces linearly as the relative gate opening increases. The pressure decreases indicating the occurrence of cavitation (Pfister et al., 2012).

3.5. Conclusions

This paper combines numerical and physical models to examine the hydraulic characteristics of vertical plane gated and ungated ogee spillways under high head ratios. The numerical models were developed using three turbulence models (realizable k-ε, RNG k-ε, and k-ω SST models) through the CFD software OpenFOAM. The experiments were conducted using an Acoustic Doppler Velocimeter (ADV) to measure the velocity profile, and ultrasonic sensor wave gauges, which recorded the time history of the water surface profile. Based on this research, the following conclusions can be drawn:

- Based on the comparison of numerical and experimental models with respect to the velocity and water surface profiles over gated and ungated ogee spillways, it was shown that the numerical simulation results agreed well with the experimental measurement data. These results indicated that all three turbulence models could predict the hydraulic characteristics successfully in the vicinity of the gated and ungated spillways.
- Velocity profiles suggest that the result of the simulation for all turbulence models improved as the head ratio increased, especially at the section near the spillway. Among the three turbulence models, the realizable k-ε model provided the best simulation results and, as such, it which was chosen for the following detailed discussion about the velocity field, corner eddy zone, and pressure field.
- To improve the discharge equation of the vertical plane gated spillway, a revised equation involving the gate opening and the upstream head was proposed. After modification, the mean absolute percentage error of the calculated discharge was reduced from 18.8% to 0.9%.
- For both the gated and ungated spillways, the vertical location of the maximum velocity occurred (*dm*) exhibited a linear relationship with the distance from the spillway crest (*x)*. The *dm* of the ungated spillway increases linearly with the *x*, while the dm of the gated spillway decreases linearly with the *x*.
- The corner separation zone upstream of the spillway provides describes complex hydrodynamics characterizing this region. In this study, the better numerical simulation exhibits a significant corner eddy. The size of the corner eddy increases with an increase in the head ratio, a fact that implies reduced numerical diffusion, which also explains why

the simulation gets improved in the near-spillway section with increasing head ratios in this research.

- The minimum pressure over the crest was investigated. The minimum negative pressure decreased linearly with an increase in the relative gate opening, which means the absolute value of pressure will increase with the increasing heads.

The numerical models employed in this study are only based on the RANS approach. Future investigation should employ more complex and advanced models, such as LES and DES.

Chapter 4 Conclusions and recommendations for future work

4.1. Conclusions

The present study was designed to employ numerical and physical models to determine the effect of the high head ratio on the hydraulic efficiency of ogee spillways, which include both ungated and gated spillways. By comparing the results of numerical and experimental models, the accuracy of numerical simulation could be investigated. In this study, the experimental measurement showed good agreement with the numerical simulation, especially in the sections located further away from the spillway, whereas, in the region closer to the spillway, the numerical simulation results were less accurate. Among the three applied turbulence models (realizable k-ε, RNG k-ε, and k-ω SST models), the realizable k-ε model provided the simulation results closest to the experimental ones, and its performance improved in the near-spillway section with an increase in the head ratio and in the relative gate opening. Moreover, a revised equation for calculating the discharge over a vertical plane gated spillway was proposed based on the experimental measurements, which involves the gate opening and the actual head. Further discussion on the hydraulic characteristics, such as the velocity fields at various locations, the vertical location of the maximum velocity, the corner separation zone, and the minimum pressure, were conducted by applying the realizable k-ε model.

The results of this investigation have led to three observations. Firstly, the vertical location where the maximum velocity occurs (*dm)* exhibits a linear relationship with the distance from the spillway axis, *x*. For the gated spillway, *dm* decreases linearly with *x*, while it increases linearly with *x* for the case of ungated spillway.

Secondly, the size of the corner separation zone allows for determining the quality of the numerical simulation in this study. A larger corner eddy indicates a lower level of numerical diffusion. Furthermore, the eddy size increase with the increasing head ratio.

Thirdly, the minimum pressure over the spillway crest was examined. This minimum pressure, which is negative, decreases with an increase in the head. This explains why the minimum pressure reduces with increasing relative gate opening and an increase in the head ratio. In other words, the absolute value of minimum pressure will increase with increasing heads.

This study attempts to provide a deeper insight into the vertical plane gated spillway and the ungated spillway with high head ratios. The numerical models developed in this study can be used as a complementary tool to physical models with the purpose of measuring various hydraulic characteristics of the ogee spillway.

With respect to the impact of this research on practical engineering aspects, two key aspects can be mentioned here. Firstly, climatic changes in various parts of the world have contributed to the actual head of the spillway being now more frequently larger than the initial design head. Therefore, it is necessary to learn the effect of high head ratios on spillways. Secondly, the analysis of the minimum pressure in this research indicates that the negative pressure should be carefully considered to prevent the ogee spillway from cavitation damage.

As mentioned in the scope of Chapter 1, this study was limited in several aspects, such as the accuracy of measurement instruments and the limited number of investigated turbulence models. Therefore, to investigate the hydraulic properties of the ogee spillway more accurately, further study is needed.

4.2. Recommendations for future work

Based on the findings and limitations of physical and numerical models presented in this study, the following recommendations are proposed for future work studies.

- Different gate openings, particularly for the case of high relative heads and also for the same inlet discharge, should be examined in more detail using numerical and physical models for a more thorough analysis of the gated spillway.
- More advanced and optimized numerical methods should be considered in the future for gated and ungated spillways. For example, mesh generation using snappyHexMesh, or working with unstructured grids.
- More sophisticated numerical models, such as LES and DES, should be explored in analyzing the high head ratio and the different relative gate opening for the ogee spillways.
- To capture the velocity profiles and streamlines over the spillway more accurately and effectively, some advanced velocity measurement devices should be used in the future, such as the Particle Image Velocimetry (PIV) method.
- Further investigations are necessary to determine the general applicability of the revised discharge equation proposed in this study for the vertical plane gated spillway, particularly for low normalized head situations.
- To calibrate the numerical models in more aspects, the pressure distribution at the spillway crest and chute should be measured by conducting the experiments using precise pressure sensors. Moreover, the negative pressure zone along the spillway crest and chute should be paid more attention to since it may pose a cavitation hazard to the ogee spillway.

Reference

Aghaei, Y., Kilanehei, F., Faghihirad, S., & Nazari-Sharabian, M. (2022). Dynamic Pressure at Flip Buckets of Chute Spillways: A Numerical Study. *International Journal of Civil Engineering*, *20*(4), 421–432. https://doi.org/10.1007/s40999-021-00670-4

Ansar, M., & Gonzalez-Castro, J. A. (2003). Submerged Weir Flow at Prototype Gated Spillways. *World Water & Environmental Resources Congress 2003*, 1–6. https://doi.org/10.1061/40685(2003)198

Bhajantri, M. R. (n.d.). *DOCTOR OF PHILOSOPHY*. 275.

Bhajantri, M. R., Eldho, T. I., & Deolalikar, P. B. (2007). Modeling hydrodynamic flow over spillway using weakly compressible flow equations. *Journal of Hydraulic Research*, *45*(6), 844–852. https://doi.org/10.1080/00221686.2007.9521822

Chanel, P. G., & Doering, J. C. (2008). Assessment of spillway modeling using computational fluid dynamics. *Canadian Journal of Civil Engineering*, *35*(12), 1481–1485. https://doi.org/10.1139/L08-094

Chatila, J., & Tabbara, M. (2004). Computational modeling of flow over an ogee spillway. *Computers & Structures*, *82*(22), 1805–1812. https://doi.org/10.1016/j.compstruc.2004.04.007

Darmawan, S., & Tanujaya, H. (2019). CFD Investigation of Flow Over a Backward-facing Step using an RNG k-ε Turbulence Model. *International Journal of Technology*, *10*(2), 280. https://doi.org/10.14716/ijtech.v10i2.800

Design of Small Dams. (1987).

Devolder, B., Troch, P., & Rauwoens, P. (2018). Performance of a buoyancy-modified k-ω and k-ω SST turbulence model for simulating wave breaking under regular waves using OpenFOAM®. *Coastal Engineering*, *138*, 49–65. https://doi.org/10.1016/j.coastaleng.2018.04.011

Erpicum, S., Blancher, B., Vermeulen, J., Peltier, Y., & Archambeau, P. (2018). *Experimental Study of Ogee Crested Weir Operation Above the Design Head and Influence of the Upstream Quadrant Geometry*. https://doi.org/10.15142/T3DH1M

Falvey, H. T. (1990). *Cavitation In Chutes and Spillways*. 165.

Ferziger, J. H., & Perić, M. (2002). *Computational Methods for Fluid Dynamics*. Springer Berlin Heidelberg. https://doi.org/10.1007/978-3-642-56026-2

Fleit, G., Baranya, S., & Bihs, H. (2017). CFD Modeling of Varied Flow Conditions Over an Ogee-Weir. *Periodica Polytechnica Civil Engineering*. https://doi.org/10.3311/PPci.10821

Hager, W. H. (1987). Continuous Crest Profile for Standard Spillway. *Journal of Hydraulic Engineering*, *113*(11), 1453–1457. https://doi.org/10.1061/(ASCE)0733-9429(1987)113:11(1453)

Hager, W. H. (1991). EXPERIMENTS ON STANDARD SPILLWAY FLOW (INCLUDING APPENDIX). *Proceedings of the Institution of Civil Engineers*, *91*(3), 399–416. https://doi.org/10.1680/iicep.1991.15622

Hager, W. H., & Bremen, R. (1988). Plane Gate on Standard Spillway. *Journal of Hydraulic Engineering*, *114*(11), 1390–1397. https://doi.org/10.1061/(ASCE)0733-9429(1988)114:11(1390)

Imanian, H., & Mohammadian, A. (2019). Numerical simulation of flow over ogee crested spillways under high hydraulic head ratio. *Engineering Applications of Computational Fluid Mechanics*, *13*(1), 983–1000. https://doi.org/10.1080/19942060.2019.1661014

Imanian, H., Mohammadian, A., & Hoshyar, P. (2021). Experimental and numerical study of flow over a broad-crested weir under different hydraulic head ratios. *Flow Measurement and Instrumentation*, *80*, 102004. https://doi.org/10.1016/j.flowmeasinst.2021.102004

Jacobsen, N. G., Fuhrman, D. R., & Fredsøe, J. (2012). A wave generation toolbox for the open-source CFD library: OpenFoam®. *International Journal for Numerical Methods in Fluids*, *70*(9), 1073–1088. https://doi.org/10.1002/fld.2726

Jafari-Nodoushan, E., Hosseini, K., Shakibaeinia, A., & Mousavi, S.-F. (2016). Meshless particle modelling of free surface flow over spillways. *Journal of Hydroinformatics*, *18*(2), 354–370. https://doi.org/10.2166/hydro.2015.096

Karim, R. A., & Mohammed, J. R. (2020). A comparison study between CFD analysis and PIV technique for velocity distribution over the Standard Ogee crested spillways. *Heliyon*, *6*(10), e05165. https://doi.org/10.1016/j.heliyon.2020.e05165

Kazemzadeh-Parsi, M. J. (2014). Numerical flow simulation in gated hydraulic structures using smoothed fixed grid finite element method. *Applied Mathematics and Computation*, *246*, 447–459. https://doi.org/10.1016/j.amc.2014.08.016

Khatsuria, R. M. (2005). *Hydraulics of spillways and energy dissipators*. Marcel Dekker.

Kim, D. G., & Park, J. H. (2005). Analysis of flow structure over ogee-spillway in consideration of scale and roughness effects by using CFD model. *KSCE Journal of Civil Engineering*, *9*(2), 161–169. https://doi.org/10.1007/BF02829067

Kocaer, Ö., & Yarar, A. (2020). Experimental and Numerical Investigation of Flow Over Ogee Spillway. *Water Resources Management*, *34*(13), 3949–3965. https://doi.org/10.1007/s11269-020-02558-9

Launder, B. E., Reece, G. J., & Rodi, W. (1975). Progress in the development of a Reynolds-stress turbulence closure. *Journal of Fluid Mechanics*, *68*(3), 537–566. https://doi.org/10.1017/S0022112075001814

Lee, C.-H. (2018). Rough boundary treatment method for the shear-stress transport *k—ω* model. *Engineering Applications of Computational Fluid Mechanics*, *12*(1), 261–269. https://doi.org/10.1080/19942060.2017.1410497

Mazumdar, S. K., & Roy, I. D. (1997). ORIFICE FLOW IN A GATED SPILLWAY. *ISH Journal of Hydraulic Engineering*, *3*(2), 44–52. https://doi.org/10.1080/09715010.1997.10514609

Menter, F. R. (1993). *ZONAL TWO EQUATION k-w TURBULENCE MODELS FOR AERODYNAMIC FLOWS*. 22.

Menter, F. R. (1994). Two-equation eddy-viscosity turbulence models for engineering applications. *AIAA Journal*, *32*(8), 1598–1605. https://doi.org/10.2514/3.12149

Morales, V., Tokyay, T. E., & Garcia, M. (2012). *NUMERICAL MODELING OF OGEE CREST SPILLWAY AND TAINTER GATE STRUCTURE OF A DIVERSION DAM ON CAN˜ AR RIVER, ECUADOR*. 9.

Nguyen, C.-T., Wang, L., & Tang, H. (2015). The effect of a curved bed on the discharge equation in a spillway with a breast wall. *Journal of Hydrodynamics*, *27*(2), 311–318. https://doi.org/10.1016/S1001-6058(15)60486-3

Novkovic, D., Burazer, J., Cocic, A., & Lecic, M. (2018). On the influence of turbulent kinetic energy level on accuracy of k − ε and LRR turbulence models. *Theoretical and Applied Mechanics*, *45*(2), 139–149. https://doi.org/10.2298/TAM171201009N

Peltier, Y., Dewals, B., Archambeau, P., Pirotton, M., & Erpicum, S. (2018). Pressure and velocity on an ogee spillway crest operating at high head ratio: Experimental measurements and validation. *Journal of Hydro-Environment Research*, *19*, 128–136. https://doi.org/10.1016/j.jher.2017.03.002

Pfister, M., Duarte, R., Müller, M., & Cesare, G. D. (2012). Cavitation risk estimation at orifice spillway based on UVP and dynamic pressure measurements. *On Ultrasonic Doppler Methods for Fluid Mechanics and Fluid Engineering*, 137–140.

Rubinstein, R., & Barton, J. M. (1992). Renormalization group analysis of the Reynolds stress transport equation. *Physics of Fluids A: Fluid Dynamics*, *4*(8), 1759–1766. https://doi.org/10.1063/1.858396

Salazar, F., Morán, R., Rossi, R., & Oñate, E. (2013). Analysis of the discharge capacity of radial-gated spillways using CFD and ANN – Oliana Dam case study. *Journal of Hydraulic Research*, *51*(3), 244–252. https://doi.org/10.1080/00221686.2012.755714

Saunders, K., Prakash, M., Cleary, P. W., & Cordell, M. (2014). Application of Smoothed Particle Hydrodynamics for modelling gated spillway flows. *Applied Mathematical Modelling*, *38*(17–18), 4308–4322. https://doi.org/10.1016/j.apm.2014.05.008

Savage, B. M., & Johnson, M. C. (2001). Flow over Ogee Spillway: Physical and Numerical Model Case Study. *Journal of Hydraulic Engineering*, *127*(8), 640–649. https://doi.org/10.1061/(ASCE)0733-9429(2001)127:8(640)

Schohl, G. (2016). *Discharge Correlations for Spillways with Radial Gates*. https://doi.org/10.15142/T3410628160853

Shaheed, R., Mohammadian, A., & Kheirkhah Gildeh, H. (2019). A comparison of standard k–ε and realizable k–ε turbulence models in curved and confluent channels. *Environmental Fluid Mechanics*, *19*(2), 543–568. https://doi.org/10.1007/s10652-018-9637-1

Shakibaeinia, A., & Jin, Y.-C. (2009). A weakly compressible MPS method for modeling of open-boundary free-surface flow. *International Journal for Numerical Methods in Fluids*, n/a-n/a. https://doi.org/10.1002/fld.2132

Shih, T.-H., Liou, W. W., Shabbir, A., Yang, Z., & Zhu, J. (1995). A NEW k-ε EDDY VISCOSITY MODEL FOR HIGH REYNOLDS NUMBER TURBULENT FLOWS. *Computers & Fluids*, *24*(3), 227–238.

Speziale, C. G., & Thangam, S. (1992). Analysis of an RNG based turbulence model for separated flows. *International Journal of Engineering Science*, *30*(10), 1379-IN4. https://doi.org/10.1016/0020-7225(92)90148-A

The Greenville News. (2016). All 12 spillway gates opened at Hartwell Dam [photograph], Retrieve from: https://www.tennessean.com/story/news/environment/2016/01/22/all-12-spillway-gates-opened-hartwell-dam/79196586/

Vermeyen, T. B. (1992). *Uncontrolled ogee crest research*. US Department of the Interior. Bureau of Reclamation.

Versteeg, H. K., & Malalasekera, W. (1995). *An introduction to computational fluid dynamics* (1st ed.). Longman Science & Technical, Harlow.

Villemonte, J. R. (1947). Submerged Weir Discharge Studies. *Eng. News Records*, 866–869.

Wu, S., & Rajaratnam, N. (1996). Submerged Flow Regimes of Rectangular Sharp-Crested Weirs. *Journal of Hydraulic Engineering*, *122*(7), 412–414. https://doi.org/10.1061/(ASCE)0733-9429(1996)122:7(412)

Yakhot, V., Orszag, S. A., Thangam, S., Gatski, T. B., & Speziale, C. G. (1992). Development of turbulence models for shear flows by a double expansion technique. *Physics of Fluids A: Fluid Dynamics*, *4*(7), 1510–1520. https://doi.org/10.1063/1.858424

Zawawi, M. H., Aziz, N. A., Radzi, M. R. M., Hassan, N. H., Ramli, M. Z., Zahari, N. M., Abbas, M. A., Saleha, A., Salwa, A., & Muda, Z. C. (2018). *Computational fluid dynamic analysis at dam spillway due to different gate openings*. 020245. https://doi.org/10.1063/1.5066886